YANG-BAXTER FIELD FOR SPIN HALL-LITTLEWOOD SYMMETRIC FUNCTIONS

ALEXEY BUFETOV1 and LEONID PETROV2,3

¹ Massachusetts Institute of Technology, Department of Mathematics, 77 Massachusetts Avenue, Cambridge, MA 02139, USA;

email: alexey.bufetov@gmail.com

² University of Virginia, Department of Mathematics, 141 Cabell Drive, Kerchof Hall, P.O. Box 400137, Charlottesville, VA 22904, USA

³ Institute for Information Transmission Problems, Bolshoy Karetny per. 19, Moscow 127994, Russia;

email: lenia.petrov@gmail.com

Received 25 January 2018; accepted 22 September 2019

Abstract

Employing bijectivization of summation identities, we introduce local stochastic moves based on the Yang–Baxter equation for $U_q(\widehat{\mathfrak{sl}_2})$. Combining these moves leads to a new object which we call the spin Hall–Littlewood Yang–Baxter field—a probability distribution on two-dimensional arrays of particle configurations on the discrete line. We identify joint distributions along down-right paths in the Yang–Baxter field with spin Hall–Littlewood processes, a generalization of Schur processes. We consider various degenerations of the Yang–Baxter field leading to new dynamic versions of the stochastic six-vertex model and of the Asymmetric Simple Exclusion Process.

2010 Mathematics Subject Classification: 60K35 (primary); 60C05, 05E05, 82B23 (secondary)

1. Introduction

1.1. Overview. The past two decades have seen a wave of progress in understanding large-scale, long-time asymptotics of driven nonequilibrium stochastic particle systems in the one space and one time dimension belonging to the Kardar–Parisi–Zhang (KPZ) universality class (to know more about the KPZ class, see, for example, [Cor12, Cor16, HHT15]). Much of this progress has been achieved by discovering exact distributional formulas in these particle systems and leveraging these formulas toward asymptotic analysis. Stochastic particle

[©] The Author(s) 2019. This is an Open Access article, distributed under the terms of the Creative Commons Attribution licence (http://creativecommons.org/licenses/by/4.0/), which permits unrestricted re-use, distribution, and reproduction in any medium, provided the original work is properly cited.



systems possessing such exact formulas are known under the name *integrable*. Since the early days (for example, [Joh00]), success in discovering integrability (at least for special initial data) has often been triggered by applications of techniques coming from the algebra of symmetric functions [Mac95, Ch. I]. Among the most notable frameworks for these applications are Schur processes [Oko01, OR03, Bor11, BBB+14] and Macdonald processes [BC14, BCGS16]. The success of this approach naturally leads to a more extensive study of structural properties of various families of symmetric functions and their relations to probabilistic systems.

In this work, we investigate stochastic systems related to *spin Hall–Littlewood symmetric rational functions* introduced in [Bor17a]. These functions are naturally at the interplay of the theory of symmetric functions and the Yang–Baxter equation (see, for example, [Tsi06, BW16, BWZJ15, WZJ16] for other related examples). The main results of the present paper are the following:

- We consider the general idea of bijectivization (Section 2) and apply it to the Yang-Baxter equation, obtaining local stochastic moves acting on vertex model configurations (Section 3). We hope that the usefulness of this general idea will not be limited by the results of this paper.
- We introduce the spin Hall-Littlewood Yang-Baxter field (Section 6), a twodimensional array of random particle configurations on the discrete line. Its main properties are explicit formulas for distributions along any down-right path (Theorem 6.3) and Markov projections turning the Yang-Baxter field into a two-dimensional scalar field or its multilayer versions (Propositions 6.2 and 7.3).
- We consider a number of degenerations of the Yang-Baxter field, including new dynamic versions of the stochastic six-vertex model (Section 7) and the Asymmetric Simple Exclusion Process (ASEP) (Appendix A.13). Our results about these dynamic models generalize those of the recent works [BBW18] and [BM18].

Let us describe our results in more detail.

1.2. Random fields of Young diagrams. One of the key properties behind probabilistic applications of Macdonald (in particular, Schur) symmetric functions is that they satisfy *Cauchy summation identities* [Mac95, Ch. I.4 and VI.2] (see also Section 4.3 for Cauchy identities for the spin Hall–Littlewood symmetric functions). Regarding these identities as expressing probability normalizing constants (= partition functions) allows to define and analyze



Macdonald processes. These are certain probability distributions on collections of Young diagrams whose probability weights are proportional to products of the (skew) Macdonald symmetric polynomials. (In probabilistic applications, Young diagrams are often interpreted as particle configurations on the discrete line.) A lot of recent research is devoted to the study of these processes and their degenerations, with applications to KPZ type and other asymptotics; for example, see [O'C12, COSZ14, OSZ14, BC14, BCFV15, BG15, BP14].

It is much less articulated in the existing literature that one can consider Macdonald (Schur, etc.) *fields*—certain ways to couple many processes together leading to two-dimensional arrays of random Young diagrams. Such fields are highly nonunique, and coming up with a 'good' way to couple processes together involves additional considerations like the presence of Markov projections (see below). Various elements of Young diagram random fields have appeared in the literature mainly as ways to match observables of (1+1)-dimensional stochastic interacting particle systems with observables of Macdonald or Schur processes. The latter observables then can be analyzed to the point of asymptotics, thanks to the algebraic structure coming from symmetric functions. Two ways to construct such random fields were mainly employed, which we will briefly discuss in Sections 1.3 and 1.4.

1.3. Robinson–Schensted–Knuth (RSK) type fields. RSK type fields were applied in probabilistic context in connection with Schur measures as early as in [BDJ99, Joh00, PS02] to study asymptotics of longest increasing subsequences, last passage percolation, Totally Asymmetric Simple Exclusion Process (TASEP), and polynuclear growth. These fields arise (in the Schur case) as results of applying the RSK insertion algorithm to a random input, hence the name. More precisely, a Schur RSK type field can be realized using Fomin growth diagrams (an equivalent way to interpret the RSK insertion [Fom86, Fom95]) with random integer inputs. The idea to apply RSK insertion to random input seems to have first appeared in [VK86] and was substantially developed in [Bar01, O'C03b, O'C03a].

Recently, RSK type fields associated with deformations of Schur processes (see Figure 1) were constructed for Whittaker processes [O'C12, COSZ14, OSZ14], *q*-Whittaker processes [OP13, BP16, Pei13, MP17, Pei16], and Hall–Littlewood processes [BP15, BBW18, BM18]. Constructions at the Whittaker level relied on the geometric (also sometimes called 'tropical') lifting of the RSK correspondence [Kir01, NY04], while the *q*-Whittaker and Hall–Littlewood developments required nontrivial randomizations of the original RSK insertion algorithm.



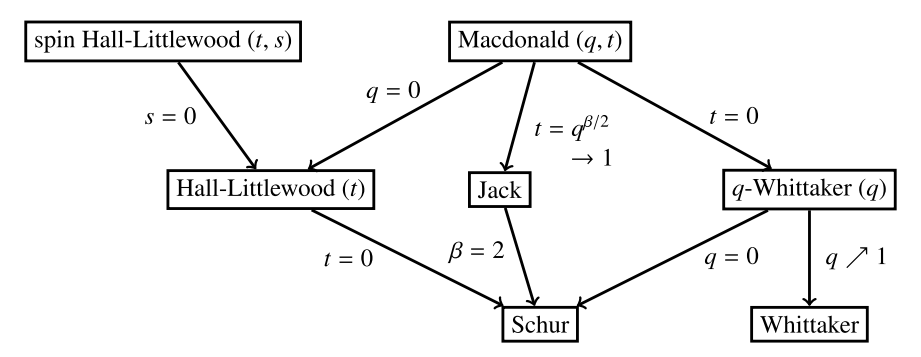


Figure 1. A part of the hierarchy of symmetric functions satisfying summation identities of Cauchy type. Arrows mean degenerations.

Via Markov projections, this work uncovered connections of Whittaker, q-Whittaker, and Hall–Littlewood processes with known and new (1 + 1)-dimensional stochastic particle systems. In the Whittaker case, these are various integrable models of directed random polymers [OY02, Sep12]. For the q-Whittaker processes, these are the q-TASEP and related systems [BC15, CP15, MP17]. In the Hall–Littlewood case, these are the ASEP [MGP68, Spi70] and the stochastic six-vertex model [GS92, BCG16].

1.4. Borodin–Ferrari type fields. Another method of constructing random fields of Young diagrams is based on interpreting the skew Cauchy identity as an intertwining relation between certain Markov transition matrices and stitching these matrices together into a multivariable Markov chain using an idea of Diaconis and Fill [**DF90**]. In the symmetric functions context, this method was first applied (in the Schur case) in a work by Borodin and Ferrari [**BF14**], hence the name.

In principle, this approach is applicable to a wider variety of models than the RSK one and does not require intricate combinatorial constructions. This generality comes at a cost of having fewer Markovian projections than the RSK constructions, especially away from the Schur case. An exception in the literature is that the half-continuous BF type field in the setting of q-Whittaker processes has led to the discovery of the continuous time q-TASEP, a notable deformation of the TASEP with a richer algebraic structure [BC14].

A unified approach to both the RSK type and the BF type fields in the half-continuous setting (details on half-continuous degenerations of random fields may be found in Appendices A.6 and A.9) was suggested in [BP16]. In a fully discrete setting, elements of BF type fields for Schur polynomials appeared in [WW09, BF14].



1.5. Yang–Baxter field. We present a third way of constructing random fields associated with symmetric functions and the corresponding processes. Our approach is based on the Yang–Baxter equation which is behind many families of symmetric functions including Schur, Hall–Littlewood, and spin Hall–Littlewood ones. We focus on the latter family for which Cauchy summation identities were recently established in [Bor17a] with the help of the Yang–Baxter equation for the quantum \mathfrak{sl}_2 [Bax07].

In the setting of spin Hall–Littlewood processes, random fields have not been considered in the literature yet. The Yang–Baxter field we construct in the present paper yields a new object even in the most basic Schur case (Appendix A.9). The main advantages of our approach are its simplicity and clear structure of Markov projections, yielding new (1 + 1)-dimensional stochastic systems (see Section 1.7). In comparison, an RSK type approach would likely require very nontrivial combinatorial considerations (see [BM18] for the Hall–Littlewood case), further complicated by the fact that the spin Hall–Littlewood functions are not homogeneous polynomials while the usual Hall–Littlewood ones are (see Remark A.2 for more details). A BF type approach, while clearly being applicable in the spin Hall–Littlewood case, might not readily produce Markov projections.

Our construction of the Yang-Baxter field uses a very basic idea of bijectivization of the Yang-Baxter equation. We briefly describe this idea next.

1.6. Bijectivization of the Yang–Baxter equation. In probability theory, it is well known that considering couplings of probability measures is a powerful idea. For our construction of the Yang–Baxter field, we apply a similar idea to summation identities which form the Yang–Baxter equation for quantum \mathfrak{sl}_2 . We refer to it as a *bijectivization* of these combinatorial summation identities. As a byproduct of couplings thus constructed, we obtain conditional distributions, and we regard them as local stochastic (Markov) moves acting on vertex model configurations. The bijectivization of the Yang–Baxter equation we consider is also not unique, but the space of possible parameters is quite small. We use this freedom to choose a bijectivization with the least 'noise', in the spirit of RSK type approach, see [**BP16**, Section 7.4]. See Section 3.6 for details.

We believe that one of the important novelties of this paper is the application of this idea of coupling to combinatorial summation identities. Here we use it in only one situation, in the setting of the Yang–Baxter equation powering the spin Hall–Littlewood symmetric functions. However, it seems likely that this idea might lead to new interesting constructions and results for other forms of the Yang–Baxter equation as well.



1.7. Dynamic stochastic six-vertex model and dynamic ASEP. A certain Markov projection of our Yang–Baxter random field yields a scalar-valued random field indexed by the nonnegative integer quadrant. This scalar field can be interpreted as a random field of values of the height function in a certain generalization of the stochastic six-vertex model in which the vertex probabilities additionally depend on the value of the height function. For this reason, one can call this model a *dynamic stochastic six-vertex (DS6V) model*. Its detailed description is given in Section **7.1**.

The joint distribution of the values of the height function in DS6V along down-right paths can be identified with that of certain observables of a spin Hall-Littlewood process (Corollary 7.4). (Also referred to as space-like paths in the language of stochastic particle systems; see [DLSS91, Fer08, BF08].) In the degeneration turning the spin Hall-Littlewood symmetric functions into the Hall-Littlewood ones, the DS6V model becomes the usual stochastic six-vertex model of [GS92, BCG16], and Corollary 7.4 turns into the statement established in [BM18].

Along with single-layer projections leading to DS6V, one can consider multilayer projections of the full Yang–Baxter field, as was done in [BM18, Sections 4.4 and 4.5] for the Hall–Littlewood RSK field. In particular, one can check that the two-layer projection of our Yang–Baxter field, in the Hall–Littlewood degeneration, coincides with the two-layer stochastic six-vertex model of [BM18, Section 4.4]. However, the corresponding degeneration of the full Yang–Baxter field is different from the full Hall–Littlewood RSK field. Details may be found in Appendix A.

In a continuous time limit around the diagonal, the DS6V model turns into the following dynamic version of the ASEP depending on parameters $t\geqslant 0, -1 < s\leqslant 0$, and u>0. Consider a continuous time particle system $\{y_i(\tau)\}_{i\in\mathbb{Z}_{\geqslant 1},\tau\in\mathbb{R}_{\geqslant 0}}$ on \mathbb{Z} (no more than one particle at a site), started from the step initial configuration $y_i(0)=-i$. In continuous time, each particle $y_i,\ i\geqslant 1$, tries to jump to the right by one at rate $(u-st^i)/(u-st^{i-1})$ and to the left by one at rate $t((u-st^{i-1})/(u-st^i))$. (That is, the waiting time till the jump is an independent exponential random variable with mean equal to $(\text{rate})^{-1}$.) If the destination is occupied, the corresponding jump is blocked and y_i does not move; see Figure 2. The height function in this dynamic ASEP can be identified in distribution with a certain limit of observables of spin Hall–Littlewood processes. When s=0, the dynamic dependence of jump rates on the height function disappears and the system turns into the usual ASEP. See [BM18] for connections of ASEP to Hall–Littlewood processes.

The connection between spin Hall–Littlewood process and DS6V and dynamic ASEP hints at the possible integrability of the latter models, which might lead to



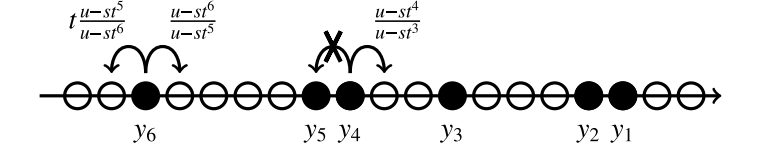


Figure 2. A new dynamic version of the ASEP.

asymptotic results for them. We do not address this question in the present paper. Note also that other dynamic generalizations of the stochastic six-vertex model and the ASEP were recently considered in [Bor17b, Agg17, BC17] in connection with vertex models related to the Yang–Baxter equation for the elliptic quantum group $E_{\tau,\eta}(\mathfrak{sl}_2)$. These dynamic models are different from the ones introduced in the present work.

Outline. In Section 2, we outline the general idea of bijectivization of summation identities. In Section 3, we describe the higher spin six-vertex weights, the Yang-Baxter equation they satisfy, and its bijectivization with minimal 'noise'. In Section 4, we recall the spin Hall-Littlewood symmetric functions and Cauchy summation identities they satisfy. This section closely follows [Bor17a]. In Section 5, we use our bijectivization of the Yang–Baxter equation sequentially to produce a bijective proof of the skew Cauchy identity for the spin Hall-Littlewood symmetric functions. In Section 6, we define our main object, the Yang-Baxter field, and discuss its connection with spin Hall-Littlewood measure and processes. In Section 7, we consider a projection of the Yang-Baxter field onto the column number zero leading to a new dynamic version of the stochastic six-vertex model. We also discuss a dynamic Yang-Baxter equation for these dynamic six-vertex weights. In Appendix A, we consider various degenerations of the DS6V model. One of these degenerations produces a new dynamic version of the ASEP. In Appendix B, we explicitly list all identities comprising the Yang-Baxter equation. In Appendix C, we discuss other versions of the skew Cauchy identity satisfied by the spin Hall-Littlewood symmetric functions. In Appendix D, we briefly outline extensions of our main constructions to the case of inhomogeneous parameters spin Hall-Littlewood symmetric functions.

2. Bijectivization of summation identities

2.1. General formalism. Here we explain the formal concept of bijectivization of summation identities which will be applied to the Yang–Baxter equation in Section 3. Let *A* and *B* be two fixed finite nonempty sets, and



each of the elements $a \in A$ and $b \in B$ is assigned certain weights w(a) and w(b), respectively. Assume that the following summation identity holds:

$$\sum_{a \in A} w(a) = \sum_{b \in B} w(b). \tag{2.1}$$

DEFINITION 2.1. We say that the following data provides a *bijectivization* of identity (2.1):

• There are forward transition weights $p^{\text{fwd}}(a, b)$ which satisfy

$$\sum_{b \in R} p^{\text{fwd}}(a, b) = 1 \quad \text{for each } a \in A;$$

• there are backward transition weights $p^{\text{bwd}}(b, a)$ which satisfy

$$\sum_{a \in A} p^{\text{bwd}}(b, a) = 1 \quad \text{for each } b \in B;$$

• the transition weights satisfy the reversibility condition

$$w(a)p^{\text{fwd}}(a,b) = w(b)p^{\text{bwd}}(b,a)$$
 for each $a \in A$ and $b \in B$. (2.2)

The term 'bijectivization' is justified by the following two observations. First, if A and B have the same numbers of elements, w(a) = w(b) = 1 for all $a \in A$, $b \in B$, and each $p^{\text{fwd}}(a, b)$ and $p^{\text{bwd}}(b, a)$ is either 0 or 1, then such a bijectivization is simply a bijection between A and B.

Second, let us get back to the general situation of Definition 2.1 and assume that a bijectivization $\{p^{\text{fwd}}(a,b), p^{\text{bwd}}(b,a)\}$ is given. Start from the left-hand side of (2.1) and write

$$\sum_{a \in A} w(a) = \sum_{a \in A} w(a) \left(\sum_{b \in B} p^{\text{fwd}}(a, b) \right) = \sum_{b \in B} w(b) \left(\sum_{a \in A} p^{\text{bwd}}(b, a) \right) = \sum_{b \in B} w(b).$$

Then, due to the reversibility condition (2.2), in the middle two double sums the terms are in *one-to-one correspondence*. Thus, one can say that the transition weights $\{p^{\text{fwd}}(a,b), p^{\text{bwd}}(b,a)\}$ produce a *refinement* (or a *bijective proof*) of the initial identity (2.1).

REMARK 2.2. Clearly, if both A and B have more than one element, then a bijectivization is highly nonunique. However, in a concrete situation (such as for the Yang–Baxter equation in Section 3), a particular bijectivization might be more natural than the others. This choice would depend on additional structure of individual terms in (2.1).



2.2. Stochastic bijectivization. Now assume that the weights w(a) and w(b) in (2.1) are stochastic; that is, they are positive and sum to one: $\sum_{a \in A} w(a) = \sum_{b \in B} w(b) = 1$. (If some weights are equal to zero, then let us remove the corresponding elements from A and B.) The latter condition can always be achieved for positive weights w(a), w(b) by dividing (2.1) by their sum. If the transition weights in a bijectivization $\{p^{\text{fwd}}(a,b), p^{\text{bwd}}(b,a)\}$ are all nonnegative, we call such a bijectivization stochastic. Another standard term used in the probability theory for such an object is coupling.

A stochastic bijectivization may be interpreted as a joint probability distribution on $A \times B$ having prescribed marginal distributions $\{w(a)\}_{a \in A}$ and $\{w(b)\}_{b \in B}$. The forward and backward transition weights become families of conditional distributions coming from this joint distribution on $A \times B$. The reversibility condition (2.2) simply states the compatibility between the two conditional distributions p^{fwd} and p^{bwd} .

One can also interpret $\{p^{\text{fwd}}(a,b)\}_{a\in A,b\in B}$ as a Markov transition matrix from A to B, and similarly for p^{bwd} . This explains the terms 'transition weights' and 'reversibility condition'.

If a stochastic bijectivization has all transition weights p^{fwd} , p^{bwd} equal to 0 or 1, we call such a bijectivization *deterministic*.

- **2.3. Examples.** Let us discuss two examples of bijectivization relevant to the Yang–Baxter equation considered in Section 3.
- 2.3.1. One of the sets is a singleton. For the first example, assume that $B = \{b\}$ is a singleton, while $A = \{a_1, \ldots, a_n\}$ is an arbitrary finite set. The bijectivization is unique in this case and is given by

$$p^{\text{fwd}}(a_i, b) = 1, \quad p^{\text{bwd}}(b, a_i) = \frac{w(a_i)}{w(b)}, \quad i = 1, \dots, n.$$

2.3.2. Both sets have two elements. For the second example, consider the situation when both sets $A = \{a_1, a_2\}$, $B = \{b_1, b_2\}$ have two elements, and all the four weights $w(a_i)$, $w(b_j)$ are nonzero. In this case, there are eight forward and backward transition weights which must solve four equations of the form $p^{\text{fwd}}(a_1, b_1) + p^{\text{fwd}}(a_1, b_2) = 1$ plus four more reversibility equations involving the weights $w(a_i)$, $w(b_j)$. However, since the weights satisfy (2.1), the reversibility equations are not independent, and hence the rank of the system of linear equations on the transition weights is equal to 7. (Another way to see this is to use quantities from (2.2) as variables: there are four variables and three linearly independent conditions on them.)



Therefore, there is a one-parameter family of bijectivizations. One readily checks that these solutions can be expressed in the following form:

$$\begin{split} p^{\text{fwd}}(a_{1}, b_{1}) &= \gamma, \\ p^{\text{fwd}}(a_{1}, b_{2}) &= 1 - \gamma, \\ p^{\text{fwd}}(a_{2}, b_{1}) &= 1 - \frac{w(b_{2})}{w(a_{2})} + (1 - \gamma) \frac{w(a_{1})}{w(a_{2})}, \\ p^{\text{fwd}}(a_{2}, b_{2}) &= \frac{w(b_{2})}{w(a_{2})} - (1 - \gamma) \frac{w(a_{1})}{w(a_{2})}, \\ p^{\text{bwd}}(b_{1}, a_{1}) &= \gamma \frac{w(a_{1})}{w(b_{1})}, \\ p^{\text{bwd}}(b_{1}, a_{2}) &= 1 - \gamma \frac{w(a_{1})}{w(b_{1})}, \\ p^{\text{bwd}}(b_{2}, a_{1}) &= (1 - \gamma) \frac{w(a_{1})}{w(b_{2})}, \\ p^{\text{bwd}}(b_{2}, a_{2}) &= 1 - (1 - \gamma) \frac{w(a_{1})}{w(b_{2})}. \end{split}$$

Let us also consider a particular case of the above example when $w(a_1) = w(b_1)$ (thus automatically $w(a_2) = w(b_2)$). In this case, the γ -dependent general solution (2.3) simplifies. Namely, it depends on the weights $w(\cdot)$ only through the combination $(1 - \gamma)w(a_1)/w(a_2)$. Thus, the most natural bijectivization of the summation identity

$$w(a_1) + w(a_2) = w(b_1) + w(b_2), \quad w(a_1) = w(b_1), \quad w(a_2) = w(b_2)$$
 (2.4)

corresponds to choosing $\gamma = 1$, does not depend on the weights $w(\cdot)$, and is *deterministic*. Namely, the term $w(a_1)$ is simply mapped to the term $w(b_1)$ equal to it, and similarly for $w(a_2)$ and $w(b_2)$.

3. Yang-Baxter equation and its bijectivization

The goal of this section is to apply bijectivization of Section 2 to the Yang–Baxter equation for the (horizontal spin- $\frac{1}{2}$) higher spin six-vertex model. This model corresponds to the quantum group $U_q(\widehat{\mathfrak{sl}}_2)$. The main outcome of this section is the definition of forward and backward transition weights in Section 3.3.

3.1. Vertex weights. Here we recall vertex weights of the higher spin sixvertex model introduced in [KR83]. In our formulas, we adopt the parametrization used in [Bor17a].



The vertex weights depend on the main 'quantization' parameter $t \in (0, 1)$, the *vertical spin* parameter s, and the *spectral* parameter u, with only the latter explicitly indicated in the notation. (For the purpose of the Yang–Baxter equation, the parameters s, u are generic complex numbers. Later, to apply the weights to stochastic models, we impose narrower conditions on the parameters.) These weights are associated with a vertex $(i_1, j_1; i_2, j_2)$ on the lattice \mathbb{Z}^2 which has i_1 and i_2 incoming and outgoing vertical arrows and j_1 and j_2 incoming and outgoing horizontal arrows, respectively. We assume that our vertex model has horizontal spin- $\frac{1}{2}$ and generic higher vertical spin, which is equivalent to saying that the vertex weights are nonzero only if j_1 , $j_2 \in \{0, 1\}$ and i_1 , $i_2 \in \mathbb{Z}_{\geqslant 0}$. (See also Appendix A.14 for a discussion of models with finite vertical spin I obtained by specializing the vertical spin parameter s to $t^{-I/2}$, $I \in \mathbb{Z}_{\geqslant 1}$.) The arrows at any vertex should satisfy the *preservation property* $i_1 + j_1 = i_2 + j_2$. Depending on j_1 , j_2 , we will denote vertices by

$$(g, 0; g, 0) = \cdots \xrightarrow{g} (g, 0; g - 1, 1) = \cdots \xrightarrow{g} \xrightarrow{1},$$

 $(g, 1; g, 1) = \xrightarrow{g} (g, 1; g + 1, 0) = \xrightarrow{g} \xrightarrow{1}.$

$$(3.1)$$

(see also Figure 3 for a more detailed graphical representation). Here $g \in \mathbb{Z}_{\geqslant 0}$ is arbitrary, with the agreement that $g \geqslant 1$ in the second vertex. The weights of these vertices are defined as

$$\begin{bmatrix}
\dots g \\
g \dots
\end{bmatrix}_{u} := \frac{1 - st^{g}u}{1 - su}, \quad \begin{bmatrix}
g - 1 \\
g
\end{bmatrix}_{u} := \frac{(1 - s^{2}t^{g-1})u}{1 - su},
\begin{bmatrix}
\rightarrow g \\
g
\end{bmatrix}_{u} := \frac{1 - st^{g}}{1 - su}, \quad \begin{bmatrix}
g + 1 \\
g \dots
\end{bmatrix}_{u} := \frac{1 - t^{g+1}}{1 - su}.$$
(3.2)

Weights (3.2) are very special in that they satisfy a Yang–Baxter equation which we recall in the next subsection.

REMARK 3.1. The higher spin weights (3.2) of [KR83] generalize the original six-vertex weights [Pau35, Lie67, Bax07] to the case when the vertical representation is the arbitrary highest weight (corresponding to the spin parameter s), and the horizontal representation is still two-dimensional. Using a procedure called fusion [KR87], one can define vertex weights corresponding to both representations being arbitrary. Explicit formulas for fused vertex weights may be found in, for example, [Man14]; see also [CP16] for a probabilistic interpretation. In the present paper, we only use the simpler weights (3.2) and do not employ the fused ones.



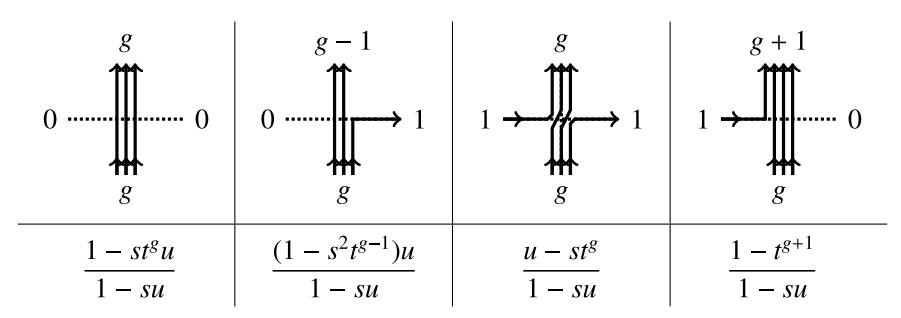


Figure 3. Possible vertices in the (horizontal spin- $\frac{1}{2}$) higher spin six-vertex model, with their weights (3.2).

REMARK 3.2. We denote the quantization parameter of the higher spin sixvertex model by t instead of q used in [Bor17a, CP16, BP18a]. This is done to highlight properties (in particular, Cauchy summation identities) of the spin Hall–Littlewood symmetric functions which degenerate at s=0 to the corresponding properties of the usual Hall–Littlewood symmetric polynomials. Vertex models in the context of Hall–Littlewood polynomials and their properties were recently studied in, for example, [BBW18, BM18], and we follow these papers when using the parameter t. Note that setting s=t=0 reduces the picture to the one associated with the classical Schur polynomials; see Appendix A.

3.2. Yang-Baxter equation. The Yang-Baxter equation [Yan67, Bax07, KRS81] can be regarded as the origin of integrability of the stochastic higher spin six-vertex model; see [BP18a]. It can be written in a rather compact form involving 4 × 4 matrices containing certain combinations of vertex weights. For example, see [Bor17a, Proposition 2.5] for the statement for our particular parametrization. However, as we aim to construct a bijectivization of the Yang-Baxter equation in the sense of Section 2, we need to write the Yang-Baxter equation out in full detail, considering each of its matrix elements separately.

Let us first define weights of auxiliary *cross vertices*. The cross vertices' incoming and outgoing arrow directions are rotated by 45° , and along each direction, there can be at most one arrow. Therefore, due to the arrow preservation, there are six possible cross vertices. Their weights depend on two arbitrary spectral parameters u, v and are defined as follows:



$$\left[\left[\left[\right] \right]_{u,v} := 1, \qquad \left[\left[\left[\right] \right]_{u,v} := 1, \right]$$

$$\left[\left[\left[\right] \right]_{u,v} := 1 - \rho = \frac{(1-t)v}{u-tv}, \qquad \left[\left[\left[\right] \right]_{u,v} := \rho = \frac{u-v}{u-tv}, \qquad (3.3)$$

$$\left[\left[\left[\right] \right]_{u,v} := t\rho = \frac{t(u-v)}{u-tv}, \qquad \left[\left[\left[\right] \right]_{u,v} := 1 - t\rho = \frac{(1-t)u}{u-tv}.$$

Here we employed the shorthand notation $\rho := (u - v)/(u - tv)$.

Let us now introduce notation for weights of *pairs of vertices* where one vertex as in Figure 3 is put on top of another. Because each of the two vertices in a pair can have at most one incoming and at most one outgoing horizontal arrow, there are $2^4 = 16$ types of such pairs. Indeed, choosing the numbers of horizontal arrows and saying that there are, say, g incoming vertical arrows at the bottom determines the other numbers of vertical arrows by the arrow preservation. The weight of a pair of vertices depends on two spectral parameters u, v, where u corresponds to the bottom vertex. (The total weight of each particular arrow configuration containing several vertices is, by definition, equal to the product of weights of arrow configurations over all individual vertices.) We will denote pairs of vertices and their weights similarly to (3.1)–(3.2), as in the following example:

$$\begin{bmatrix} \dots & g \\ g + 1 \\ g & \dots \end{bmatrix}_{u,v} = \begin{bmatrix} g + 1 \\ g & \dots \end{bmatrix}_{u} \begin{bmatrix} \dots & g \\ g + 1 \end{bmatrix}_{v} = \frac{(1 - t^{g+1})(1 - s^{2}t^{g})v}{(1 - su)(1 - sv)}.$$

We are now in a position to discuss the Yang-Baxter equation. In other words, this equation states that the partition function (that is, the sum of weights of all arrow configurations) in a configuration of a cross vertex followed by a pair of vertices with spectral parameters u, v is the same as the partition function of a pair of vertices with parameters v, u followed by a cross vertex, provided that the boundary conditions on all six external edges are the same. (In fact, thus defined partition functions are always sums of at most two terms.) This leads to 16 types of identities (YB1.1)–(YB4.4) (each depending on g) which are listed in Appendix B.

REMARK 3.3. The numbering of identities (YB1.1)–(YB4.4) reflects the boundary conditions on the left and right (the first and the second number, respectively). More precisely, equation numbers $\{1, 2, 3, 4\}$ correspond to the boundary conditions $\{\dots, \dots, \dots, \dots\}$.



For example, identity (YB3.3) among these reads

$$\left[\underbrace{\times}_{u,v}^{g} \xrightarrow{g} \right]_{u,v} + \left[\underbrace{\times}_{g}^{g+1} \right]_{u,v} = \left[\underbrace{\times}_{g}^{g} \xrightarrow{g} \right]_{v,u} + \left[\underbrace{\times}_{g}^{g} \xrightarrow{g} \right]_{v,u}$$
(3.4)

Here, in the left-hand side, u is the spectral parameter of the bottom vertex, while in the right-hand side, the spectral parameter u is at the top vertex. The weights of the cross vertices on both sides are given by (3.3) and are not affected by the flipping of the spectral parameters. Writing out (3.4) as an identity between rational functions, we obtain

$$\frac{(1-t)v}{u-tv} \frac{(1-st^g u)(v-st^g)}{(1-su)(1-sv)} + \frac{u-v}{u-tv} \frac{(1-t^{g+1})(1-s^2t^g)v}{(1-su)(1-sv)}$$

$$= \frac{(1-st^g v)(u-st^g)}{(1-sv)(1-su)} \frac{(1-t)v}{u-tv} + \frac{(1-s^2t^{g-1})v(1-t^g)}{(1-sv)(1-su)} \frac{t(u-v)}{u-tv},$$

which can be readily checked by hand. All other explicit Yang–Baxter identities are listed in Appendix B.

3.3. Bijectivization of the Yang–Baxter equation. Our aim is now to bijectivize (in the sense of Section 2) each of the 16 types of identities (YB1.1)–(YB4.4) given in Appendix B. Here the sets A, B as in (2.1) are the sets of arrow configurations on three-vertex lattices with given boundary conditions. For example, both A and B in (3.4) consist of two elements each. The weights w(a), w(b) are products of the corresponding vertex weights. The forward transition weights corresponding to the Yang–Baxter equation with spectral parameters u, v will be denoted by $P_{u,v}^{\text{fwd}}$ and the backward ones by $P_{u,v}^{\text{bwd}}$. (That is, in the left-hand side of the Yang–Baxter equation, the parameter u is at the bottom vertex, v is at the top vertex, and the weights of the cross vertices on both sides are given by (3.3).)

Now, note that both sides of each of the Yang–Baxter identities (YB1.1)–(YB4.4) have at most two terms, and so the discussion from Section 2.3 applies. First, we see that Section 2.3.1 provides a unique bijectivization of 12 out of 16 types of the Yang–Baxter identities, except (YB2.2), (YB2.3), (YB3.2), and (YB3.3).

Second, among these four remaining identities, (YB2.3) and (YB3.2) are of the form (2.4); that is, we can identify equal terms on both sides. Thus, let us choose the corresponding natural deterministic bijectivizations of these identities as explained in the end of Section 2.3.2.

Finally, it remains to choose bijectivizations of identities (YB2.2) and (YB3.3) for which one cannot deterministically identify terms on both sides. Let us



consider (YB2.2), and identity (YB3.3) can be treated very similarly. Moreover, for any bijectivization of the former identity, there is a unique bijectivization of the latter satisfying the symmetries discussed in Section 3.4. Thus, having a bijectivization of (YB2.2), we will then simply write down the bijectivization of (YB3.3) obtained using these symmetries.

Identity (YB2.2) has the form $w(a_1) + w(a_2) = w(b_1) + w(b_2)$, where

$$a_1 = \underbrace{\times}_{g}^{g}, \quad a_2 = \underbrace{\times}_{g}^{g}, \quad b_1 = \underbrace{\times}_{g}^{g}, \quad b_2 = \underbrace{\times}_{g}^{g}, \quad b_3 = \underbrace{\times}_{g}^{g},$$

and the weights are given by (here, $g \ge 1$ because one of the arrow configurations contains g-1 vertical arrows)

$$w(a_1) = \frac{(1-t)u}{u-tv} \frac{(u-st^g)(1-st^gv)}{(1-su)(1-sv)},$$

$$w(a_2) = \frac{u-v}{u-tv} \frac{t(1-t^g)(1-s^2t^{g-1})u}{(1-su)(1-sv)},$$

$$w(b_1) = \frac{(1-t)u}{u-tv} \frac{(v-st^g)(1-st^gu)}{(1-sv)(1-su)},$$

$$w(b_2) = \frac{u-v}{u-tv} \frac{(1-t^{g+1})(1-s^2t^g)u}{(1-sv)(1-su)}.$$

All bijectivizations of (YB2.2) form a one-parameter family (2.3) employing the above weights. To select a particular solution out of this one-parameter family, let us argue as follows. Note that $w(a_2)$ vanishes when u=v, t=0, or $s^2=t^{1-g}$. When $w(a_2)=0$, identity (YB2.2) simplifies and, due to the discussion in Section 2.3.1, has a unique bijectivization. In particular, in this case, it should be $P_{u,v}^{\rm bwd}(b_1,a_2)=0$ (that is, no mass can be transferred into the term $w(a_2)=0$), which means that

$$\gamma(u, v, s, t, g) = \frac{w(b_1)}{w(a_1)}$$

$$= \frac{(v - st^g)(1 - st^g u)}{(u - st^g)(1 - st^g v)} \quad \text{when } u = v, t = 0, \text{ or } s^2 = t^{1-g}.$$

We will not address the question of whether the above conditions determine $\gamma(u, v, s, t, g)$ uniquely (in a suitable class of functions) but instead will take $\gamma(u, v, s, t, g)$ equal to the expression in the right-hand side *for all possible values* of u, v, s, t, g (more discussion about the choice of our particular bijectivization may be found in Section 3.6). This choice of γ leads via (2.3) to the following relatively simple forward and backward transition weights:



$$\begin{split} P_{u,v}^{\text{fwd}}(a_1,b_1) &= \frac{(v-st^g)(1-st^gu)}{(u-st^g)(1-st^gv)}, & P_{u,v}^{\text{fwd}}(a_1,b_2) &= \frac{(u-v)(1-s^2t^{2g})}{(u-st^g)(1-st^gv)}, \\ P_{u,v}^{\text{fwd}}(a_2,b_1) &= 0, & P_{u,v}^{\text{fwd}}(a_2,b_2) &= 1, \\ P_{u,v}^{\text{bwd}}(b_1,a_1) &= 1, & P_{u,v}^{\text{bwd}}(b_1,a_2) &= 0, \\ P_{u,v}^{\text{bwd}}(b_2,a_1) &= \frac{(1-t)(1-s^2t^{2g})}{(1-t^{g+1})(1-s^2t^g)}, & P_{u,v}^{\text{bwd}}(b_2,a_2) &= \frac{(t-t^{g+1})(1-s^2t^{g-1})}{(1-t^{g+1})(1-s^2t^g)}. \end{split}$$

This is the bijectivization of identity (YB2.2) that we will use in the present work.

A similar argument leads to the following forward and backward transition weights corresponding to the Yang–Baxter identity (YB3.3):

$$P_{u,v}^{\text{fwd}}\left(\underbrace{\begin{array}{c} g - 1 \\ g - 1 \end{array}}, \underbrace{\begin{array}{c} g - 1 \\ g - 1 \end{array}} \right) = 1 - P_{u,v}^{\text{fwd}}\left(\underbrace{\begin{array}{c} g - 1 \\ g - 1 \end{array}}, \underbrace{\begin{array}{c} g - 1 \\ g - 2 \end{array}} \right)$$

$$= \frac{(1 - t)(1 - s^2t^2g^{-2})}{(1 - t^g)(1 - s^2t^{g-1})};$$

$$P_{u,v}^{\text{fwd}}\left(\underbrace{\begin{array}{c} g \\ g - 2 \end{array}}, \underbrace{\begin{array}{c} g + 1 \\ g + 1 \end{array}} \right) = 1;$$

$$P_{u,v}^{\text{fwd}}\left(\underbrace{\begin{array}{c} g \\ g - 2 \end{array}}, \underbrace{\begin{array}{c} g + 1 \\ g + 1 \end{array}}, \underbrace{\begin{array}{c} g + 1 \\ g + 1 \end{array}} \right) = 1;$$

$$P_{u,v}^{\text{bwd}}\left(\underbrace{\begin{array}{c} g \\ g - 2 \end{array}}, \underbrace{\begin{array}{c} g \\ g + 1 \end{array}}, \underbrace{\begin{array}{c} g + 1 \\ g + 1 \end{array}} \right) = 1;$$

$$= \frac{(v - st^g)(1 - st^gu)}{(u - st^g)(1 - st^gu)}.$$

All the forward and backward transition weights obtained above are organized as tables in Figures 4 and 5, respectively.

3.4. Symmetries. The forward and backward transition weights just defined in Section 3.3 satisfy the following symmetries.

PROPOSITION 3.4. Fix any boundary conditions $k_1, k_2, k'_1, k'_2 \in \{0, 1\}$ and $i_1, i_2 \in \mathbb{Z}_{\geq 0}$. Then for any $g_1, g_2 \in \mathbb{Z}_{\geq 0}$, we have the following identity between forward and backward transition weights:

$$P_{u,v}^{\text{fwd}} \begin{pmatrix} k_2 & \frac{i_2}{k_1} & k'_2 & k_2 & \frac{i_2}{k_2} \\ k_1 & \frac{g_1}{k_1} & k'_1 & k_1 & \frac{g_2}{k_1} \end{pmatrix}$$



$P_{u,v}^{\mathrm{fwd}}$	$ \times $	$\mid \times$	X	X	$\mid \times \mid$	X
X	1	$\frac{(1-t)v}{u-tv} \frac{1-st^g u}{1-st^g v}$	$\frac{u-v}{u-tv} \frac{1-st^{g+1}v}{1-st^gv}$	$\frac{(1-t)u}{u-tv} \frac{1-st^g v}{1-st^g u}$	$\frac{t(u-v)}{u-tv} \frac{1-st^{g-1}u}{1-st^gu}$	1
X	1	$\frac{v - st^g}{u - st^g} \frac{1 - st^g u}{1 - st^g v}$	$\frac{u-v}{u-st^g} \frac{1-s^2t^{2g}}{1-st^gv}$	1	0	1
X	1	0	1	$\frac{1-t}{1-t^g} \frac{1-s^2 t^{2g-2}}{1-s^2 t^{g-1}}$	$\frac{t - t^g}{1 - t^g} \frac{1 - s^2 t^{g-2}}{1 - s^2 t^{g-1}}$	1
X	1	1	0	1	0	1
X	1	0	1	0	1	1
×	1	$\frac{(1-t)u}{u-tv} \frac{v-st^g}{u-st^g}$	$\frac{u-v}{u-tv}\frac{u-st^{g+1}}{u-st^g}$	$\frac{(1-t)v}{u-tv} \frac{u-st^g}{v-st^g}$	$\frac{t(u-v)}{u-tv} \frac{v-st^{g-1}}{v-st^g}$	1

Figure 4. Forward transition weights corresponding to the Yang–Baxter equation. The rows of the table are parameterized by the first argument of the function $P_{u,v}^{\text{fwd}}$, and the columns are parameterized by the second argument. Here, g is the number of vertical arrows in the middle before the move of the cross vertex. The coloring reflects the change of the number of vertical arrows in the middle after the move: pink and red correspond to transitions $g \to g + 1$ and $g \to g + 2$, while lighter and darker gray mean $g \to g - 1$ and $g \to g - 2$, respectively.

$P_{u,v}^{\mathrm{bwd}}$	$ \times $	X	$\mid \times \mid$	X	$\mid \times \mid$	X
$\overline{\times}$	1	$\frac{(1-t)u}{u-tv} \frac{1-st^g v}{1-st^g u}$	$\frac{u-v}{u-tv} \frac{1-st^{g+1}v}{1-st^gv}$	$\frac{(1-t)v}{u-tv} \frac{1-st^g u}{1-st^g v}$	$\frac{t(u-v)}{u-tv} \frac{1-st^{g-1}u}{1-st^gu}$	1
X	1	1	0	1	0	1
X	1	$\frac{1-t}{1-t^g} \frac{1-s^2 t^{2g-2}}{1-s^2 t^{g-1}}$	1	0	$\frac{t - t^g}{1 - t^g} \frac{1 - s^2 t^{g-2}}{1 - s^2 t^{g-1}}$	1
X	1	1	$\frac{u-v}{u-st^g} \frac{1-s^2t^{2g}}{1-st^gv}$	$\frac{v - st^g}{u - st^g} \frac{1 - st^g u}{1 - st^g v}$	0	1
X	1	0	1	0	1	1
X	1	$\frac{(1-t)v}{u-tv}\frac{u-st^g}{v-st^g}$	$\frac{u-v}{u-tv}\frac{u-st^{g+1}}{u-st^g}$	$\frac{(1-t)u}{u-tv}\frac{v-st^g}{u-st^g}$	$\frac{t(u-v)}{u-tv} \frac{v-st^{g-1}}{v-st^g}$	1

Figure 5. Backward transition weights corresponding to the Yang–Baxter equation. This table uses the same conventions as in Figure 4.

$$= P_{u,v}^{\text{bwd}} \left(\begin{matrix} k'_1 & -i_1 & & \\ k'_1 & -g_1 & & \\ k'_2 & -i_2 & & \\ \end{matrix} \right) \left(\begin{matrix} k_1 & k_1 & k_2 & k_1 \\ k'_2 & -g_1 & k_2 \\ \end{matrix} \right),$$

with the agreement that weights on both sides are well-defined (that is, g_1 and/or g_2 is $\geqslant 1$ if needed). In both weights, the numbers of arrows at the boundary are



given, and the number of vertical arrows in the middle $(g_1 \text{ or } g_2)$ determines the numbers of arrows along the dashed edges connecting the cross vertices with the two-vertex configurations.

Proof. Straightforward verification.

PROPOSITION 3.5. For any $k_1, k_2, k_1', k_2' \in \{0, 1\}$ and $i_1, i_2, g_1, g_2 \in \mathbb{Z}_{\geq 0}$, we have the following symmetry of the forward transition weights with respect to the change $(u, v) \to (v^{-1}, u^{-1})$ in the spectral parameters:

$$P_{u,v}^{\text{fwd}} \begin{pmatrix} k_2 \\ k_1 \end{pmatrix} \underbrace{k_2 - k_2'}_{i_1} k_1', \quad k_2 \underbrace{k_2 - k_2'}_{i_1} k_2' \\ = P_{v^{-1},u^{-1}}^{\text{fwd}} \begin{pmatrix} 1 - k_1 \\ 1 - k_2 \end{pmatrix} \underbrace{k_2 - k_2'}_{i_1} k_2', \quad 1 - k_1 \underbrace{k_2'}_{i_2} k_1' \\ = \frac{i_1}{1 - k_2} \underbrace{k_2'}_{i_2} k_2', \quad 1 - k_2 \underbrace{k_2'}_{i_2} k_2' \\ = \frac{i_1}{1 - k_2'} \underbrace{k_2'}_{i_2} k_2', \quad 1 - k_2 \underbrace{k_2'}_{i_2} k_2' \\ = \frac{i_1}{1 - k_2'} \underbrace{k_2'}_{i_2} k_2', \quad 1 - k_2 \underbrace{k_2'}_{i_2} k_2' \\ = \frac{i_1}{1 - k_2'} \underbrace{k_2'}_{i_2} k_2', \quad 1 - k_2 \underbrace{k_2'}_{i_2} k_2' \\ = \frac{i_1}{1 - k_2'} \underbrace{k_2'}_{i_2} k_2', \quad 1 - k_2 \underbrace{k_2'}_{i_2} k_2' \\ = \frac{i_1}{1 - k_2'} \underbrace{k_2'}_{i_2} k_2', \quad 1 - k_2 \underbrace{k_2'}_{i_2} k_2' \\ = \frac{i_1}{1 - k_2'} \underbrace{k_2'}_{i_2} k_2' \\ = \frac{i_2}{1 - k_2'} \underbrace{k_2'}_{i_2} k_2' \\ = \frac{i_1}{1 - k_2'} \underbrace{k_2'}_$$

An analogous identity holds for the backward transition weights.

Proof. This can also be checked in a straightforward way, but the verification can be made shorter with the help of the previous Proposition 3.4.

3.5. Nonnegativity and probabilistic interpretation. Let us now address the question of nonnegativity of the forward and backward transition weights obtained in Section 3.3.

PROPOSITION 3.6. Assume that our parameters satisfy

$$0 \le t < 1, \quad -1 < s \le 0, \quad 0 \le v \le u.$$
 (3.5)

Then all the forward and backward transition weights $P_{u,v}^{\text{fwd}}$, $P_{u,v}^{\text{bwd}}$ are nonnegative.

Proof. Observe that the nonnegativity of the forward and backward transition weights would hold if all the following quantities

$$\frac{u-v}{u-tv}, \frac{(1-st^gu)(v-st^g)}{(1-st^gv)(u-st^g)}, \frac{(1-t)(1-s^2t^{2g})}{(1-t^{g+1})(1-s^2t^g)}, \frac{1-st^{g+1}v}{1-st^gv}, \frac{t-st^{g+1}u}{1-st^{g+1}u}, \frac{tv-st^{g+1}}{v-st^{g+1}}, \frac{u-st^{g+1}}{u-st^g}$$

(with arbitrary $g \in \mathbb{Z}_{\geqslant 0}$) are between 0 and 1. The latter directly follows from (3.5).



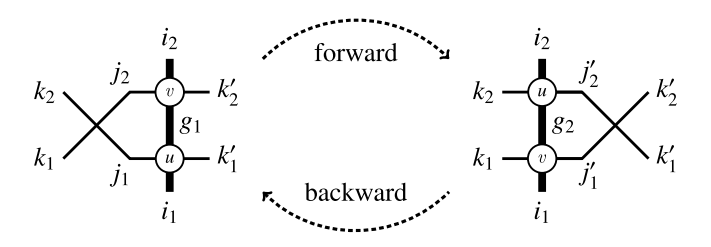


Figure 6. Randomized Yang–Baxter moves turning fixed g_1 to random g_2 or vice versa. Note that the numbers of arrows j_1 , j_2 or j'_1 , j'_2 in the middle are uniquely determined by k_1 , k_2 , k'_1 , k'_2 , i_1 , i_2 and g_1 or g_2 , respectively, and thus do not need to be specified explicitly.

Proposition 3.6 implies that under conditions (3.5), the forward and backward weights from Section 3.3 define *Markov* transition steps. We call them the (*local*, *randomized*) *Yang–Baxter moves*.

DEFINITION 3.7. The *forward Yang–Baxter move* transforms a fixed three-vertex configuration with the cross vertex on the left, given boundary conditions k_1, k_1' , $k_2, k_2' \in \{0, 1\}$, $i_1, i_2 \in \mathbb{Z}_{\geqslant 0}$, and fixed number $g_1 \in \mathbb{Z}_{\geqslant 0}$ of vertical arrows in the middle, into a three-vertex configuration with the cross vertex on the right, having the same boundary conditions and a *random* number g_2 of vertical arrows in the middle. Depending on the boundary conditions, g_2 can take at most two possible values which are two consecutive numbers chosen from $\{g_1 - 2, g_1 - 1, g_1, g_1 + 1, g_1 + 2\}$.

Similarly, the *backward Yang–Baxter move* transforms a fixed three-vertex configuration with the cross vertex on the right, given boundary conditions, and fixed g_2 , into a three-vertex configuration with the cross vertex on the left, same boundary conditions, and *random* g_1 .

The probabilities of forward and backward Yang–Baxter moves are given in Figures 4 and 5. See Figure 6 for an illustration.

3.6. On the choice of bijectivization. In Section 3.3, we presented a particular choice of bijectivization of the Yang–Baxter equation, and the rest of the paper will be devoted to the study of the objects associated with the choice. However, there are other reasonable choices, for which a very similar discussion would be possible. To simplify the exposition, we will not focus on them and just briefly mention possible variations in this section.



The Yang-Baxter equation consists of 16 identities between rational functions listed in Appendix B. Twelve of them contain only one term on at least one side of an equation and thus have a unique bijectivization. Identities (YB2.2), (YB2.3), (YB3.2), and (YB3.3) contain two terms on each side, and so according to Section 2.3.2, each of these identities admits a one-parameter family of bijectivizations. It is easy to check that the choice of bijectivizations of these identities presented in Section 3.3 is uniquely determined by the following properties:

- (1) (Nonnegativity) Transition probabilities are nonnegative.
- (2) (*Minimal 'noise' property*) As many transition probabilities as possible are equal to 0.

Indeed, in (YB2.3) and (YB3.2), two of the forward probabilities can be made zero, and in (YB2.2) and (YB3.3), one forward probability can be made zero. Which of these probabilities are zero is uniquely determined by the nonnegativeness.

Let us discuss the above conditions. The first one is a must have since we want to obtain a stochastic object. Thus, it forces our four parameters to lie within certain segments of the real line. However, the second condition has a combinatorial flavor which is not crucial for obtaining reasonable probabilistic models. For example, one can introduce another bijectivization by replacing it with a condition

(2') (*Independence from input*) Forward transition probabilities do not depend on the state of the cross vertex before the move.

Condition (2') uses the idea of [DF90] (applied in a symmetric function setting in [BF14]). Also, as far as we know, the dynamics coming from condition (2') was used by [GM14] in the context of percolation and in [Spo15] for simulations of stochastic vertex model essentially in our setting. However, this idea was not applied to bijectivize the Cauchy identity (which requires both forward and backward probabilities) or to construct a random field of signatures (Section 6).

We focus on condition (2) rather than (2') (or any other choice of four parameters satisfying condition (1)) because due to less interaction, it leads to slightly simpler models. However, since 12 out of 16 identities coming from the Yang–Baxter equation work in the same way for any bijectivization, all these models are fairly similar. In particular, the dynamic version of the six-vertex model (Section 7) and all its degenerations (Appendix A) will appear for all bijectivizations.

Finally, let us note that yet another motivation for a certain specific choice of bijectivization might come from the algebraic side related to the matrix



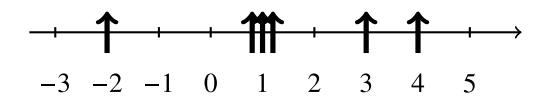


Figure 7. Representing a signature $\mu = (4, 3, 1, 1, 1, -2) \in \text{Sign}_6$ as a configuration of six vertical arrows on \mathbb{Z} .

interpretation of the Yang–Baxter equation. We were not able to find a natural condition along these lines.

4. Spin Hall–Littlewood symmetric functions

In this section, we recall the symmetric rational functions defined in [Bor17a] and their basic properties including the Cauchy summation identities. In this section, we do not assume that the transition weights are nonnegative.

4.1. Signatures. We need to introduce some notation. For each $N \in \mathbb{Z}_{\geq 1}$, let

$$\mathsf{Sign}_N := \{\lambda \in \mathbb{Z}^N : \lambda_1 \geqslant \cdots \geqslant \lambda_N\}$$

denote the set of *signatures* with N components. (Signatures are also sometimes called *highest weights* as the set Sign_N indexes irreducible representations of the unitary group U(N); for example, see [Wey97].) For $\lambda \in \mathsf{Sign}_N$, denote $\ell(\lambda) := N$ and call this the *length* of λ . By agreement, Sign_0 consists of the single empty signature \varnothing . We will also use the notation $|\lambda| := \lambda_1 + \cdots + \lambda_N$.

A signature $\lambda \in \operatorname{Sign}_N$ is called *nonnegative* if $\lambda_N \geqslant 0$. The set of nonnegative signatures is denoted by $\operatorname{Sign}_N^+ \subset \operatorname{Sign}_N$. Let us set $\operatorname{Sign} := \bigcup_{N=0}^{\infty} \operatorname{Sign}_N$ and $\operatorname{Sign}^+ := \bigcup_{N=0}^{\infty} \operatorname{Sign}_N^+$.

Nonnegative signatures are often referred to as (integer) *partitions*, which are represented pictorially as *Young diagrams*; for example, see [Mac95, Ch. I.1]. While this way of representing signatures is extremely useful in many contexts, we will employ another graphical representation of signatures which works equally well for signatures having negative parts.

Namely, associate to each $\mu \in \operatorname{Sign}_N$ a configuration of N vertical arrows on \mathbb{Z} , with multiple arrows per site allowed, by putting an arrow at each of the locations $\mu_1, \ldots, \mu_N \in \mathbb{Z}$. In other words, write μ in multiplicative notation as $\mu = \cdots (-1)^{m_{-1}} 0^{m_0} 1^{m_1} 2^{m_2} \ldots$, where $m_i := \#\{j : \mu_j = i\}, i \in \mathbb{Z}$. Then put m_i vertical arrows at each site $i \in \mathbb{Z}$. Note that all but finitely many sites $i \in \mathbb{Z}$ will be empty. See Figure 7, left, for an illustration.



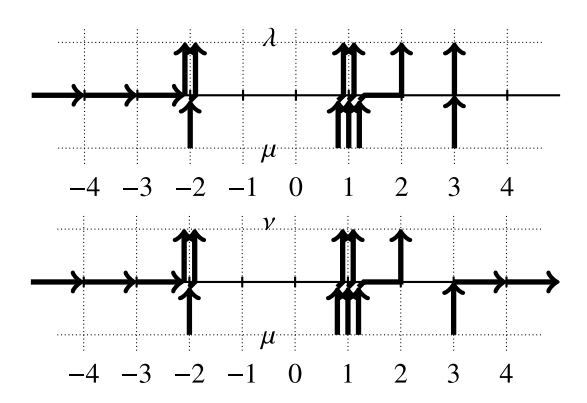


Figure 8. Left: a configuration of horizontal arrows connecting $\mu = (3, 1, 1, 1, -2)$ to $\lambda = (3, 2, 1, 1, -2, -2)$, with $\mu \prec \lambda$. Right: a configuration of horizontal arrows connecting the same μ to $\nu = (2, 1, 1, -2, -2)$, with $\nu \stackrel{\circ}{\prec} \mu$.

4.2. Definition of spin Hall–Littlewood functions. Let us now recall the definitions of the symmetric rational functions $F_{\lambda/\mu}$ and $G^c_{\lambda/\mu}$ introduced in [Bor17a]. Similar objects were also considered earlier as Bethe ansatz eigenfunctions; for example, see [KBI93, Ch. VII], and also [Pov13, BCPS15a] for more stochastic particle system connections.

We begin by defining versions of the spin Hall–Littlewood functions depending on one variable, the spectral parameter $u \in \mathbb{C}$.

4.2.1. Functions $F_{\lambda/\mu}(u)$. Let a signature $\mu \in \text{Sign}_{N-1}$ interlace with a signature $\lambda \in \text{Sign}_N$ (notation: $\mu \prec \lambda$), which, by definition, means that

$$\lambda_N \leqslant \mu_{N-1} \leqslant \lambda_{N-1} \leqslant \dots \leqslant \lambda_2 \leqslant \mu_1 \leqslant \lambda_1. \tag{4.1}$$

There exists a unique configuration of arrows on the grid $\mathbb{Z} \times \{-1, 0, 1\}$ connecting μ to λ (see Figure 8, left):

- vertical arrows $(\mu_i, -1) \rightarrow (\mu_i, 0)$ entering from the bottom;
- vertical arrows $(\lambda_i, 0) \rightarrow (\lambda_i, 1)$ exiting at the top;
- horizontal arrows along $\mathbb{Z} \times \{0\}$ such that the local configuration of arrows around each vertex of $\mathbb{Z} \times \{0\}$ looks like one of the vertices in Figure 3, and configurations of arrows at neighboring vertices are compatible. There the configuration of horizontal arrows is packed at $-\infty$ and is empty at $+\infty$.



For each $m \in \mathbb{Z}$, denote the numbers of incoming and outgoing vertical and horizontal arrows at vertex $m \times \{0\}$ by $i_1(m), i_2(m) \in \mathbb{Z}_{\geq 0}$ and $j_1(m), j_2(m) \in \{0, 1\}$, respectively (this notation follows the beginning of Section 3.1).

Using this configuration of horizontal arrows connecting μ to λ , define

$$F_{\lambda/\mu}(u) := \prod_{m=-\infty}^{-1} \frac{\left[j_1(m) \frac{i_2(m)}{i_1(m)} j_2(m) \right]_u}{\left[\underbrace{-} \right]_u} \prod_{m=0}^{\infty} \left[j_1(m) \frac{i_2(m)}{i_1(m)} j_2(m) \right]_u, \quad (4.2)$$

where we use notation (3.2) for the vertex weights depending on the spectral parameter u. Observe that both products above are finite since $i_1(-m) = i_2(-m) = i_1(m) = i_2(m) = 0$, $j_1(-m) = j_2(-m) = 1$, $j_1(m) = j_2(m) = 0$ for all sufficiently large m. If $\mu \not\prec \lambda$, set $F_{\lambda/\mu}(u) \equiv 0$.

When $\mu, \lambda \in \text{Sign}^+$, $F_{\lambda/\mu}$ defined by (4.2) coincides with the one given in [Bor17a]. Moreover, (4.2) extends the definition so that $F_{\lambda/\mu}$ for arbitrary signatures $\mu \prec \lambda$ satisfies the following translation property:

$$F_{\lambda+(r^N)/\mu+(r^{N-1})}(u) = \left(\frac{u-s}{1-su}\right)^r F_{\lambda/\mu}(u), \quad \mu \in \mathsf{Sign}_{N-1}, \quad \lambda \in \mathsf{Sign}_N, \tag{4.3}$$

where in the left-hand side we add arbitrary $r \in \mathbb{Z}$ to all parts of both μ and λ .

4.2.2. Functions $G_{\mu/\nu}^c(u)$. Let $\mu, \nu \in \text{Sign}_N$. If these signatures satisfy

$$\nu_N \leqslant \mu_N \leqslant \nu_{N-1} \dots \mu_2 \leqslant \nu_1 \leqslant \mu_1, \tag{4.4}$$

then we also say that ν and μ interlace, but we use a slightly different notation $\nu \stackrel{\circ}{\prec} \mu$ for this.

Let us connect μ to ν by a configuration of horizontal arrows in the same sense as in Section 4.2.1. Note that now the 'larger' signature μ is placed at the *bottom*. This implies that the configuration of horizontal arrows connecting μ to ν contains infinitely many horizontal arrows, both at $-\infty$ and at $+\infty$ (see Figure 8, right).

Using this configuration of arrows connecting μ to ν , define

$$G_{\mu/\nu}^{c}(u) := \prod_{m=-\infty}^{+\infty} \frac{\left[j_{1}(m) \frac{i_{2}(m)}{i_{1}(m)} j_{2}(m) \right]_{u^{-1}}}{\left[\xrightarrow{\vdots} \right]_{u^{-1}}}, \tag{4.5}$$

where we used the same notation $i_{1,2}(m)$, $j_{1,2}(m)$ for the numbers of arrows at individual vertices of $\mathbb{Z} \times \{0\}$ as in Section 4.2.1. Again, observe that the product in (4.5) is actually finite. If $v \not\prec \mu$, set $G^c_{\mu/\nu}(u) \equiv 0$.



REMARK 4.1. Let us connect (4.5) to the definition of $G_{\mu/\nu}^c$ given in [Bor17a]. Denote

$$\left[j_1 \, \frac{i_2}{i_1} \, j_2 \, \right]_u^{\bullet} := \frac{\left[j_1 \, \frac{i_2}{i_1} \, j_2 \, \right]_{u^{-1}}}{\left[\xrightarrow{} \right]_{u^{-1}}},$$

then from (3.2), we have

$$\begin{bmatrix} \cdots g \\ g \end{bmatrix}_{u}^{\bullet} = \frac{u - st^{g}}{1 - su}, \quad \begin{bmatrix} g - 1 \\ g \end{bmatrix}_{u}^{\bullet} = \frac{1 - s^{2}t^{g-1}}{1 - su},$$
$$\begin{bmatrix} g + 1 \\ g \end{bmatrix}_{u}^{\bullet} = \frac{1 - s^{2}t^{g-1}}{1 - su}, \quad \begin{bmatrix} g + 1 \\ g \end{bmatrix}_{u}^{\bullet} = \frac{(1 - t^{g+1})u}{1 - su}.$$

Observe that in the above graphical definition of $G_{\mu/\nu}^c$ the 'larger' signature μ is placed at the bottom. Replacing the right-pointing horizontal arrows by empty edges and, vice versa, replacing empty edges by *left-pointing* horizontal arrows lead to the conjugated vertex weights w_{μ}^c defined in [Bor17a]:

$$\begin{bmatrix} \leftarrow \overset{g}{g} \leftarrow \end{bmatrix}_{u}^{c} = \frac{u - st^{g}}{1 - su}, \quad \begin{bmatrix} \overset{g}{g} - \ddots & \\ & & \end{bmatrix}_{u}^{c} = \frac{1 - s^{2}t^{g}}{1 - su}, \\ \begin{bmatrix} \dots & & \\ & & \end{bmatrix}_{u}^{c} = \frac{1 - st^{g}u}{1 - su}, \quad \begin{bmatrix} \dots & & \\ & & & \end{bmatrix}_{u}^{c} = \frac{(1 - t^{g})u}{1 - su}.$$

Then $G_{\mu/\nu}^c(u)$ is equal to the product of the conjugated weights $[\cdots]_u^c$ similar to (4.5) but without the denominators (also with ν at the top and μ at the bottom). Note that [Bor17a] also defines functions $G_{\mu/\nu}(u)$ without the conjugation, but we do not use them in the present paper.

4.2.3. Multivariable functions F and G^c . Using the single-variable functions (4.2) and (4.5), one can define the corresponding multivariable functions F and G^c .

Let
$$K \in \mathbb{Z}_{\geqslant 1}$$
, $\lambda, \mu \in \text{Sign such that } \ell(\lambda) = \ell(\mu) + K$, $\ell(\mu) = N \in \mathbb{Z}_{\geqslant 0}$. Set

$$F_{\lambda/\mu}(u_1,\ldots,u_K) := \sum_{\{\kappa^{(j)}\}} F_{\lambda/\kappa}(\kappa^{-1})(u_1) F_{\kappa}(\kappa^{-1})/\kappa}(u_2) \ldots F_{\kappa}(\mu_2) \ldots F_{\kappa}(\mu_K), \quad (4.6)$$

where the sum runs over all (K-1)-tuples of signatures $\kappa^{(j)} \in \operatorname{Sign}_{N+j}$, $j=1,\ldots,K-1$ such that $\mu \prec \kappa^{(1)} \prec \cdots \prec \kappa^{(K-1)} \prec \lambda$. Equivalently, $F_{\lambda/\mu}(u_1,\ldots,u_K)$ can be thought of as the partition function of a path configuration similar to the one in Figure 8, left, but consisting of K horizontal layers. The signatures μ and λ encode, respectively, the bottom and the top boundary conditions, and there are additional K paths entering on the left.



The multivariable version of G^c is defined in a similar way. Fix $K \in \mathbb{Z}_{\geq 1}$, $N \in \mathbb{Z}_{\geq 0}$, and let $\mu, \nu \in \mathsf{Sign}_N$. Set

$$G_{\mu/\nu}^{c}(u_{1},\ldots,u_{K}):=\sum_{\{\kappa^{(i)}\}}G_{\mu/\kappa^{(K-1)}}^{c}(u_{1})G_{\kappa^{(K-1)}/\kappa^{(K-2)}}^{c}(u_{2})\ldots G_{\kappa^{(1)}/\nu}^{c}(u_{K}), \quad (4.7)$$

where the sum is taken over all (K-1)-tuples of signatures $\kappa^{(j)} \in \operatorname{Sign}_N$, $j=1,\ldots,K-1$, satisfying $\nu \stackrel{\circ}{\sim} \kappa^{(1)} \stackrel{\circ}{\sim} \cdots \stackrel{\circ}{\sim} \kappa^{(K-1)} \stackrel{\circ}{\sim} \mu$. Equivalently, $G^c_{\mu/\nu}(u_1,\ldots,u_K)$ is the partition function of path configurations similar to the one in Figure 8, right, but consisting of K horizontal layers. The signatures μ and ν encode, respectively, the bottom and the top boundary conditions.

The Yang–Baxter equation for the vertex weights used to define the functions $F_{\lambda/\mu}(u_1,\ldots,u_K)$ and $G^c_{\mu/\nu}(u_1,\ldots,u_K)$ readily implies that these functions are symmetric with respect to permutations of the u_j 's. See [Bor17a, Theorem 3.5] for details.

In special cases when the lower diagram is simple, the skew functions F and G^c admit explicit formulas expressing them as sums over permutations. Let us recall such a formula for $F_{\lambda/\varnothing}$. A formula for $G^c_{\mu/(0,\dots,0)}$ (where the number of zeros is the same as the number of components in μ) is of similar nature but is more complicated, so we omit it here and refer to [Bor17a, Theorem 5.1], [BP18a, Theorem 4.14] for details on the statements and their proofs. For the function $F_{\lambda/\varnothing}$ with $\lambda \in \text{Sign}^+_N$, we have

$$F_{\lambda/\varnothing}(u_1, \dots, u_N) = \frac{(1-t)^N}{\prod_{i=1}^N (1-su_i)} \sum_{\sigma \in S(N)} \prod_{1 \le i < j \le N} \frac{u_{\sigma(i)} - tu_{\sigma(j)}}{u_{\sigma(i)} - u_{\sigma(j)}} \prod_{i=1}^N \left(\frac{u_{\sigma(i)} - s}{1 - su_{\sigma(i)}}\right)^{\lambda_i}.$$
(4.8)

4.3. Cauchy summation identities. One of the central properties of the functions F and G^c described in Section 4.2 is that they satisfy summation identities of Cauchy type [Bor17a]. The most basic of these identities is the one for the single-variable functions.

THEOREM 4.2 (Single-variable skew Cauchy identity [Bor17a, Theorem 4.2]). Let $s, u, v \in \mathbb{C}$ satisfy

$$\left| \frac{(u-s)(1-sv)}{(v-s)(1-su)} \right| < 1. \tag{4.9}$$



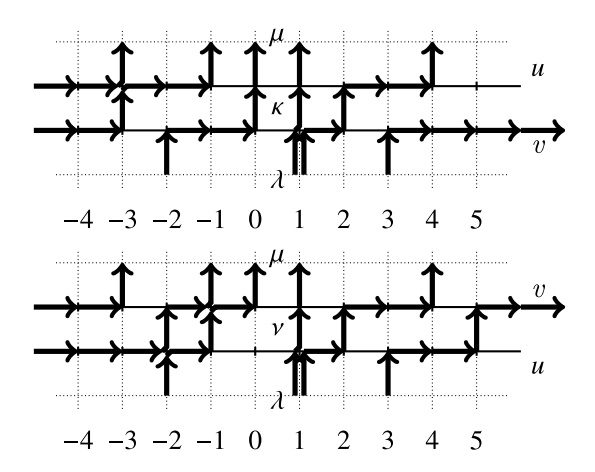


Figure 9. Illustration of the sums in the skew Cauchy identity (4.10) with $\lambda = (3, 1, 1, -2)$, $\mu = (4, 1, 0, -1, -3)$, and N = 4. Left: the (finite) sum runs over $\kappa \in \text{Sign}_N$ with $\lambda \stackrel{\circ}{\succ} \kappa \prec \mu$. Right: the (infinite) sum runs over $\nu \in \text{Sign}_{N+1}$ with $\lambda \prec \nu \stackrel{\circ}{\succ} \mu$. Spectral parameters corresponding to the two horizontal layers are also indicated.

Then for any $N \in \mathbb{Z}_{\geq 0}$, $\lambda \in \text{Sign}_N$, $\mu \in \text{Sign}_{N+1}$, we have (see Figure 9 for a graphical illustration of both sides of the sum)

$$\sum_{\kappa \in \text{Sign}_{N}} G_{\lambda/\kappa}^{c}(v^{-1}) F_{\mu/\kappa}(u) = \frac{v - u}{v - tu} \sum_{\nu \in \text{Sign}_{N+1}} F_{\nu/\lambda}(u) G_{\nu/\mu}^{c}(v^{-1}). \tag{4.10}$$

REMARK 4.3. In Theorem 4.2, the sum over κ in the left-hand side is finite, while the sum over ν in the right-hand side is infinite. Condition (4.9) is needed to ensure the convergence of this infinite sum.

In Section 5.2, we will present a new bijective proof of the skew Cauchy identity of Theorem 4.2 employing the forward and backward transition weights developed in Section 3. This bijective proof motivates a new version of the skew Cauchy identity which we present in Appendix C.

COROLLARY 4.4 (Multivariable skew Cauchy identity). Let $u_1, \ldots, u_K, v_1, \ldots, v_L \in \mathbb{C}$ be such that each pair (u_i, v_i) satisfies (4.9). For any $N \in \mathbb{Z}_{\geq 0}$, $\lambda \in \text{Sign}_N$,



and $\mu \in \mathsf{Sign}_{N+K}$, we have

$$\begin{split} & \sum_{\kappa \in \mathrm{Sign}_{N}} G_{\lambda/\kappa}^{c}(v_{1}^{-1}, \dots, v_{L}^{-1}) F_{\mu/\kappa}(u_{1}, \dots, u_{K}) \\ & = \prod_{i=1}^{K} \prod_{j=1}^{L} \frac{v_{j} - u_{i}}{v_{j} - tu_{i}} \sum_{v \in \mathrm{Sign}_{N+K}} F_{v/\lambda}(u_{1}, \dots, u_{K}) G_{v/\mu}^{c}(v_{1}^{-1}, \dots, v_{L}^{-1}). \end{split} \tag{4.11}$$

Proof. Use branching rules (4.6) and (4.7) to break each of the multivariable functions into a sum of products of single-variable ones. Then apply the single-variable skew Cauchy identity of Theorem 4.2 for each pair of the variables v_i^{-1} and u_i , LK times in total.

Next, setting $\lambda = \emptyset$ and $\mu = (0^K)$ in Corollary 4.4, we get the following.

COROLLARY 4.5 (Ordinary Cauchy identity). Let $u_1, \ldots, u_K, v_1, \ldots, v_L \in \mathbb{C}$ be such that each pair (u_i, v_i) satisfies (4.9). Then we have

$$\prod_{i=1}^{K} \frac{1-t^{i}}{1-su_{i}} = \prod_{i=1}^{K} \prod_{j=1}^{L} \frac{v_{j}-u_{i}}{v_{j}-tu_{i}} \sum_{v \in \text{Sign}_{K}^{+}} F_{v/\varnothing}(u_{1},\ldots,u_{K}) G_{v/(0^{K})}^{c}(v_{1}^{-1},\ldots,v_{L}^{-1}).$$

$$(4.12)$$

Note that, here, the sum runs over nonnegative signatures because all parts of $\mu = (0^K)$ are nonnegative.

5. Transition probabilities U^{fwd} and U^{bwd} on signatures

In this section, employing the vertex-level forward and backward transition probabilities from Section 3, we define the transition probabilities on signatures $U^{\text{fwd}}_{v,u}(\kappa \to \nu \mid \lambda, \mu)$ and $U^{\text{bwd}}_{v,u}(\nu \to \kappa \mid \lambda, \mu)$. The latter probabilities are, in particular, used to give a new bijective proof of the skew Cauchy identity (Theorem 4.2).

5.1. Definition of transition probabilities on signatures. Throughout this section, we assume that our parameters satisfy

$$0 \le t < 1, \quad -1 < s \le 0, \quad 0 \le u < v < 1$$
 (5.1)

so that the probabilities $P_{v,u}^{\text{fwd}}$ and $P_{v,u}^{\text{bwd}}$ of the local Yang–Baxter moves are nonnegative (thanks to Proposition 3.6). In particular, this implies the convergence



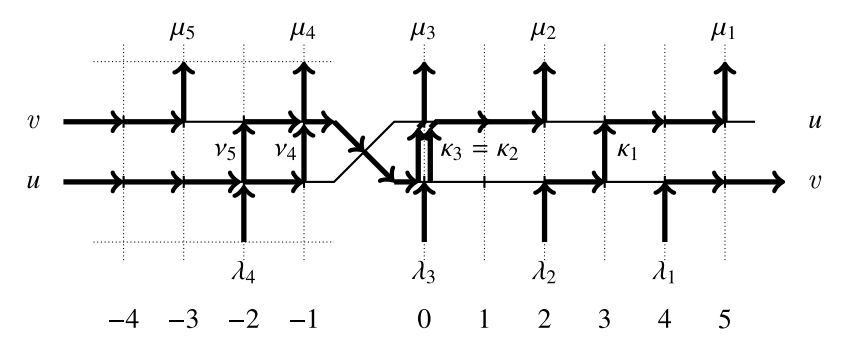


Figure 10. Performing randomized Yang–Baxter moves to sample ν given κ under $U_{\nu,u}^{\text{fwd}}$ (dragging the cross to the right) or κ given ν under $U_{\nu,u}^{\text{bwd}}$ (the cross is dragged the left).

condition (4.9) in Cauchy identities. Note that we need a strict inequality in (4.9), and for that, we require u < v.

The condition v < 1 (hence u < 1) included in (5.1) ensures that the vertex weights (3.2) with spectral parameters u and v are nonnegative. This property will be essential in Section 6.

REMARK 5.1. In this and the following sections (in comparison with Section 3), we swap the parameters $(u, v) \leftrightarrow (v, u)$ in probabilities of the local Yang–Baxter moves. The swapped parameters (corresponding to $P_{v,u}^{\text{fwd}}$ and $P_{v,u}^{\text{bwd}}$) match the skew Cauchy identities of Section 4.3 (see Figure 9).

Fix $N \in \mathbb{Z}_{\geqslant 0}$, and let $\kappa, \lambda \in \mathsf{Sign}_N$ and $\mu \in \mathsf{Sign}_{N+1}$ such that $\lambda \stackrel{\circ}{\succ} \kappa \prec \mu$ be fixed. For each $\nu \in \mathsf{Sign}_{N+1}$, we define the forward transition probability $\mathsf{U}^{\mathsf{fwd}}_{\nu,\mu}(\kappa \to \nu \mid \lambda, \mu)$ by constructing a random signature ν as follows.

Consider the two-layer arrow configuration as in Figure 9, left, with signatures λ, κ, μ appearing from bottom to top. Observe that this configuration has boundary conditions \rightrightarrows on the far left and \rightrightarrows on the far right and, moreover, cannot contain vertical arrows to the left of μ_{N+1} and to the right of λ_1 . Add the cross vertex \bigstar to the left of an arbitrary location $M \leqslant \mu_{N+1}$. Then for each $r = M, M+1, \ldots$ perform the forward randomized Yang–Baxter move which drags the cross to the right through the column number r. Let these forward Yang–Baxter moves have probabilities $P_{v,u}^{\text{fwd}}$ given in Figure 4. This sequence of forward Yang–Baxter moves will not affect the signatures λ, μ and will randomly change κ ; see Figure 10.



LEMMA 5.2. As $r \to +\infty$, the state of the cross vertex stabilizes at χ .

Proof. Once the cross vertex passes to the right of λ_1 , it can only be in one of the two states, X or X, since the boundary conditions far to the right are $\stackrel{\dots}{\longrightarrow}$. From the table in Figure 4, we see that $P_{v,u}^{\text{fwd}}(X,X) = 1$. Moreover, since there are no vertical arrows to the right of λ_1 , we have

$$P_{v,u}^{\text{fwd}}(X,X) = 1 - \frac{(u-s)(1-sv)}{(v-s)(1-su)},$$

which is strictly positive by (4.9). Therefore, the state \times of the cross vertex eventually turns into \times with probability 1 (which, in fact, corresponds to choosing ν_1 somewhere to the right of λ_1), and the latter state is preserved forever.

We see that the process of (randomized) dragging of the cross vertex to the right essentially terminates. Cutting cross vertex \searrow which has stabilized far on the right, we obtain the final two-layer arrow configuration which looks as in Figure 9, right. That is, the boundary conditions are now \rightrightarrows on the far left and \varinjlim on the far right, while the fixed signature $\kappa \in \text{Sign}_N$ in the middle has been replaced by a *random* signature $\nu \in \text{Sign}_{N+1}$. Moreover, this new signature satisfies $\lambda \prec \nu \stackrel{\circ}{\succ} \mu$ because in the final two-layer configuration, there can be at most one horizontal arrow per edge.

DEFINITION 5.3. The law of the random signature $\nu \in \text{Sign}_{N+1}$ described above will be denoted by $\mathsf{U}^{\text{fwd}}_{v,u}(\kappa \to \nu \mid \lambda, \mu)$. We will call $\mathsf{U}^{\text{fwd}}_{v,u}$ the *forward transition probabilities* (on signatures).

The backward transition probabilities $U^{\text{bwd}}_{v,u}(\nu \to \kappa \mid \lambda, \mu)$ (where the signatures $\lambda \in \text{Sign}_N, \nu, \mu \in \text{Sign}_{N+1}$ with $\lambda \prec \nu \stackrel{>}{\succ} \mu$ are given) are defined in a similar way, but now the cross vertex \times is added to the right of ν_1 and is dragged to the left using the backward Yang–Baxter moves having probabilities $P^{\text{bwd}}_{v,u}$ given in Figure 5. The process of dragging the cross vertex to the left terminates at μ_{N+1} when the cross vertex has the state \times . This process does not affect the signatures λ and μ and turns the fixed signature $\nu \in \text{Sign}_{N+1}$ in the middle into a *random* signature $\kappa \in \text{Sign}_N$.

DEFINITION 5.4. The law of the random signature $\kappa \in \text{Sign}_N$ just described will be denoted by $\bigcup_{v,u}^{\text{bwd}}(v \to \kappa \mid \lambda, \mu)$. We will call $\bigcup_{v,u}^{\text{bwd}}$ the *backward transition probabilities* (on signatures).



Clearly, by the very construction,

$$\sum_{\nu \in \mathsf{Sign}_{N+1}} \mathsf{U}^{\mathsf{fwd}}_{\nu,u}(\kappa \to \nu \mid \lambda, \mu) = 1, \quad \text{for every } \lambda, \kappa, \mu \text{ with } \lambda \overset{\circ}{\succ} \kappa \prec \mu;$$

$$\sum_{\kappa \in \mathsf{Sign}_{N}} \mathsf{U}^{\mathsf{bwd}}_{\nu,u}(\nu \to \kappa \mid \lambda, \mu) = 1, \quad \text{for every } \lambda, \nu, \mu \text{ with } \lambda \prec \nu \overset{\circ}{\succ} \mu.$$
(5.2)

The first of these sums is infinite and converges due to (5.1). The second of the sums is finite.

PROPOSITION 5.5. Let $N \in \mathbb{Z}_{\geqslant 0}$, $\lambda, \kappa \in \text{Sign}_N$, and $\mu, \nu \in \text{Sign}_{N+1}$ be fixed. The forward transition probability $\bigcup_{v,u}^{\text{fwd}}(\kappa \to \nu \mid \lambda, \mu)$ on signatures is equal to the product of finitely many local forward transition probabilities $P_{v,u}^{\text{fwd}}$ over columns with numbers from μ_{N+1} to ν_1 . Similarly, $\bigcup_{v,u}^{\text{bwd}}(\nu \to \kappa \mid \lambda, \mu)$ is the product of finitely many local backward transition probabilities $P_{v,u}^{\text{bwd}}$ over columns from μ_{N+1} to ν_1 .

Proof. We argue only about forward transition probabilities; the case of the backward ones is analogous. Let the multiplicative notations of the signatures $\lambda, \kappa, \nu, \mu$ be $\lambda = \cdots (-1)^{\ell_{-1}} 0^{\ell_0} 1^{\ell_1} 2^{\ell_2} \ldots, \kappa = \cdots (-1)^{k_{-1}} 0^{k_0} \ldots, \nu = \cdots (-1)^{n_{-1}} 0^{n_0} \ldots$, and $\mu = \cdots (-1)^{m_{-1}} 0^{m_0} \ldots$. Consider the situation in the definition of $U_{v,u}^{\text{fwd}}$ when the cross vertex is moved through the column number r (for example, r=0 in Figure 10). Assume that the following data is known before the move of the cross vertex:

- the state of the cross vertex (that is, one of six states as in (3.3));
- the numbers ℓ_r , k_r , m_r of vertical arrows at the rth column before the move of the cross vertex:
- the numbers ℓ_r , n_r , m_r of vertical arrows at the rth column after the move of the cross vertex;
- the numbers of horizontal arrows in both layers of the arrow configuration as in Figure 10 between the (r-1)st column and the cross vertex as well as between the rth and the (r+1)st columns.

One readily sees that the state of the cross vertex after the forward randomized Yang–Baxter move (placing the cross vertex one step to the right) is completely determined by the above data.

The state of the cross vertex and all the above data at the far left is known. Therefore, by induction, all the intermediate states of the cross vertex in the



definition of $\mathsf{U}^{\mathrm{fwd}}_{v,u}(\kappa \to \nu \mid \lambda, \mu)$ are completely determined by the four signatures $\lambda, \kappa, \nu, \mu$. This implies that the transition probability $\mathsf{U}^{\mathrm{fwd}}_{v,u}(\kappa \to \nu \mid \lambda, \mu)$ on signatures is indeed equal to the product of the local transition probabilities $P^{\mathrm{fwd}}_{v,u}$ depending on these intermediate cross vertex states. This completes the proof. \square

5.2. Bijective proof of the skew Cauchy identity. The key observation leading to our bijective proof of Theorem 4.2 is the following.

PROPOSITION 5.6 (Reversibility on signatures). *Fix arbitrary* $N \in \mathbb{Z}_{\geq 0}$, $\lambda, \kappa \in \text{Sign}_N$, and $\mu, \nu \in \text{Sign}_{N+1}$. We have for any (u, v) satisfying (5.1):

$$\left[\sum_{v,u} G_{\lambda/\kappa}^{c}(v^{-1}) F_{\mu/\kappa}(u) \mathsf{U}_{v,u}^{\text{fwd}}(\kappa \to \nu \mid \lambda, \mu) \right]$$

$$= \left[\sum_{v,u} F_{v/\lambda}(u) G_{v/\mu}^{c}(v^{-1}) \mathsf{U}_{v,u}^{\text{bwd}}(v \to \kappa \mid \lambda, \mu), \right]$$
(5.3)

where the weights of the cross vertices are given in (3.3) (modulo the swap, see Remark 5.1).

REMARK 5.7. Both sides of (5.3) are nonzero only if $\lambda \stackrel{\circ}{\succ} \kappa \prec \mu$ and $\lambda \prec \nu \stackrel{\circ}{\succ} \mu$. Indeed, if, say, the condition $\kappa \prec \mu$ is violated, then $F_{\mu/\kappa}(u)$ is zero by the very definition. At the same time, $U_{v,u}^{\text{bwd}}(v \to \kappa \mid \lambda, \mu)$ also vanishes because $\kappa \not\prec \mu$ implies that κ cannot arise as the middle signature in the two-layer arrow configuration after dragging the cross vertex from far right to the left.

Proof of Proposition 5.6. By (4.2), (4.5), and Proposition 5.5, the skew functions F, G^c as well as the transition probabilities $U_{v,u}$ on both sides of (5.3) can be expressed as products over the columns in the two-layer arrow configurations as in Figure 9. The desired identity (5.3) then follows by repeatedly applying the local reversibility condition at each column for the probabilities of the Yang–Baxter moves $P_{v,u}^{\text{fwd}}$ and $P_{v,u}^{\text{bwd}}$. This local reversibility condition is given by (2.2) in the general setting. In our vertex model context, it means that the weight of the left picture in Figure 6 times the forward transition probability equals the weight of the right picture times the backward transition probability. The local reversibility holds precisely because the probabilities $P_{v,u}^{\text{fwd}}$ and $P_{v,u}^{\text{bwd}}$ come from a bijectivization. The quantities $\left[\mathbf{X}\right]_{v,u} G_{\lambda/\kappa}^c(v^{-1}) F_{\mu/\kappa}(u)$ and $\left[\mathbf{X}\right]_{v,u} F_{v/\lambda}(u) G_{v/\mu}^c(v^{-1})$ collect the weights entering the local reversibility conditions, while the probabilities $U_{v,u}^{\text{fwd}}$, $U_{v,u}^{\text{bwd}}$ collect the local probabilities $P_{v,u}^{\text{fwd}}$, $P_{v,u}^{\text{bwd}}$. This implies (5.3).



Proof of Theorem 4.2. Summing (5.3) over both $\kappa \in \operatorname{Sign}_N$ and $\nu \in \operatorname{Sign}_{N+1}$ and recalling that $\left[\times \right]_{v,u} = 1$ and $\left[\times \right]_{v,u} = (v-u)/(v-tu)$, we have

$$\sum_{\kappa \in \operatorname{Sign}_{N}} G_{\lambda/\kappa}^{c}(v^{-1}) F_{\mu/\kappa}(u) \left(\sum_{\nu \in \operatorname{Sign}_{N+1}} \mathsf{U}_{v,u}^{\operatorname{fwd}}(\kappa \to \nu \mid \lambda, \mu) \right) \\
= \frac{v - u}{v - tu} \sum_{\nu \in \operatorname{Sign}_{N+1}} F_{\nu/\lambda}(u) G_{\nu/\mu}^{c}(v^{-1}) \left(\sum_{\kappa \in \operatorname{Sign}_{N}} \mathsf{U}_{v,u}^{\operatorname{bwd}}(\nu \to \kappa \mid \lambda, \mu) \right). \tag{5.4}$$

By (5.2), the sums in the parentheses on both sides are equal to 1, which implies the desired identity (4.10).

We call the above proof of the skew Cauchy identity (4.10) *bijective* because (5.4) provides a *refinement* of (4.10) (involving summation over κ , ν on both sides), in which the terms on both sides are bijectively identified with each other with the help of the reversibility condition (5.3). Thus, the transition probabilities $U_{\nu,u}^{\text{fwd}}$ and $U_{\nu,u}^{\text{bwd}}$ show how to split terms on both sides of the original identity (4.10) into smaller ones, such that these smaller terms are identified with each other.

5.3. Markov projection of the forward transition onto first columns. For notational convenience, in this subsection, we assume that both λ and μ are nonnegative signatures (that is, whose parts are all nonnegative). Then the signatures κ , ν entering $\mathsf{U}^{\mathrm{fwd}}_{v,u}(\kappa \to \nu \mid \lambda, \mu)$ (as well as $\mathsf{U}^{\mathrm{bwd}}_{v,u}(\nu \to \kappa \mid \lambda, \mu)$) should also be nonnegative, otherwise these transition probabilities vanish for interlacing reasons. Fix any $h \in \mathbb{Z}_{\geq 1}$. For any nonnegative signature ρ having multiplicative notation $\rho = 0^{r_0} 1^{r_1} 2^{r_2} \dots$, let $\rho^{[<h]} := (r_0, r_1, \dots, r_{h-1}) \in \mathbb{Z}_{\geq 0}^h$ and $\rho^{[\geqslant h]} := (r_h, r_{h+1}, \dots)$ be the corresponding configurations of arrows in the first h columns and in the rest of the nonnegative integer lattice. Using the fact that the forward transition probabilities $\mathsf{U}^{\mathrm{fwd}}_{v,u}$ were defined in Section 5.1 in a sequential way (from left to right columns), we can express them as follows (for every fixed $h \geqslant 1$):

$$U_{v,u}^{\text{fwd}}(\kappa \to \nu \mid \lambda, \mu) = U_{v,u}^{[< h], \text{fwd}}(\kappa^{[< h]} \to \nu^{[< h]} \mid \lambda^{[< h]}, \mu^{[< h]})
\times U_{v,u}^{[\geqslant h], \text{fwd}}(\kappa^{[\geqslant h]} \to \nu^{[\geqslant h]} \mid \lambda, \mu, \kappa^{[< h]}, \nu^{[< h]}).$$
(5.5)

A crucial property in (5.5) is that $U_{v,u}^{[< h],\text{fwd}}$, the transition probability describing the evolution of the first h columns, does not depend on configurations of arrows in columns $h, h+1, \ldots$ In other words, in the transition $\kappa \to \nu$ under $U_{v,u}^{\text{fwd}}$, the first h columns are (randomly) transformed in a *marginally Markovian way*. We will say that the forward transition probabilities $U_{v,u}^{\text{fwd}}$ on signatures *admit*



Markov projections onto the first h columns for every $h \ge 1$. In (5.5), this Markov projection is denoted by $\bigcup_{v=h}^{[< h], \text{fwd}}$.

Representation (5.5) is possible because the forward transition probabilities are defined via dragging the cross vertex from left to right. A similar representation for the backward transition probabilities based on their definition via dragging the cross vertex from right to left would show that in the transition $v \to \kappa$ under $\mathsf{U}^{\mathsf{bwd}}_{v,u}$, the columns $h,h+1,\ldots$ evolve in a marginally Markovian way. Since this Markov projection of the backward probabilities always involves infinitely many columns, we will not focus on this right-to-left Markov property in the present paper.

Let us now consider the case h=1. For shorter notation in this case, we will write [0] instead of [< 1] in the superscripts. Let us write down the Markov projection $\mathsf{U}^{[0],\mathrm{fwd}}_{v,u}$ onto the column number 0. In this case, the quantity $\rho^{[0]}$ for any nonnegative signature ρ is simply the number of zero parts in ρ . There are six possible types of transitions in the first column which can be read off the last row of the table in Figure 4 (recall that we swap the parameters u and v; see Remark 5.1):

$$U_{v,u}^{[0]}(g \to g \mid g - 1, g + 1) = 1,
U_{v,u}^{[0]}(g \to g \mid g, g + 1) = \frac{(1 - t)v}{v - tu} \frac{u - st^g}{v - st^g}
U_{v,u}^{[0]}(g \to g + 1 \mid g, g + 1) = \frac{v - u}{v - tu} \frac{v - st^{g+1}}{v - st^g},
U_{v,u}^{[0]}(g \to g \mid g - 1, g) = \frac{(1 - t)u}{v - tu} \frac{v - st^g}{u - st^g}
U_{v,u}^{[0]}(g \to g - 1 \mid g - 1, g) = \frac{t(v - u)}{v - tu} \frac{u - st^{g-1}}{u - st^g},
U_{v,u}^{[0]}(g \to g \mid g, g) = 1.$$
(5.6)

These transitions depend on arbitrary $g \in \mathbb{Z}_{\geq 0}$ with the understanding that $g \geq 1$ in the first and the third lines in (5.6).

6. Yang-Baxter field

In this section, we introduce our main stochastic object, the *spin Hall–Littlewood Yang–Baxter random field* (called simply the *Yang–Baxter field* throughout the paper), and discuss its main properties.

6.1. Spin Hall–Littlewood measures and processes. Fix $(x, y) \in \mathbb{Z}_{\geq 0}^2$, and let v_1, \ldots, v_x and u_1, \ldots, u_y be spectral parameters such that $0 \leq u_i < v_j < 1$ for



all i, j. As in Section 5, we continue to assume that $0 \le t < 1$ and $-1 < s \le 0$. Define the following probability measure on the set of nonnegative signatures of length y:

$$\mathcal{H}_{x,y}(\lambda) := \frac{1}{\prod_{x,y}} G^{c}_{\lambda/(0^{y})}(v_{1}^{-1}, \dots, v_{x}^{-1}) F_{\lambda/\varnothing}(u_{1}, \dots, u_{y}), \quad \lambda \in \mathsf{Sign}_{y}^{+}. \quad (6.1)$$

The weights under $\mathcal{H}_{x,y}$ are nonnegative and their sum over $\lambda \in \text{Sign}_y^+$ converges, thanks to our conditions on parameters. The normalization constant in (6.1) has the following product form due to the Cauchy identity of Corollary 4.5:

$$\Pi_{x,y} = \prod_{i=1}^{y} \left(\frac{1 - t^{i}}{1 - su_{i}} \prod_{j=1}^{x} \frac{v_{j} - tu_{i}}{v_{j} - u_{i}} \right). \tag{6.2}$$

We call the measures $\mathcal{H}_{x,y}$ (6.1) the *spin Hall–Littlewood measures* by analogy with the Macdonald measures [BC14] (and their several degenerations, most notably, the Schur measures [Oko01]). As in the Macdonald setting, skew Cauchy identities allow to extend the measures (6.1) to spin Hall–Littlewood processes which are probability measures on certain sequences of nonnegative signatures. For simplicity, we will only consider a particular case of spin Hall–Littlewood processes suitable for our needs.

Fix $k \in \mathbb{Z}_{\geqslant 1}$ and sequences

$$\vec{x} := (0 = x_1 \leqslant x_2 \leqslant \ldots \leqslant x_k), \quad \vec{y} := (y_1 \geqslant y_2 \geqslant \ldots \geqslant y_{k-1} \geqslant y_k = 0).$$
 (6.3)

Consider the following down-right path in $\mathbb{Z}^2_{\geq 0}$ corresponding to these sequences:

$$\mathcal{P}_{\vec{x},\vec{y}} := \{(x_1, y_1), (x_2, y_1), (x_2, y_2), (x_3, y_2), \dots, (x_k, y_{k-1}), (x_k, y_k)\}.$$
(6.4)

Let v_1, \ldots, v_{x_k} and u_1, \ldots, u_{y_1} be spectral parameters satisfying the same conditions as for the measures (6.1). The *spin Hall–Littlewood process* $\mathcal{HP}_{\vec{x},\vec{y}}$ indexed by the down-right path $\mathcal{P}_{\vec{x},\vec{y}}$ depending on these spectral parameters is a probability measure on sequences of nonnegative signatures λ^p , $p \in \mathcal{P}_{\vec{x},\vec{y}}$, with $\lambda^{(0,y_1)} = (0^{y_1})$ and $\lambda^{(x_k,0)} = \varnothing$, defined as

$$\mathcal{H}\mathcal{P}_{\vec{x},\vec{y}}(\lambda^{p}: p \in \mathcal{P}_{\vec{x},\vec{y}})$$

$$:= \frac{1}{\Pi_{\vec{x},\vec{y}}} \prod_{i=1}^{k-1} G^{c}_{\lambda^{(x_{i+1},y_{i})}/\lambda^{(x_{i},y_{i})}}(v_{x_{i}+1}^{-1}, \dots, v_{x_{i+1}}^{-1}) \prod_{i=2}^{k} F_{\lambda^{(x_{i},y_{i-1})}/\lambda^{(x_{i},y_{i})}}(u_{y_{i}+1}, \dots, u_{y_{i-1}}).$$
(6.5)



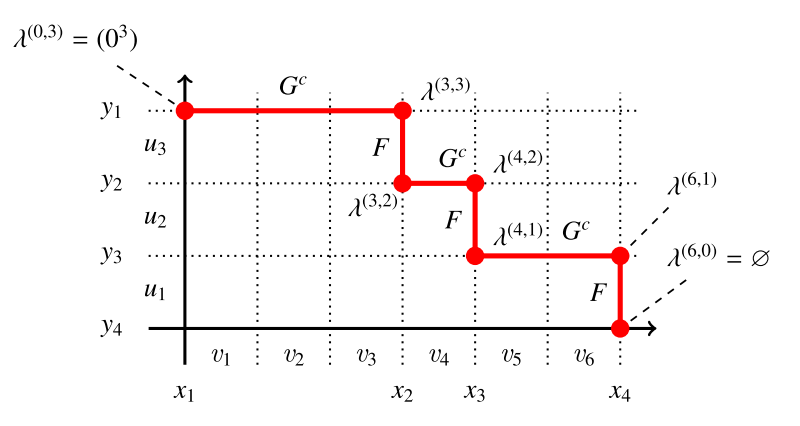


Figure 11. An illustration of the spin Hall–Littlewood process indexed by sequences $\vec{x} = (0, 3, 4, 6)$ and $\vec{y} = (3, 2, 1, 0)$. The second product (over in (i, j)) in (6.6) runs over all boxes inside the region bounded by the down-right path $\mathcal{P}_{\vec{x}, \vec{y}}$. For this particular path, the product contains 13 terms.

Here, $\lambda^{(x,y)} \in \text{Sign}_y^+$, and the normalization constant in (6.5) can be read off the skew Cauchy identities (see Section 4.3):

$$\Pi_{\vec{x}, \vec{y}} = \left(\prod_{i=1}^{y} \frac{1 - t^{i}}{1 - su_{i}} \right) \prod_{\substack{(i,j) \in \mathbb{Z}_{\geqslant 1}^{2}: \\ \text{box } (i,j) \text{ is below } \mathcal{P}_{\vec{x}, \vec{y}}}} \frac{v_{j} - tu_{i}}{v_{j} - u_{i}}.$$
(6.6)

A graphical illustration of a spin Hall–Littlewood process is given in Figure 11. One of the properties of spin Hall–Littlewood processes is that under $\mathcal{HP}_{\bar{x},\bar{y}}$ (6.5), for fixed x, y, the marginal distribution of the signature $\lambda^{(x,y)} \in \operatorname{Sign}_y^+$ is given by the Hall–Littlewood measure $\mathcal{H}_{x,y}$ (6.1) (here, by 'marginal distribution', we mean the distribution of $\lambda^{(x,y)}$ after 'integrating out' all other signatures). More generally, take any subpath \mathcal{Q} of $\mathcal{P}_{\bar{x},\bar{y}}$ such that \mathcal{Q} is itself a down-right path. Then the marginal distribution of the signatures $\{\lambda^q: q\in \mathcal{Q}\}$ under the original spin Hall–Littlewood process $\mathcal{HP}_{\bar{x},\bar{y}}$ (6.5) is itself a spin Hall–Littlewood process corresponding to the path \mathcal{Q} .

6.2. Yang-Baxter field. Let us now introduce the Yang-Baxter field with the help of the forward transition probabilities on signatures discussed in Section 5. The field depends on $t \in [0, 1)$, $s \in (-1, 0]$, and two sequences of spectral parameters $v_1, v_2, \ldots, u_1, u_2, \ldots$ such that $0 \le u_i < v_j < 1$ for all i, j. The Yang-Baxter field is a probability distribution on the space of nonnegative signatures



 $\lambda^{(x,y)}$ indexed by points of the quadrant $(x, y) \in \mathbb{Z}^2_{\geq 0}$ such that $\lambda^{(x,y)} \in \mathsf{Sign}^+_y$, the signatures interlace as (see Section 4.1 for notation)

$$\lambda^{(x,y)} \prec \lambda^{(x,y+1)}, \quad \lambda^{(x,y)} \stackrel{\circ}{\prec} \lambda^{(x+1,y)}, \quad (x,y) \in \mathbb{Z}^2_{\geq 0},$$

and satisfy the boundary conditions $\lambda^{(x,0)} \equiv \emptyset$, $\lambda^{(0,y)} = (0^y)$.

DEFINITION 6.1. We construct the *Yang–Baxter field* $\Lambda := \{\lambda^{(x,y)}\}_{x,y\geqslant 0}$ inductively. Initialize the boundary values in the following nonrandom way: $\lambda^{(x,0)} = \emptyset$, $\lambda^{(0,y)} = (0^y)$ for all $x,y\geqslant 0$. Now, for some $n\geqslant 1$, let the field be already defined for all $(x',y')\in\mathbb{Z}^2_{\geqslant 0}$ such that $x'+y'\leqslant n$. Conditioned on $\{\lambda^{(x',y')}\}_{x'+y'\leqslant n}$, independently sample the random signatures $\lambda^{(x,y)}$ with $x+y=n+1,x,y\geqslant 1$, according to

$$\operatorname{Prob}(\boldsymbol{\lambda}^{(x,y)} = \nu \mid \{\boldsymbol{\lambda}^{(x',y')}\}_{x'+y' \leqslant n}) = \mathsf{U}^{\operatorname{fwd}}_{v_x,u_y}(\boldsymbol{\lambda}^{(x-1,y-1)} \to \nu \mid \boldsymbol{\lambda}^{(x,y-1)}, \boldsymbol{\lambda}^{(x-1,y)}). \tag{6.7}$$

This defines the Yang–Baxter field for (x, y) with $x + y \le n + 1$, and the induction step completes the definition of the field for all $(x, y) \in \mathbb{Z}^2_{\ge 0}$. See Figure 12 for an illustration.

The discussion in Section 5.3 readily implies the following Markov projection property of the Yang–Baxter field.

PROPOSITION 6.2. Fix any $h \in \mathbb{Z}_{\geq 1}$. Under the Yang–Baxter field, the first h columns of the signatures $\lambda^{(x,y)}$ evolve in a marginally Markovian way (that is, independently of the columns $h+1,h+2,\ldots$).

This evolution of the first h columns defines a random field indexed by $\mathbb{Z}^2_{\geq 0}$ with values in $\mathbb{Z}^h_{\geq 0}$ which can be regarded as an h-layer stochastic vertex model. In Section 7 and Appendix A, we discuss the case h = 1 in detail. Details on the two-layer case for s = 0 may be found in [BM18, Section 4.4].

The next theorem states a key property of the Yang–Baxter field Λ .

THEOREM 6.3. Under the Yang–Baxter field, for any down-right path $\mathcal{P}_{\vec{x},\vec{y}}$ as in (6.3)–(6.4), the joint distribution of the signatures $\{\lambda^p : p \in \mathcal{P}_{\vec{x},\vec{y}}\}$ is given by the spin Hall–Littlewood process $\mathcal{HP}_{\vec{x},\vec{y}}$ (6.5).

Proof. Extend the path $\mathcal{P}_{\bar{x},\bar{y}}$ by adding to it all the intermediate vertices so that the distance between each two consecutive vertices along the extended path is equal to 1 (see Figure 12). Let us also add vertices $(0, y_1 + 1)$ and $(x_k + 1, 0)$ in the beginning and the end of the path, respectively. If we establish the claim for such



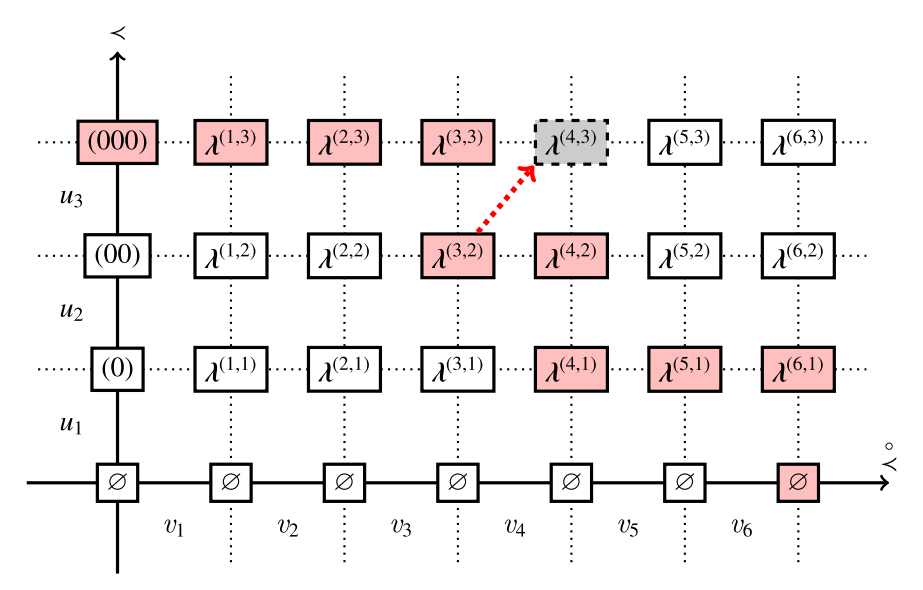


Figure 12. Yang–Baxter random field. Signatures along a down-right path (the extension of the path in Figure 11) are highlighted in red. The signature $\lambda^{(3,2)}$ is replaced by $\lambda^{(4,3)}$ in this path with the help of the forward transition probability; see the proof of Theorem 6.3.

extended paths, then the original claim will follow; see the remark at the end of Section 6.1.

Using the inductive definition of Λ , we establish the modified claim by induction on the down-right path. The base of the induction is the case when the path goes along the coordinate axes, that is, has the form

$$\{(0, y_1 + 1), (0, y_1), \dots, (0, 1), (0, 0), (1, 0), \dots, (x_k + 1, 0)\}.$$

In this case, the random signatures along this path are, in fact, deterministic and coincide with the corresponding signatures under the spin Hall–Littlewood process corresponding to this path.

In the induction step, we replace one down-right corner of the form $\{(x, y+1), (x, y), (x+1, y)\}$ by the right-down corner $\{(x, y+1), (x+1, y+1), (x+1, y)\}$ (see an example in Figure 12 where (x, y) = (3, 2)). Denote the old and the new paths by \mathcal{P} and \mathcal{P}' , respectively. For shorter notation, set

$$\kappa := \lambda^{(x,y)}, \quad \mu := \lambda^{(x,y+1)}, \quad \lambda := \lambda^{(x+1,y)}, \quad \nu := \lambda^{(x+1,y+1)}.$$



Assume that the joint distribution of the signatures along \mathcal{P} is given by the corresponding spin Hall–Littlewood process. The joint distribution along \mathcal{P}' can be obtained from the joint distribution along \mathcal{P} with the help of the conditional distribution of ν given λ , κ , μ . By Definition 6.1, the latter conditional distribution is given by the forward transition probability. Thus, we see that the joint distribution of all four signatures λ , κ , μ , ν is proportional to the left-hand side of (5.3) (with $u = u_{\nu+1}$, $v = v_{\nu+1}$). Using this identity and summing over κ , we see from the right-hand side of (5.3) that the joint distribution of λ , ν , μ is proportional to $F_{\nu/\lambda}(u_{\nu+1})$ $G^c_{\nu/\mu}(v^{-1}_{\nu+1})$ as it should be under the spin Hall–Littlewood process corresponding to the path \mathcal{P}' . This completes the induction step and the proof of the proposition.

Theorem 6.3 and Proposition 5.6 readily imply a backward version of the conditional distribution (6.7) in the Yang–Baxter field.

COROLLARY 6.4. Under the Yang–Baxter field, for any $(x, y) \in \mathbb{Z}_{\geq 0}$, the conditional distribution of $\lambda^{(x,y)}$ given the signatures to the right and above it is equal to the backward transition probability:

$$\begin{split} \operatorname{Prob} & \big(\boldsymbol{\lambda}^{(x,y)} = \kappa \mid \boldsymbol{\lambda}^{(x+1,y)}, \boldsymbol{\lambda}^{(x,y+1)}, \boldsymbol{\lambda}^{(x+1,y+1)} \big) \\ & = \mathsf{U}^{\operatorname{bwd}}_{v_{x+1},u_{y+1}} \big(\boldsymbol{\lambda}^{(x+1,y+1)} \to \kappa \mid \boldsymbol{\lambda}^{(x+1,y)}, \boldsymbol{\lambda}^{(x,y+1)} \big). \end{split}$$

7. A dynamic stochastic six-vertex model

Here we consider the Markov projection of the Yang–Baxter field onto the column number zero. This produces a new dynamic version of the stochastic sixvertex model. The original stochastic six-vertex model was introduced in [GS92], and its asymptotic behavior was studied in [BCG16] and subsequent works. We recall this original model in Appendix A.1.

7.1. Dynamic vertex weights. Let $\Lambda = \{\lambda^{(x,y)}\}_{x,y\geqslant 0}$ be the Yang–Baxter field constructed in Section 6. Recall that each $\lambda^{(x,y)}$ is a random nonnegative signature (of length y). For each $(x,y)\in\mathbb{Z}^2_{\geqslant 0}$, let $\ell^{(x,y)}:=(\lambda^{(x,y)})^{[0]}\in\mathbb{Z}_{\geqslant 0}$ denote the number of arrows in the zeroth column of the arrow configuration encoded by the signature $\lambda^{(x,y)}$. (Equivalently, $(\lambda^{(x,y)})^{[0]}$ is the number of zero parts in the signature $\lambda^{(x,y)}$.) Since $\lambda^{(x,y)}\in \text{Sign}_y$, we have $\ell^{(x,y)}\leqslant y$. Proposition 6.2 implies that the scalar random field $\mathbf{L}:=\{\ell^{(x,y)}\}_{x,y\geqslant 0}$ does not depend on the rest of the Yang–Baxter field (that is, of the numbers of arrows in $\lambda^{(x,y)}$ in columns $\geqslant 1$). In this way, we say that \mathbf{L} is a marginally Markovian projection of the Yang–Baxter field Λ onto the column number zero.



$\begin{array}{c c} \ell+1 & \ell \\ \hline \ell & \ell-1 \end{array}$	$\begin{array}{c c} \ell+1 & \ell \\ \hline \ell & \ell \end{array}$	$\begin{array}{c c} \ell+1 & \ell+1 \\ \hline \ell & \ell \end{array}$	$ \begin{array}{c c} \ell & \ell \\ \ell & \ell-1 \end{array} $	$\begin{array}{c c} \ell & \ell-1 \\ \hline \ell & \ell-1 \end{array}$	ℓ ℓ ℓ
1		$\frac{v-u}{v-tu} \frac{v-st^{\ell+1}}{v-st^{\ell}}$		$\frac{t(v-u)}{v-tu} \frac{u-st^{\ell-1}}{u-st^{\ell}}$	1

Figure 13. Conditional probabilities in the random field \mathbf{L} on $\mathbb{Z}^2_{\geqslant 0}$. In the top row, all possible values of the field in the square $\{x,x+1\}\times\{y,y+1\}$ are listed, where $\ell\in\mathbb{Z}_{\geqslant 0}$ (and $\ell\geqslant 1$ in the first, fourth, and fifth pictures). The bottom row contains the corresponding conditional probabilities to sample the top-right value $\ell^{(x+1,y+1)}$ of the field, given the three other values. The spectral parameters are $v=v_{x+1}$ and $u=u_{y+1}$. The arrows represent identification with the six-vertex configurations.

Let us now present an independent description of **L**. From the definition of the Yang–Baxter field via conditional probabilities (6.7), it follows that for each $(x, y) \in \mathbb{Z}^2_{\geq 0}$, the value of $\ell^{(x+1,y+1)}$ is randomly determined using $\ell^{(x+1,y)}$, $\ell^{(x,y)}$, and $\ell^{(x,y+1)}$, and the corresponding conditional probabilities can be read from (5.6). In the language of values of the field **L**, these conditional probabilities are given in Figure 13. The nature of the six possible configurations of the values of **L** at 2×2 squares allow to *identify* **L** with the height function in a dynamic version of the stochastic six-vertex model. Let us describe this model in more detail.

First, we define the space of configurations in our DS6V model. Consider an ensemble of infinite up-right paths in the positive integer quadrant with the following properties:

- paths go along edges of the shifted lattice $(\mathbb{Z}_{\geq 0} + \frac{1}{2})^2$;
- each edge of $(\mathbb{Z}_{\geqslant 0} + \frac{1}{2})^2$ is occupied by at most one path;
- paths can touch each other at a vertex but cannot cross each other;
- on the boundary of the quadrant, no paths enter from below, and at each height $n + \frac{1}{2}$, $n \ge 0$, a new path enters through the left part of the boundary.

Fix such a configuration of up-right paths. At each (x, y) in the original nonshifted lattice $\mathbb{Z}^2_{\geqslant 0}$, define the value of the *height function*, $\mathfrak{h}(x, y)$, to be the number of paths passing below (x, y). See Figure 14 for an illustration.

DEFINITION 7.1 (DS6V). The (*DS6V model*) is a probability distribution on ensembles of up-right paths (depending on the parameters $t \in [0, 1)$, $s \in (-1, 0]$, and two sequences v_1, v_2, \ldots and u_1, u_2, \ldots such that $0 \le u_i < v_j < 1$ for all i, j)



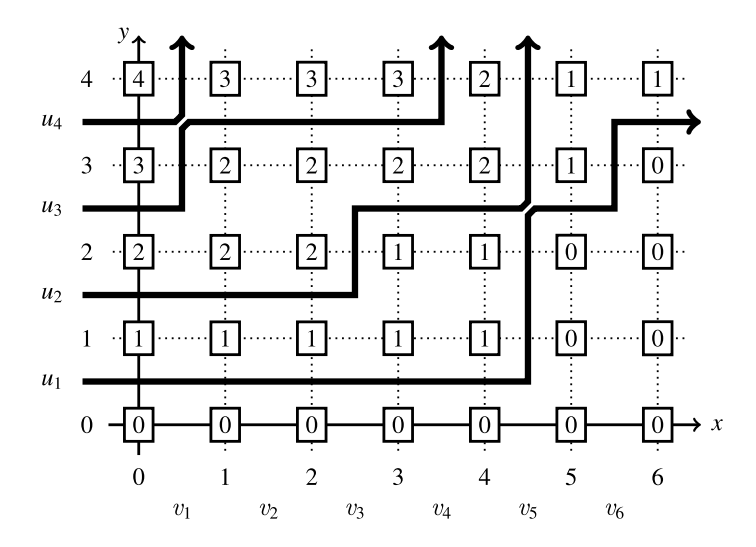


Figure 14. Path configuration of six-vertex type in a quadrant together with its height function.

defined inductively as follows. Suppose that the path configuration below the line $x+y\leqslant n$ (for some $n\in\mathbb{Z}_{\geqslant 1}$) is sampled. Thus, at each vertex $(n-\frac{1}{2},\frac{1}{2}), (n-\frac{3}{2},\frac{3}{2}),\ldots,(\frac{1}{2},n-\frac{1}{2}),$ we know the incoming configuration of paths. We also know the values of the height function at each point $(x,y)\in\mathbb{Z}_{\geqslant 0}^2$ with $x+y\leqslant n$. Using the probabilities in Figure 13, sample the outgoing configuration of paths at each vertex $(n-\frac{1}{2},\frac{1}{2}),\ldots,(\frac{1}{2},n-\frac{1}{2})$ independently, and then proceed by induction.

The weights in Figure 13 together with our conditions on the parameters of the model imply that under the DS6V model for each y, there almost surely exists x such that $\mathfrak{h}(x', y) = 0$ for all $x' \ge x$. In other words, each path almost surely reaches arbitrarily large vertical coordinates.

REMARK 7.2. The vertex model introduced in Definition 7.1 differs from the DS6V model presented recently in [Bor17b] as a degeneration of the stochastic interaction-round-a-face model (introduced in the same work). A higher spin model following the approach of the latter paper was then developed in [Agg17]. All these dynamic stochastic vertex models are closely related to versions of the Yang–Baxter equation with dynamic parameters (see Section 7.2 for our dynamic Yang–Baxter equation which seems to be simpler than the one in [Bor17b]). Therefore, we regard the model from Definition 7.1 as another dynamic version of the stochastic six-vertex model, different from the ones in [Bor17b, Agg17].



PROPOSITION 7.3. Let $\mathfrak{H}:=\{\mathfrak{h}(x,y)\}_{x,y\geqslant 0}$ be the random field of values of the height function of DS6V (Definition 7.1). Let $\mathbf{L}=\{\boldsymbol{\ell}^{(x,y)}\}_{x,y\geqslant 0}$ be the random field obtained as the projection of the Yang–Baxter random field of Definition 6.1 onto the column number zero. Then these random fields \mathfrak{H} and \mathbf{L} have the same distribution.

Proof. Straightforward from the identification of weights in \mathfrak{H} and \mathbf{L} in Figure 13 together with the identification of the boundary conditions.

From Theorem 6.3 and Proposition 7.3, we immediately get the following interpretation of the distribution of the height function in DS6V.

COROLLARY 7.4. Fix a down-right path $\mathcal{P}_{\vec{x},\vec{y}}$ as in (6.3)–(6.4). The joint distribution of the random variables $\{\mathfrak{h}(p)\colon p\in\mathcal{P}_{\vec{x},\vec{y}}\}$ (that is, the values of the height function of the DS6V model along this down-right path) coincides with the joint distribution of $\{(\lambda^{(p)})^{[0]}\colon p\in\mathcal{P}_{\vec{x},\vec{y}}\}$, the numbers of zero parts in the signatures $\lambda^{(p)}$ governed by the spin Hall–Littlewood process $\mathfrak{HP}_{\vec{x},\vec{y}}$ corresponding to the down-right path $\mathcal{P}_{\vec{x},\vec{y}}$.

7.2. A dynamic Yang–Baxter equation. The probabilities of vertex configurations in DS6V (given in Figure 13) satisfy a dynamic version of the Yang–Baxter equation. It is convenient to formulate it in terms of the values of the height function since the corresponding arrow configurations can be readily recovered as in Figure 13. Consider two three-line configurations as in Figure 15. Fix the six boundary values ℓ_0 , ℓ_1 , ℓ_2 , ℓ'_1 , ℓ'_2 , $\ell_3 \in \mathbb{Z}_{\geqslant 0}$ of the height function. Clearly, these values can be arbitrary provided that they satisfy

$$\ell_1 - \ell_0, \ell_2 - \ell_1, \ell_3 - \ell_2 \in \{0, 1\}, \quad \ell'_1 - \ell_0, \ell'_2 - \ell'_1, \ell_3 - \ell'_2 \in \{0, 1\}.$$
 (7.1)

Also fix spectral parameters u_1 , u_2 , v. For the dynamic Yang–Baxter equation in Theorem 7.5, these parameters do not have to satisfy any conditions as in Definition 7.1. However, if $0 \le u_2 < u_1 < v < 1$ and $0 \le t < 1$, $-1 < s \le 0$, then all the individual vertex weights entering the dynamic Yang–Baxter equation belong to [0, 1].

THEOREM 7.5 (Dynamic Yang–Baxter equation). Form two partition functions corresponding to the left and the right three-line configurations in Figure 15. In both partition functions, the same boundary conditions satisfying (7.1) are fixed, and the summation is over all possible values (in fact, no more than two) of the height function '?' inside the triangle. The spectral parameters U₁, U₂, V are attached to the three lines, and at each intersection, the corresponding



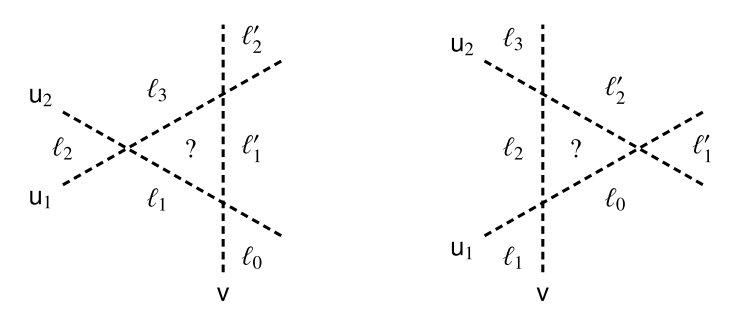
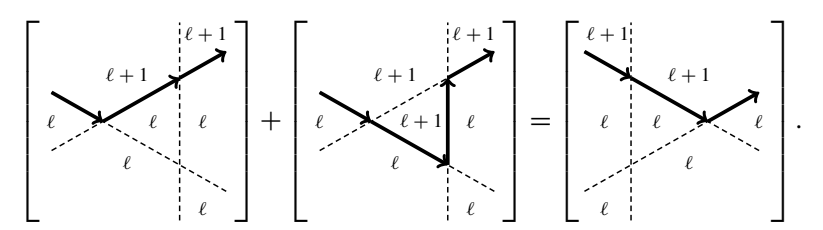


Figure 15. The dynamic Yang–Baxter equation for the dynamic stochastic sixvertex weights in Figure 13.

'horizontal' and 'vertical' parameters replace u and v, respectively, in the weights in Figure 13.

Then these two partition functions are equal to each other.

Proof. There are totally 20 types of identities corresponding to various choices of the boundary conditions satisfying (7.1) and depending on one particular value of the height function, say, $\ell_0 = \ell$. Each of these identities is readily verified by hand. For illustration, let us present one such identity:



This translates into the following identity between rational functions

$$\begin{split} &\frac{(1-t)\mathsf{u}_1(\mathsf{u}_2-st^\ell)}{(\mathsf{u}_1-t\mathsf{u}_2)(\mathsf{u}_1-st^\ell)} \frac{(\mathsf{v}-\mathsf{u}_1)(st^{\ell+1}-\mathsf{v})}{(\mathsf{v}-t\mathsf{u}_1)(st^\ell-\mathsf{v})} \\ &+ \frac{(\mathsf{u}_1-\mathsf{u}_2)(\mathsf{u}_1-st^{\ell+1})}{(\mathsf{u}_1-t\mathsf{u}_2)(\mathsf{u}_1-st^\ell)} \frac{(1-t)\mathsf{v}(\mathsf{u}_2-st^\ell)}{(\mathsf{v}-t\mathsf{u}_2)(\mathsf{v}-st^\ell)} \frac{(1-t)\mathsf{u}_1(\mathsf{v}-st^{\ell+1})}{(\mathsf{v}-t\mathsf{u}_1)(\mathsf{u}_1-st^{\ell+1})} \\ &= \frac{(\mathsf{v}-\mathsf{u}_2)(st^{\ell+1}-\mathsf{v})}{(\mathsf{v}-t\mathsf{u}_2)(st^\ell-\mathsf{v})} \frac{(1-t)\mathsf{u}_1(\mathsf{u}_2-st^\ell)}{(\mathsf{u}_1-t\mathsf{u}_2)(\mathsf{u}_1-st^\ell)}, \end{split}$$

which is readily verified by hand. The remaining 19 identities comprising the dynamic Yang–Baxter equation are checked in a similar way, and the theorem follows.



REMARK 7.6. The dynamic Yang–Baxter equation of Theorem 7.5 is, in fact, a certain 'gauge' of the usual Yang–Baxter equation for the stochastic six-vertex model [ABB18]. However, we do not use this fact here.

The dynamic Yang–Baxter equation of Theorem 7.5 satisfied by the probabilities in the DS6V model hints at the model's integrability (that is, that certain observables of this model are computable in explicit form). We do not discuss these problems in the present work, though in Appendix A, we consider degenerations of DS6V for which certain observables indeed can be computed in explicit form.

Appendix A. Degenerations and limits

Here we discuss a number of degenerations of the DS6V model and its properties stated in Theorem 6.3 and Corollary 7.4. Some of these degenerations correspond to degenerations of the spin Hall–Littlewood symmetric functions outlined in [Bor17a, Section 8]. The tables in Figures 16 and 17 list various degenerations of the DS6V weights considered in Appendices A.1–A.11. Additional (less direct) degenerations are discussed in Appendices A.12–A.14. We also discuss two degenerations of the full Yang–Baxter field in Appendices A.1 and A.9 and compare them to known systems.

REMARK A.1. Every degeneration of the DS6V model we consider can be lifted to a k-layer model, where $k \geqslant 2$ is arbitrary. Indeed, such a model would arise by taking the corresponding degeneration of the full Yang–Baxter field and looking at its Markov projection onto the first k columns as in Section 5.3. Such multilayer models for s=0 were explicitly written down in [BM18] for the RSK type field. The Yang–Baxter field of the present paper produces different k-layer versions for $k \geqslant 3$. For shortness, we will not address multilayer extensions in the present work.

For simplicity, we assume that the spectral parameters are constant, $u_i \equiv u$ and $v_j \equiv v$, but most constructions (except the ASEP type limit in Appendix A.13) work for the inhomogeneous parameters u_i , v_i too.

A.1. Hall-Littlewood degeneration and stochastic six-vertex model. Setting s = 0 and keeping other parameters makes the DS6V weights independent of the height function. Moreover, in this degeneration, the weights depend only on the ratio u/v and not on the individual parameters u, v; see Figure 16(a). Thus, in this limit, the DS6V turns into the usual stochastic six-vertex model introduced



		$\begin{array}{c c} \ell+1 & \ell \\ \hline \ell & \ell \end{array}$	$\begin{array}{c c} \ell+1 & \ell+1 \\ \hline \ell & \ell \end{array}$	$-\frac{\ell + \ell}{\ell + 1}$	$\begin{array}{c c} \ell & \ell-1 \\ \hline \ell & \ell-1 \end{array}$
	Original	$(1-t)v \ u - st^{\ell}$	$v - u \ v - st^{\ell+1}$	$(1-t)u\ v-st^{\ell}$	$t(v-u)u-st^{\ell-1}$
	weights	$v - tu \overline{v - st^{\ell}}$	$v - tu v - st^{\ell}$	$\overline{v-tu} \overline{u-st^{\ell}}$	$v - tu u - st^{\ell}$
(a)	Appendix A.1	$\frac{(1-t)u/v}{1-tu/v}$	$\frac{1 - u/v}{1 - tu/v}$	$\frac{1-t}{1-tu/v}$	$\frac{t(1-u/v)}{1-tu/v}$
(b)	Appendix A.2	$\frac{u - s1_{\ell=0}}{v - s1_{\ell=0}}$	$\frac{v-u}{v-s1_{\ell=0}}$	1	0
(c)	Appendix A.3	u/v	1 - u/v	1	0
(d)	Appendix A.4	$\frac{(1-t)v}{v-tu}\frac{u+t^{\ell}}{v+t^{\ell}}$	$\frac{v-u}{v-tu}\frac{v+t^{\ell+1}}{v+t^{\ell}}$	$\frac{(1-t)u}{v-tu}\frac{v+t^{\ell}}{u+t^{\ell}}$	$\frac{t(v-u)}{v-tu} \frac{u+t^{\ell-1}}{u+t^{\ell}}$
(e)	Appendix A.5	$\frac{u+1_{\ell=0}}{v+1_{\ell=0}}$	$\frac{v - u}{v + 1_{\ell=0}}$	1	0

Figure 16. Direct degenerations of the dynamic stochastic six-vertex weights from Section 7 considered in the first part of Appendix A. Here $\ell \in \mathbb{Z}_{\geqslant 0}$ (and $\ell \geqslant 1$ in the last two cases) is the parameter corresponding to the height function, and $\mathbf{1}_{\dots}$ denotes the indicator of an event. The vertices (1,1;1,1) and (0,0;0,0) always having weight 1 are not shown.

		$\begin{array}{c c} \ell+1 & \ell \\ \hline \ell & \ell \\ \hline \text{Rate} \end{array}$	$\begin{array}{c c} \ell+1 & \ell+1 \\ \hline \ell & \ell \\ \hline \end{array}$ Probability	$ \begin{array}{c c} \ell & \ell \\ \ell & \ell-1 \end{array} $ Probability	$ \begin{array}{c c} \ell & \ell - 1 \\ \ell & \ell - 1 \end{array} $ Probability
(a)	Appendix A.6	$(1-t)(u-st^{\ell})$	$1 - O(v^{-1})$	$\frac{(1-t)u}{u-st^{\ell}}$	$\frac{tu - st^{\ell}}{u - st^{\ell}}$
(b)	Appendix A.7	(1-t)u	$1 - O(v^{-1})$	1-t	t
(c)	Appendix A.8	$u - s1_{\ell=0}$	$1 - O(v^{-1})$	1	0
(d)	Appendix A.9	и	$1 - O(v^{-1})$	1	0
(e)	Appendix A.10	$(1-t)(u+t^{\ell})$	$1 - O(v^{-1})$	$\frac{(1-t)u}{u+t^{\ell}}$	$\frac{tu - st^{\ell}}{u + t^{\ell}}$
(f)	Appendix A.11	$u + 1_{\ell=0}$	$1 - O(v^{-1})$	1	0

Figure 17. The half-continuous DS6V model and its various degenerations. The vertices (1, 1; 1, 1) and (0, 0; 0, 0) always having weight 1 are not shown.

in [GS92] and studied in integrable probability since [BCG16]. The spin Hall–Littlewood symmetric functions F and G^c turn (up to simple factors) into the Hall–Littlewood symmetric polynomials [Mac95, Ch. III]. The correspondence between the stochastic six-vertex model and Hall–Littlewood processes following



from Corollary 7.4 was obtained earlier in [Bor16] (at the level of formulas), [BBW18] (for a half-continuous degeneration, see Appendix A.7) and in full form in [BM18].

The Yang–Baxter field $\Lambda := \{\lambda^{(x,y)}\}_{x,y\geqslant 0}$ for s=0 becomes a certain field of random Young diagrams indexed by $\mathbb{Z}^2_{\geqslant 0}$ related to Hall–Littlewood measures and processes. This random field *differs* from the Hall–Littlewood RSK field introduced in [BM18] despite the following:

- In both fields, joint distributions along down-right paths are the same and are given by the Hall–Littlewood processes as in Corollary 7.4.
- The projection onto the first column in both fields produces the stochastic sixvertex model.

The existence of two different random fields with these properties might seem surprising, but such nonuniqueness of two-dimensional stochastic dynamics was observed before, for example, in [BP16] or [BP14, Section 4]. The fact that the s = 0 Yang-Baxter field and the Hall-Littlewood RSK field are indeed different will be evident in Appendix A.9 when we take further degenerations and obtain different objects.

REMARK A.2. The Hall–Littlewood RSK field of [BM18] has an additional structure coming from the fact that the skew Hall–Littlewood symmetric functions in one variable are proportional to a power of the variable. Using this fact, analogues of the probabilities $U_{v,u}^{\text{fwd}}$ and $U_{v,u}^{\text{bwd}}$ for the Hall–Littlewood RSK field lead to *randomized RSK correspondences*: having Young diagrams μ , κ , λ , and an integer $r \in \mathbb{Z}_{\geq 0}$ (corresponding to the power of u/v), the randomized RSK produces a random output Young diagram ν . See [BM18, Section 3.6] for details on this reduction of a random field of Young diagrams to randomized RSK correspondences with input.

However, for $s \neq 0$, the skew spin Hall–Littlewood symmetric functions in one variable are not simply proportional to powers of the variables. This presents a clear obstacle to a possible reduction of the Yang–Baxter field or another such random field of signatures to a randomized correspondence with integer input. Therefore, we do not address this issue in the present work.

Observables of Hall–Littlewood processes pertaining to the projection onto first columns can be extracted using the action of Hall–Littlewood versions of Macdonald difference operators (for example, see [Dim16]). Thus, the connection between the stochastic six-vertex model and Hall–Littlewood processes produces tools for the analysis of the former model alternative to the original approach of [BCG16]. See, for example, [Bor16] for an analysis via Hall–Littlewood measures.



A.2. Schur degeneration and modified discrete time PushTASEP. Setting t = 0 and keeping all other parameters makes the DS6V weights look as in Figure 16(b). These weights are still dynamic in the sense that they retain dependence on the height function. However, this dependence only singles out the bottommost path: the behavior of all other paths follows the same weights.

As noted in [Bor17a, Section 8.3], the spin Hall–Littlewood functions F and G^c for t=0 turn into certain determinants generalizing Schur polynomials, thus making the spin Hall–Littlewood measures and processes in this degeneration potentially more tractable.

Let us reinterpret the t=0 degeneration of DS6V as a discrete time particle system by regarding the horizontal direction as time (a similar interpretation is valid for the general DS6V model too, only the corresponding particle system becomes more complicated).

DEFINITION A.3. Consider a discrete time particle system living on half infinite particle configurations $x_1(t) < x_2(t) < \cdots$, $t \in \mathbb{Z}_{\geq 0}$, on \mathbb{Z} . Identify this system with the t = 0 degeneration of the DS6V model as follows:

$$x_i(t) = k \iff \mathfrak{h}(t, k - 1) = i - 1 \text{ and } \mathfrak{h}(t, k) = i;$$
 (A.1)

see Figure 14 and the definition of the height function in Section 7.1. The boundary condition with arrows on the right in DS6V translates into the *step* initial condition $x_i(0) = i$, $i \in \mathbb{Z}_{\geq 1}$.

The particle system on \mathbb{Z} thus defined evolves as follows. In discrete time, particles jump to the right by one or stay put (indeed, this is because the weight of the vertex (1,0;1,0) is zero). At each time step $t \to t+1$, the first particle flips a coin with the probability of success (u-s)/(v-s), and each of the other particles flip independent coins with probability of success u/v. Then in the order from left to right, each particle x_i , $i=1,2,\ldots$ jumps to the right by one if either

- the coin of x_i is a success
- or if $x_i(t) = x_{i-1}(t) + 1 = x_{i-1}(t+1)$. In other words, if the particle x_{i-1} is moving to the right by one and its destination is occupied by x_i , then x_i is pushed to the right by one (and then the coin of x_i does not matter). If the destination of x_i is also occupied, the pushing propagates further to the right to x_{i+1} , and so on.

At each time step, almost surely the update eventually terminates after a final push to the right by one of the infinite densely packed configurations.

The particle system of Definition A.3 is a *modified discrete time PushTASEP* with a special behavior of the first particle (the original discrete time PushTASEP is discussed in Appendix A.3 next). To the best of the authors' knowledge,



this modified PushTASEP was not studied before by methods of integrable probability.

A.3. Discrete time PushTASEP and Schur measures. Setting s = t = 0 in DS6V turns it into the discrete time pushing Totally Asymmetric Simple Exclusion Process (PushTASEP). That is, interpreting the vertex model as a particle system as in (A.1), we get the following evolution. Initially, $x_i(0) = i$, $i \in \mathbb{Z}_{\geq 1}$. At each discrete time step $t \to t+1$, each particle x_1, x_2, \ldots (in this order) independently jumps to the right by one with probability u/v, following the pushing mechanism described in Definition A.3.

When s = t = 0, the spin Hall-Littlewood symmetric functions turn into the Schur symmetric polynomials [Mac95, Ch. II.3], and the measures and processes from Section 6.1 turn into the Schur measures and processes, which are determinantal with explicit double contour integral kernels [Oko01, OR03].

The discrete time PushTASEP just described is a known particle system associated with Schur measures and processes. (This discrete time PushTASEP is known as the Bernoulli one. There is also geometric PushTASEP in which particles jump to the right by arbitrary distance according to some distribution. These processes can be read off from, for example, [BF14]; concise discrete time definitions are also obtained by setting q=0 in [MP17, Sections 5.2 and 6.3]. The continuous time version of the PushTASEP (which is a suitable limit of both the Bernoulli and the geometric PushTASEPs) is discussed in Appendix A.9.) However, its relation to the Schur measures following from our Corollary 7.4 differs from the one in [BF14]. A connection similar to the latter one was employed in [BF08] for asymptotic analysis. Let us compare these two connections in the single-point case (though both of them can be lifted to suitable multipoint statements).

PROPOSITION A.4 [BF14]. For the discrete time PushTASEP with step initial condition and probability of jump u/v, we have the following equality in distribution for all $N \ge 1$, $t \ge 0$:

$$x_N(t) \stackrel{d}{=} \lambda_1 + N$$
,

where $\lambda = (\lambda_1, \dots, \lambda_N) \in \mathsf{Sign}_N^+$ is a random signature distributed according to the Schur measure

$$\operatorname{Prob}(\lambda) = \frac{1}{Z} s_{\lambda}(\underbrace{1, \dots, 1}_{N}) s_{\lambda'} \left(\underbrace{\frac{u}{v}, \dots, \frac{u}{v}}_{N}\right).$$



Here, Z is the normalizing constant and λ' denotes the transposition (in the language of Young diagrams) of λ .

Recall that via the identification (A.1), the vertex model height function can be interpreted as $\mathfrak{h}(t, x) := \#\{\text{particles at time } t \text{ which are } \leq x\}$, which is natural to view as the height function of the PushTASEP.

PROPOSITION A.5 (t = s = 0 in Corollary 7.4). For the discrete time PushTASEP as above, we have for all $N \ge 1$ and $t \ge 0$:

$$\mathfrak{h}(\mathfrak{t},N)\stackrel{d}{=}\mu^{[0]},$$

where $\mu = (\mu_1, \dots, \mu_N) \in \mathsf{Sign}_N^+$ is distributed according to the Schur measure

$$\operatorname{Prob}(\mu) = \frac{1}{Z} s_{\mu}(\underbrace{v^{-1}, \dots, v^{-1}}_{t}) s_{\mu}(\underbrace{u, \dots, u}_{N}). \tag{A.2}$$

Here, Z is the normalizing constant and $\mu^{[0]}$ denotes the number of zero parts in the signature μ (in other words, $\mu^{[0]} = N - \mu'_1$).

Note that when t < N, $\operatorname{Prob}(\mu)$ given by (A.2) automatically vanishes if $\mu_{t+1} > 0$, as it should be. Indeed, after time t < N, there are at least N-t particles in the PushTASEP at locations $\leq N$, so the value of the height function $N-\mu_1'$ must be at least N-t.

These two connections between PushTASEP and Schur measures admit different deformations along the hierarchy of symmetric functions. Namely, Proposition A.4 can be generalized by inserting the q-Whittaker parameter $q \in (0,1)$, which gives rise to q-PushTASEP connected with q-Whittaker measures and processes [BP16, CP15, MP17]. On the other hand, Proposition A.5 is generalized to our Corollary 7.4, and thus the PushTASEP is lifted to the DS6V model depending on two additional parameters $t \in (0,1)$ and $s \in (-1,0)$ and related to the spin Hall–Littlewood measures and processes.

Moreover, Proposition A.4 can be generalized to PushTASEP with particle-dependent jumping probabilities, while Proposition A.5 can be extended to PushTASEP in inhomogeneous space. In the latter version of PushTASEP, the jumping probability of a particle depends on the current location of the particle and not on the particle itself. The asymptotics of PushTASEP in inhomogeneous space are studied in the forthcoming work [Pet20].

We postpone the discussion of the t = s = 0 degeneration of the Yang–Baxter field to Appendix A.9 where a half-continuous rescaling further simplifies the object.



A.4. Hall–Littlewood degeneration with rescaling. Renaming (u, v) to (-su, -sv) makes the DS6V weights independent of s; see Figure 16(d). The new degenerate weights still contain the dynamic dependence on the value of the height function. They are nonnegative for $0 \le t < 1$ and $0 \le u < v < 1$.

Taking variables $-su_i$ and $-sv_j$ in the spin Hall–Littlewood functions F and G^c , respectively, we can then send $s \to 0$. This limit requires a rescaling of the functions themselves, but the spin Hall–Littlewood measures and processes have $s \to 0$ limits without any rescaling. The symmetric functions F and G^c in this $s \to 0$ limit become polynomials in u_i and v_j , respectively, whose top degree homogeneous components are the classical Hall–Littlewood symmetric polynomials [Bor17a, Section 8.2]. The functions $F_{\lambda/\varnothing}$ under this degeneration can also be viewed as eigenfunctions of the stochastic q-Boson particle system [BCPS15b].

This $s \to 0$ limit with rescaling of the spin Hall–Littlewood measures could be easier to analyze (to the point of asymptotics) than the measures (6.1) before the limit. Via Corollary 7.4, this would give tools for asymptotic analysis of a dynamic model with the weights given in Figure 16(d).

- **A.5.** Schur degeneration with rescaling. Further setting t = 0 in the model of Appendix A.4 produces a model with vertex weights in Figure 16(e) which are very similar to the ones considered in Appendix A.2. Interpreting the vertex model as a discrete time particle system as in Definition A.3 produces another version of the discrete time PushTASEP with a special behavior of the first particle.
- **A.6. Half-continuous DS6V model.** In Appendices A.6–A.11, we discuss the rescaling of DS6V to the continuous horizontal direction, beginning with the half-continuous DS6V model itself. The degenerations of the half-continuous DS6V model considered in Appendices A.7–A.11 are summarized in Figure 17.

Taking the expansion as $v \to +\infty$ of the DS6V vertex weights in Figure 14, we see that

$$\begin{bmatrix} \ell+1 & \ell \\ \hline \ell & \ell \end{bmatrix} = v^{-1}(1-t)(u-st^{\ell}) + O(v^{-2}),$$

$$\begin{bmatrix} \ell+1 & \ell+1 \\ \hline \ell & \ell \end{bmatrix} = 1 - O(v^{-1}),$$

$$\begin{bmatrix} -\ell & \ell \\ \hline \ell & \ell \end{bmatrix} = \frac{(1-t)u}{u-st^{\ell}} + O(v^{-2}),$$



$$\begin{bmatrix} -\ell & \uparrow & \ell - 1 \\ -\ell & \uparrow & \ell - 1 \end{bmatrix} = \frac{tu - st^{\ell}}{u - st^{\ell}} + O(v^{-2}),$$

$$\begin{bmatrix} \ell + 1 & \uparrow & \ell \\ \ell & \uparrow & \ell - 1 \end{bmatrix} = \begin{bmatrix} -\ell & \ell \\ \ell & \ell \end{bmatrix} = 1.$$

Thus, for $v \gg 1$, taking into account the DS6V boundary conditions, we see that all up-right paths will go to the right in most of the steps. Occasionally with probability proportional to v^{-1} , a path might turn up using the vertex (0,1;1,0), move some random distance up using several vertices (1,0;1,0), and either turn right using (1,0;0,1) or hit a neighboring path above it using (1,1;1,1) (recall that the paths can touch each other at a vertex but cannot cross each other). In the latter case, this neighboring path now faces up and, in turn, should make a number of upward steps and either eventually turn right or hit the next path, and so on. The update in this vertical slice eventually terminates after some path decides to turn right or after the infinite densely packed cluster of paths is pushed up by one.

In the limit, as $v \to +\infty$, we thus obtain a probability distribution on up-right paths in the half-continuous quadrant $\mathbb{R}_{\geqslant 0} \times (\mathbb{Z}_{\geqslant 0} + \frac{1}{2})$. All paths enter through the left boundary and nothing enters from below. Each ith path from below, $i \in \mathbb{Z}_{\geqslant 1}$, carries an independent Poisson process of rate $(1-t)(u-st^{i-1})$ (one should think that $i=\ell+1$, where ℓ is the parameter in Figure 17). Outside arrivals of these Poisson processes, all paths go to the right. (To rigorously define the system, note that the behavior of the paths up to vertical coordinate M does not depend on the behavior of the system above M, for any $M\geqslant 1$. Thus, the evolution of any finite part of the system with vertical coordinate $\leqslant M$ is well-defined, and for different M, these processes are compatible, thus defining the measure on the full half-continuous quadrant.) When there is an arrival in the ith Poisson process, the corresponding path turns up and then behaves as explained in the previous paragraph using probabilities of the vertices (1,0;1,0), (1,0;0,1), and (1,1;1,1).

Similarly to Definition A.3, one can interpret this half-continuous DS6V model as a continuous time particle system $x_1(\tau) < x_2(\tau) < \cdots$, $\tau \in \mathbb{R}_{\geq 0}$, started from the step initial configuration $x_i(0) = i$, $i \geq 1$. Namely, in continuous time, each particle $x_i(\tau)$ wakes up at rate $(1-t)(u-st^{i-1})$ and instantaneously moves to the right by a random number of steps according to the probabilities in Figure 17(a). If the particle x_{i+1} is in the way of x_i , then x_i stops at where x_{i+1} was before. At the same time moment, x_{i+1} is pushed to the right by one, wakes up, and can instantaneously move further to the right, and so on.

The height function of the half-continuous DS6V is identified (via a limit of Corollary 7.4) with an observable of a limit of the spin Hall–Littlewood measure



- (6.1) as $v \to +\infty$ and the number of the variables v^{-1} in G^c grows as τv . (This identification can also be extended to multipoint observables.) Such limits of the spin Hall–Littlewood measures and processes exist and can be constructed via the corresponding half-continuous rescaling of the Yang–Baxter field. We will not discuss the half-continuous Yang–Baxter field in the full generality of parameters and, instead in Appendix A.9, focus on the simpler s=t=0 case which can be readily compared to existing (2+1)-dimensional dynamics associated with Schur processes.
- **A.7.** Half-continuous stochastic six-vertex model. Setting s=0 in the half-continuous DS6V model turns the rates and probabilities in this model into the ones in Figure 17(b). The vertex weights stop being dynamic (that is, they no longer depend on the value ℓ of the height function), and the model becomes a half-continuous version of the stochastic six-vertex model. This model and its connection to Hall–Littlewood measures and processes was considered in [BBW18].
- **A.8.** Continuous time modified PushTASEP. Setting t = 0 in the half-continuous DS6V model but keeping the parameter $s \in (-1, 0]$ and identifying the vertex model with a continuous time particle system $x_1(\tau) < x_2(\tau) < \cdots$ yields the following system. Initially, $x_i(0) = i$, $i \ge 1$. Each particle has an independent exponential clock, x_1 with a higher rate u s, and each of the other ones with rate u. When the clock of x_i rings, it jumps to the right by one. If the destination is occupied and, more generally, if there is a packed cluster of particles immediately to the right of x_i (that is, $x_i = x_{i+1} 1 = \cdots = x_{i+k-1} k + 1 = x_{i+k} k$ before the jump), then each of the particles x_{i+1}, \ldots, x_{i+k} in this cluster is pushed to the right by one.
- **A.9.** Continuous time PushTASEP and (2 + 1)-dimensional Yang–Baxter dynamics. Setting t = 0 in the half-continuous stochastic six-vertex model of Appendix A.7 or, which is the same, setting s = 0 in the model of Appendix A.8 leads to the usual continuous time *PushTASEP*. In this continuous time particle system on \mathbb{Z} , each particle independently jumps to the right by one at rate u and pushes to the right the particles which are in the way.

The spin Hall–Littlewood measures turn into the Schur measures, and the limit $v \to +\infty$ in the specialization (v^{-1}, \ldots, v^{-1}) $(v^{-1}$ is repeated τv times) corresponds to the so-called Plancherel specialization of symmetric functions. In this way, both Propositions A.4 and A.5 readily lead to corresponding statements for the continuous time PushTASEP.



Let us address what happens to the Yang-Baxter field under this half-continuous s=t=0 degeneration and compare it with other known (2+1)-dimensional continuous time dynamics associated with Schur measures and processes. Let us first introduce a suitable framework. Fix any $M \in \mathbb{Z}_{\geq 1}$. A collection of signatures $\lambda^{(1)} \prec \lambda^{(2)} \prec \cdots \prec \lambda^{(M)}$, $\lambda^{(i)} \in \text{Sign}_i^+$ (see (4.1) for notation) is called an *interlacing array* of depth M. (Also, often in connection with representation theory, referred to as a Gelfand-Tsetlin pattern.) We interpret the integers $\lambda_i^{(k)}$, $1 \leq i \leq k \leq M$, as coordinates of particles in the space $\mathbb{Z}_{\geq 0} \times \{1, \ldots, M\}$. There are exactly k particles on each level $k=1,\ldots,M$.

We will consider a class of continuous time stochastic dynamics on interlacing arrays called *sequential update dynamics* introduced in [BP16]. They evolve as follows:

- (Independent jumps and blocking by particles below) Each particle $\lambda_i^{(k)}$ has an independent exponential clock of rate $w_i^{(k)} \geqslant 0$ which may depend on the whole array. When the clock rings, the particle $\lambda_i^{(k)}$ tries to jump to the right by one (that is, the coordinate $\lambda_i^{(j)}$ wishes to increase by one). If this particle is blocked by the lower right neighbor, that is, $\lambda_i^{(k)} = \lambda_{i-1}^{(k-1)}$ before the jump, then the jump of $\lambda_i^{(k)}$ is forbidden.
- (*Move propagation*) Denote the signature after the jump at level k by $\nu^{(k)}$. After a jump at level k, the update $\lambda^{(k)} \to \nu^{(k)}$ may initiate a sequential cascade of instantaneous updates on all the upper levels, $\lambda^{(k+1)} \to \nu^{(k+1)}, \ldots, \lambda^{(M)} \to \nu^{(M)}$, according to the transition probabilities $U_j(\lambda^{(j)} \to \nu^{(j)} \mid \lambda^{(j-1)} \to \nu^{(j-1)})$. Here, each $\nu^{(j)}$ differs from $\lambda^{(j)}$ by a move of at most one particle to the right by one.
- (*Mandatory pushing to preserve interlacing*) In order to preserve interlacing, the probabilities U_j must be equal to one in the case when $\nu_i^{(j-1)} = \lambda_i^{(j-1)} + 1 = \lambda_i^{(j)} + 1$ and $\nu_i^{(j)} = \lambda_i^{(j)} + 1$. In other words, if a particle $\lambda_i^{(j-1)}$ moves and this breaks the interlacing with level j, then an instantaneous move of $\lambda_i^{(j)}$ must be made to restore the interlacing.

Under certain conditions on $w_i^{(k)}$ and the transition probabilities U_k , the sequential update dynamics acts nicely on Schur processes; see [BP16]. (That is, joint distributions in the dynamics started from the packed initial configuration $\lambda_j^{(k)}(0) \equiv 0$ are given by Schur processes along down-right paths as in our Theorem 6.3.) These conditions might be interpreted as providing a bijectivization of the skew Cauchy identity for Schur polynomials when one of the specializations is Plancherel.

The connection between the framework of interlacing arrays and the half-continuous rescaling of the Yang–Baxter field is the following. Under the rescaling of the horizontal coordinate x to continuum, the Yang–Baxter field (or any of its degenerations considered in Appendices A.1–A.5) $\{\lambda^{(x,y)}\}$ indexed by



 $(x, y) \in \mathbb{Z}_{\geqslant 0}$ turns into a field $\{\lambda^{(\tau, y)}\}$ indexed by $\tau \in \mathbb{R}_{\geqslant 0}$, $y \in \mathbb{Z}_{\geqslant 0}$. The boundary conditions are $\lambda^{(0, y)} = (0^y)$, $y \in \mathbb{Z}_{\geqslant 0}$, and $\lambda^{(\tau, 0)} = \varnothing$, $\tau \in \mathbb{R}_{\geqslant 0}$. We interpret the first M rows $\{\lambda^{(\tau, k)}\}_{k=1,\dots,M}$ of the half-continuous random field of signatures as a continuous time Markov dynamics (where τ is time) on interlacing arrays of depth M via $\lambda^{(k)}(\tau) = \lambda^{(\tau, k)}$, with initial condition $\lambda^{(k)}(0) = (0^k)$.

In sequential update dynamics we describe below the quantities $w_i^{(k)}$ and U_k are essentially independent of k, that is, the jumping and move propagation mechanisms are the same at all levels of the interlacing array. Thus, to describe such a dynamics, let us fix k and denote

$$\kappa = \lambda^{(k-1)}(\tau), \quad \mu = \lambda^{(k)}(\tau), \quad \lambda = \lambda^{(k-1)}(\tau), \quad \nu = \lambda^{(k)}(\tau)$$
 (A.3)

(that is, these are signatures at levels k-1 and k before and after the jump at time τ , respectively). The jump rates $w_i \equiv w_i^{(k)}, i=1,\ldots,k$, correspond to independent jumps of the particles of μ when $\lambda = \kappa$, and the transition probabilities $U(\mu \to \nu \mid \kappa \to \lambda)$ describe how the move at level k-1 propagates to level k.

We are now in a position to describe the half-continuous t = s = 0 degeneration of the Yang–Baxter field.

DEFINITION A.6. The Yang–Baxter continuous time dynamics on interlacing arrays looks as follows at each pair of consecutive levels (k-1,k) (using notation (A.3)). When $\lambda = \kappa$, the rate of independent jump of each particle μ_i is, in general, equal to u, except the following:

- (blocking from below) the rate of independent jump of μ_i is zero if $\mu_i = \lambda_{i-1}$;
- (special blocking) the rate of independent jump of μ_i is also zero if

$$\mu_i = \lambda_i = \mu_{i+1} = \lambda_{i+1} = \dots = \mu_{i+m} = \lambda_{i+m} > \mu_{i+m+1}$$
 for some $m \geqslant 0$. (A.4)

When $\lambda \neq \kappa$ and the difference is only in $\lambda_i = \kappa_i + 1$, the transition probability $U(\mu \to \nu \mid \kappa \to \lambda)$ is, in general, equal to $\mathbf{1}_{\nu=\mu}$ (no move propagation), except the following:

- (mandatory pushing to restore interlacing) if $\lambda_i = \mu_i + 1 = \kappa_i + 1$, this leads to $\nu_i = \mu_i + 1$ with probability 1;
- (special pushing) if

$$\mu_i = \lambda_i = \mu_{i-1} = \lambda_{i-1} = \dots = \mu_{i-m} = \lambda_{i-m} < \lambda_{i-m-1}$$
 for some $m \ge 0$, (A.5)

then together with $\lambda_i = \kappa_i + 1$, this leads to $\nu_{i-m} = \mu_{i-m} + 1$ with probability 1. In particular, in this dynamics, the difference between λ and κ as well as between ν and μ is in the move of at most one particle to the right by one (in the language of Young diagrams, in adding one box).



$P_{v,u}^{\mathrm{fwd}}$	$ \times $	X	X	X	X	X
\overline{X}	1	$v^{-1}u$	$1 - O(v^{-1})$	1	0	1
X	1	$v^{-1}u$	$1 - O(v^{-1})$	1	0	1
X	1	0	1	1	0	1
X	1	1	0	1	0	1
X	1	0	1	0	1	1
X	1	$v^{-1}u$	$1 - O(v^{-1})$	1	0	1

Figure 18. Behavior of the forward local Yang–Baxter transition probabilities for s = t = 0 as $v \to +\infty$. The coloring of the table cells is explained in Figure 4. Note that the parameters u, v are swapped compared to Figure 4; see Remark 5.1.

PROPOSITION A.7. The half-continuous t = s = 0 Yang-Baxter field is identified with the dynamics in Definition A.6.

Proof. The Yang–Baxter field is determined using the forward transition probabilities $U_{v,u}^{\rm fwd}$, which, in turn, are products of the local probabilities $P_{v,u}^{\rm fwd}$; see Definitions 5.3 and 6.1. Setting s=t=0 and expanding the latter as $v\to +\infty$, we get the quantities given in the table in Figure 18. Note that these quantities do not depend on the multiplicity g of arrows in the middle as was the case for $s,t\neq 0$. Because of this, we can assume without loss of generality that all the multiplicities in the middle are 0 or 1. It remains to match the corresponding expansions as $v\to +\infty$ of $U_{v,u}^{\rm fwd}$ to rates w_j and update probabilities $U(\mu\to v\mid \kappa\to \lambda)$ given in Definition A.6. We do this in two steps, for $\lambda=\kappa$ (considering jump rates) and $\lambda\neq\kappa$ (dealing with move propagation).

Jump rates. First, consider the case $\lambda = \kappa$. Then the arrow configuration $\lambda \stackrel{\circ}{\succ} \kappa \prec \mu$ (see Figures 9 and 10) looks as in Figure 19(a), and we need to drag the cross vertex through this configuration from left to right. The nonnegative integer line $\mathbb{Z}_{\geqslant 0}$ is divided into segments of two types: type I segments $[\lambda_i, \mu_i)$ and type II segments $[\mu_{i+1}, \lambda_i)$. When λ_i, μ_i are sufficiently apart, these types of segments interlace, but it can also happen that segments of the same type can be neighbors.

The cross vertex starts in state \times in type I segment, and this state cannot change throughout type I segment. Observe that on the boundary from type I to type II segment (say, corresponding to the arrow at μ_i), if the length of type II segment is positive, the cross vertex transforms (while moving to the right) as follows:



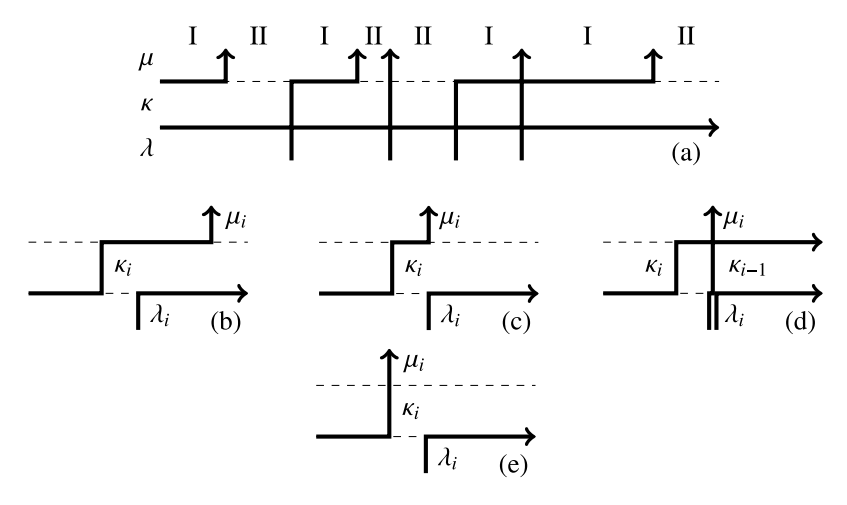


Figure 19. Arrow configurations $\lambda \stackrel{\circ}{\succ} \kappa \prec \mu$ in the proof of Proposition A.7.

- $\times \sim \times \sim \times$ with probability $v^{-1}u + O(v^{-2})$ (that is, at rate u) if the length of the type II segment is greater than 1, or if the length of the type II segment is 1 and the following type I segment has zero length;
- $\times \sim \times \sim \times$ with probability $v^{-1}u + O(v^{-2})$ (that is, at rate u) if the length of the type II segment is equal to 1 and the next segment is type I of positive length;
- $\times \sim \times$ with probability $1 O(v^{-1})$.

In the first two cases, this move places an arrow in the middle at $v_i = \mu_i + 1$, and in the second case, an arrow is placed at $v_i = \mu_i$. As $v \to +\infty$, the move leading to $v_i = \mu_i + 1$ can occur only once in the process of dragging the cross vertex, which proves the claim that, in general, the rates w_i are equal to u.

The cross vertex does not change throughout type II segments and leaves such a segment as χ (unless event of probability $v^{-1}u$ occurs and the length of type II segment is 1, but this is already considered above). When entering type I segment of positive length (at, say, the boundary corresponding to $\lambda_j = \kappa_j$), the cross vertex transforms as $\chi \rightsquigarrow \chi$, and this removes an arrow in the middle at κ_j .

A type II segment of zero length corresponds to $\mu_{i+1} = \kappa_i = \lambda_i$ for some i, which blocks the independent jump of μ_{i+1} . A type I segment of zero length does not change the state of the cross from χ which it has while traveling through type II segment; this behavior corresponds to the special case (A.4) in which the jump rate is zero. This establishes the claim about the jump rates.



Move propagation. Assume now that $\lambda \neq \kappa$, and the difference between these two signatures at level k-1 can be only at one location, $\lambda_i = \kappa_i + 1$. This fact would follow by induction on levels of the array after we show that the move propagation mechanism is as in Definition A.6. Indeed, this would imply that a single move of a particle by one cannot result in a move of a particle by more than one, or moves by more than one particle, at the level one higher.

Then in the process of dragging the cross vertex through the arrow configuration $\lambda \stackrel{\circ}{\succ} \kappa \prec \mu$ to obtain the signature ν , all updates are deterministic: an event with probability $O(\nu^{-1})$ has already occurred at level k-1 or below, and at a single time moment, two or more such events cannot occur. Updates through the parts of the configuration where $\lambda_j = \kappa_j$ have been considered above: they all lead to setting $\nu_j = \mu_j$. Thus, it remains to consider the update coming from the passing of the cross vertex through the part of the configuration where $\lambda_i = \kappa_i + 1$. There are four basic cases (see Figure 19(b)–(e)):

- (b) When $\mu_i > \lambda_i$ and $\mu_{i+1} < \kappa_i$, the cross vertex is updated as $\chi \leadsto \chi \leadsto \chi$. This removes the arrow at κ_i and corresponds to $U(\mu \to \nu \mid \kappa \to \lambda) = \mathbf{1}_{\nu=\mu}$.
- (c) When $\mu_i = \lambda_i = \kappa_i + 1 < \lambda_{i-1}$, the update is $\times \sim \times \sim \times$, which removes the arrow at κ_i and places a new arrow (corresponding to ν_i after the update) at $\lambda_i + 1$, which corresponds to the push under conditions (A.5).
- (d) When $\mu_i = \lambda_i = \kappa_i + 1 = \lambda_{i-1}$, the update is $\times \sim \times \sim \times$, which removes the arrow at κ_i , and does not affect the arrow at $\kappa_{i-1} = \lambda_{i-1}$ which becomes $\nu_i = \mu_i$. This case violates (A.5), and thus the update rule is $U(\mu \rightarrow \nu \mid \kappa \rightarrow \lambda) = \mathbf{1}_{\nu=\mu}$.
- (e) When $\mu_i < \lambda_i$ (and necessarily $\mu_i = \lambda_i + 1$), the update is $\chi \leadsto \chi$ $\leadsto \chi$, which removes an arrow at κ_i and adds a new arrow for ν_i at λ_i . This corresponds to the mandatory pushing to restore interlacing.

Each of the cases (c)–(e) admits a slight variation when $\mu_{i+1} = \kappa_i > \kappa_{i+1}$. Then in the update of the cross vertex state, the initial state is \mathbb{X} instead of \mathbb{X} , but the rows of the table in Figure 18 corresponding to these two states are the same up to $O(v^{-1})$. There is also another variation of (e) when $\lambda_{i-1} = \kappa_{i-1} = \lambda_i < \mu_{i-1}$, in which case the update is $\mathbb{X} \leadsto \mathbb{X}$. This does not remove an arrow at κ_{i-1} which becomes ν_i after the passing of the cross, and this agrees with the mandatory pushing. This completes the proof.

REMARK A.8. One can directly check that the Yang–Baxter dynamics on interlacing arrays described in Proposition A.7 in the language of interlacing arrays satisfies [BP16, Equation (2.20)]. This equation implies that the dynamics acts nicely on Schur processes (that is, in agreement with Theorem 6.3). However,



after establishing Proposition A.7, this fact also follows as a degeneration of Theorem 6.3.

The dynamics of Proposition A.7 is very similar to the one constructed in $[\mathbf{BF14}]$ using an idea of coupling Markov chains from $[\mathbf{DF90}]$. Namely, in the latter dynamics, the absence of independent jumps and additional pushing in the special cases $(\mathbf{A.4})$ and $(\mathbf{A.5})$ are eliminated. In other words, in the dynamics of $[\mathbf{BF14}]$, every particle simply jumps to the right by one at rate u while obeying the blocking and the mandatory pushing rules.

On the other hand, the Hall–Littlewood RSK field introduced in [BM18] in the half-continuous t=0 limit turns into a continuous time dynamics on interlacing arrays related to the column insertion RSK correspondence. In this dynamics, only the leftmost particles $\lambda_j^{(j)}$ can independently jump. At the same time, each move (to the right by one) of a particle $\lambda_i^{(j)}$ triggers a move of a particle to the right of it on the upper level. Typically, this triggered particle is $\lambda_i^{(j+1)}$, but the move is donated to the right if it is blocked. We refer to [BP16, Section 7] for a detailed description of this dynamics related to the (column) RSK.

Since this RSK dynamics differs from the one coming from the Yang–Baxter field via Proposition A.7, we see that the Hall–Littlewood RSK field of [BM18] also differs from the s = 0 Yang–Baxter field of Appendix A.1.

A.10. Half-continuous Hall-Littlewood degeneration with rescaling. Renaming u = -su and slowing the continuous time (equivalently, rescaling the continuous horizontal direction in the vertex model language) by the factor (-s) makes the rates and probabilities in the half-continuous DS6V independent of s. Then we can send $s \to 0$ and obtain a well-defined dynamic half-continuous vertex model. This model can be also obtained as a half-continuous limit $v \to +\infty$ of the one described in Appendix A.4. The resulting rates and probabilities for this model are listed in Figure 17(e).

- **A.11.** Half-continuous Schur degeneration with rescaling. Further setting t = 0 in the model of Appendix A.10 turns the rates and probabilities into the ones in Figure 17(f). Via a simple time rescaling, this model becomes the same as the modified continuous time PushTASEP considered in Appendix A.8.
- **A.12.** Rational limit $t \to 1$. In this and the following subsections, we return to the original DS6V weights as in Figure 13. Let us take limit $t \to 1$ in these weights, simultaneously rescaling all other parameters:

$$t = e^{\varepsilon}, \quad s = e^{\varepsilon \zeta}, \quad u = e^{x\varepsilon}, \quad v = e^{-y\varepsilon}, \quad \varepsilon \to 0.$$



In this limit, the vertex weights turn into the following:

$$\begin{bmatrix} \ell+1 & \ell & \ell \\ \ell & \ell-1 \end{bmatrix} = 1, \quad \begin{bmatrix} \ell & \ell & \ell \\ \ell & \ell & \ell \end{bmatrix} = 1,$$

$$\begin{bmatrix} \ell+1 & \ell & \ell \\ \ell & \ell & \ell \end{bmatrix} = \frac{\ell-x+\zeta}{(x+y+1)(\ell+y+\zeta)},$$

$$\begin{bmatrix} \ell+1 & \ell+1 \\ \ell & \ell \end{bmatrix} = \frac{(x+y)(\ell+y+\zeta+1)}{(x+y+1)(\ell+y+\zeta)},$$

$$\begin{bmatrix} \ell+1 & \ell+1 \\ \ell & \ell \end{bmatrix} = \frac{(x+y)(\ell+y+\zeta+1)}{(x+y+1)(\ell-x+\zeta)} \mathbf{1}_{\ell \geq 1},$$

$$\begin{bmatrix} \ell & \ell+1 \\ \ell & \ell \end{pmatrix} = \frac{\ell+y+\zeta}{(x+y+1)(\ell-x+\zeta)} \mathbf{1}_{\ell \geq 1},$$

$$\begin{bmatrix} \ell & \ell-1 \\ \ell & \ell-1 \end{bmatrix} = \frac{(x+y)(\ell-x+\zeta-1)}{(x+y+1)(\ell-x+\zeta)} \mathbf{1}_{\ell \geq 1}.$$
(A.6)

These weights are dynamic in the sense that they depend on the height function ℓ . Moreover, under certain restrictions on the parameters (for example, if x, y > 0 and $\zeta > x$), these weights are between 0 and 1 for all $\ell \in \mathbb{Z}_{\geq 0}$. Thus, the weights (A.6) define a dynamic stochastic vertex model. Its height function is identified via Corollary 7.4 with an observable of a measure constructed out of rational symmetric functions of [Bor17a, Section 8.5].

The Hall-Littlewood case (s=0) corresponds to setting $\zeta \to +\infty$ in the weights (A.6). This vertex model is no longer dynamic; it has symmetric vertex weights (that is, the probabilities for a path to turn right or left are both equal to 1/(1+x+y)) and can be regarded as a discrete time version of the symmetric simple exclusion process (SSEP). One can thus say that the limit $t \to 1$ for s=0 corresponds to the transition from the XXZ to the XXX model, and the model (A.6) can be regarded as a dynamic version of SSEP/XXX.

A.13. Limit to a dynamic version of ASEP. Here we consider a limit of DS6V to a continuous time particle system generalizing the ASEP. For the stochastic six-vertex model, a limit to the usual ASEP was observed in [GS92] (see also [BCG16] for details).

Recall that the spectral parameters of the DS6V weights satisfy $0 \le u < v < 1$. Taylor expanded the vertex weights as $v - u \to 0$ (we omit the vertices (0, 0; 0, 0) and (1, 1; 1, 1) always having weight 1):

$$\begin{bmatrix} \ell+1 & \ell \\ \ell & \ell \end{bmatrix} = 1 + O(v-u),$$



$$\begin{bmatrix} \ell+1 & \ell+1 \\ \ell & \ell \end{bmatrix} = \frac{(v-u)(u-st^{\ell+1})}{(1-t)u(u-st^{\ell})} + O(v-u)^2,$$

$$\begin{bmatrix} -\ell & \ell \\ \ell & \ell \end{bmatrix} = 1 + O(v-u),$$

$$\begin{bmatrix} \ell & \ell \\ \ell & \ell \end{bmatrix} = 0$$

$$\begin{bmatrix} \ell & \ell \\ \ell & \ell \end{bmatrix} = 0$$

$$\begin{bmatrix} \ell & \ell \\ \ell & \ell \end{bmatrix} = 0$$

$$\begin{bmatrix} \ell & \ell \\ \ell & \ell \end{bmatrix} = 0$$

$$\begin{bmatrix} \ell & \ell \\ \ell & \ell \end{bmatrix} = 0$$

$$\begin{bmatrix} \ell & \ell \\ \ell & \ell \end{bmatrix} = 0$$

$$\begin{bmatrix} \ell & \ell \\ \ell & \ell \end{bmatrix} = 0$$

$$\begin{bmatrix} \ell & \ell \\ \ell & \ell \end{bmatrix} = 0$$

$$\begin{bmatrix} \ell & \ell \\ \ell & \ell \end{bmatrix} = 0$$

$$\begin{bmatrix} \ell & \ell \\ \ell & \ell \end{bmatrix} = 0$$

$$\begin{bmatrix} \ell & \ell \\ \ell & \ell \end{bmatrix} = 0$$

$$\begin{bmatrix} \ell & \ell \\ \ell & \ell \end{bmatrix} = 0$$

$$\begin{bmatrix} \ell & \ell \\ \ell & \ell \end{bmatrix} = 0$$

$$\begin{bmatrix} \ell & \ell \\ \ell & \ell \end{bmatrix} = 0$$

$$\begin{bmatrix} \ell & \ell \\ \ell & \ell \end{bmatrix} = 0$$

$$\begin{bmatrix} \ell & \ell \\ \ell & \ell \end{bmatrix} = 0$$

$$\begin{bmatrix} \ell & \ell \\ \ell & \ell \end{bmatrix} = 0$$

$$\begin{bmatrix} \ell & \ell \\ \ell & \ell \end{bmatrix} = 0$$

$$\begin{bmatrix} \ell & \ell \\ \ell & \ell \end{bmatrix} = 0$$

$$\begin{bmatrix} \ell & \ell \\ \ell & \ell \end{bmatrix} = 0$$

$$\begin{bmatrix} \ell & \ell \\ \ell & \ell \end{bmatrix} = 0$$

$$\begin{bmatrix} \ell & \ell \\ \ell & \ell \end{bmatrix} = 0$$

$$\begin{bmatrix} \ell & \ell \\ \ell & \ell \end{bmatrix} = 0$$

$$\begin{bmatrix} \ell & \ell \\ \ell & \ell \end{bmatrix} = 0$$

$$\begin{bmatrix} \ell & \ell \\ \ell & \ell \end{bmatrix} = 0$$

$$\begin{bmatrix} \ell & \ell \\ \ell & \ell \end{bmatrix} = 0$$

$$\begin{bmatrix} \ell & \ell \\ \ell & \ell \end{bmatrix} = 0$$

$$\begin{bmatrix} \ell & \ell \\ \ell & \ell \end{bmatrix} = 0$$

$$\begin{bmatrix} \ell & \ell \\ \ell & \ell \end{bmatrix} = 0$$

$$\begin{bmatrix} \ell & \ell \\ \ell & \ell \end{bmatrix} = 0$$

$$\begin{bmatrix} \ell & \ell \\ \ell & \ell \end{bmatrix} = 0$$

$$\begin{bmatrix} \ell & \ell \\ \ell & \ell \end{bmatrix} = 0$$

$$\begin{bmatrix} \ell & \ell \\ \ell & \ell \end{bmatrix} = 0$$

$$\begin{bmatrix} \ell & \ell \\ \ell & \ell \end{bmatrix} = 0$$

$$\begin{bmatrix} \ell & \ell \\ \ell & \ell \end{bmatrix} = 0$$

$$\begin{bmatrix} \ell & \ell \\ \ell & \ell \end{bmatrix} = 0$$

$$\begin{bmatrix} \ell & \ell \\ \ell & \ell \end{bmatrix} = 0$$

$$\begin{bmatrix} \ell & \ell \\ \ell & \ell \end{bmatrix} = 0$$

$$\begin{bmatrix} \ell & \ell \\ \ell & \ell \end{bmatrix} = 0$$

$$\begin{bmatrix} \ell & \ell \\ \ell & \ell \end{bmatrix} = 0$$

$$\begin{bmatrix} \ell & \ell \\ \ell & \ell \end{bmatrix} = 0$$

$$\begin{bmatrix} \ell & \ell \\ \ell & \ell \end{bmatrix} = 0$$

$$\begin{bmatrix} \ell & \ell \\ \ell & \ell \end{bmatrix} = 0$$

$$\begin{bmatrix} \ell & \ell \\ \ell & \ell \end{bmatrix} = 0$$

$$\begin{bmatrix} \ell & \ell \\ \ell & \ell \end{bmatrix} = 0$$

$$\begin{bmatrix} \ell & \ell \\ \ell & \ell \end{bmatrix} = 0$$

$$\begin{bmatrix} \ell & \ell \\ \ell & \ell \end{bmatrix} = 0$$

$$\begin{bmatrix} \ell & \ell \\ \ell & \ell \end{bmatrix} = 0$$

$$\begin{bmatrix} \ell & \ell \\ \ell & \ell \end{bmatrix} = 0$$

$$\begin{bmatrix} \ell & \ell \\ \ell & \ell \end{bmatrix} = 0$$

$$\begin{bmatrix} \ell & \ell \\ \ell & \ell \end{bmatrix} = 0$$

$$\begin{bmatrix} \ell & \ell \\ \ell & \ell \end{bmatrix} = 0$$

$$\begin{bmatrix} \ell & \ell \\ \ell & \ell \end{bmatrix} = 0$$

$$\begin{bmatrix} \ell & \ell \\ \ell & \ell \end{bmatrix} = 0$$

$$\begin{bmatrix} \ell & \ell \\ \ell & \ell \end{bmatrix} = 0$$

$$\begin{bmatrix} \ell & \ell \\ \ell & \ell \end{bmatrix} = 0$$

$$\begin{bmatrix} \ell & \ell \\ \ell & \ell \end{bmatrix} = 0$$

$$\begin{bmatrix} \ell & \ell \\ \ell & \ell \end{bmatrix} = 0$$

$$\begin{bmatrix} \ell & \ell \\ \ell & \ell \end{bmatrix} = 0$$

$$\begin{bmatrix} \ell & \ell \\ \ell & \ell \end{bmatrix} = 0$$

$$\begin{bmatrix} \ell & \ell \\ \ell & \ell \end{bmatrix} = 0$$

$$\begin{bmatrix} \ell & \ell \\ \ell & \ell \end{bmatrix} = 0$$

$$\begin{bmatrix} \ell & \ell \\ \ell & \ell \end{bmatrix} = 0$$

$$\begin{bmatrix} \ell & \ell \\ \ell & \ell \end{bmatrix} = 0$$

$$\begin{bmatrix} \ell & \ell \\ \ell & \ell \end{bmatrix} = 0$$

$$\begin{bmatrix} \ell & \ell \\ \ell & \ell \end{bmatrix} = 0$$

$$\begin{bmatrix} \ell & \ell \\ \ell & \ell \end{bmatrix} = 0$$

$$\begin{bmatrix} \ell & \ell \\ \ell & \ell \end{bmatrix} = 0$$

$$\begin{bmatrix} \ell & \ell \\ \ell & \ell \end{bmatrix} = 0$$

$$\begin{bmatrix} \ell & \ell \\ \ell & \ell \end{bmatrix} = 0$$

$$\begin{bmatrix} \ell & \ell \\ \ell & \ell \end{bmatrix} = 0$$

$$\begin{bmatrix} \ell & \ell \\ \ell & \ell \end{bmatrix} = 0$$

$$\begin{bmatrix} \ell & \ell \\ \ell & \ell \end{bmatrix} = 0$$

$$\begin{bmatrix} \ell & \ell \\ \ell & \ell \end{bmatrix} = 0$$

$$\begin{bmatrix} \ell & \ell \\ \ell & \ell \end{bmatrix} = 0$$

$$\begin{bmatrix} \ell & \ell \\ \ell & \ell \end{bmatrix} = 0$$

$$\begin{bmatrix} \ell & \ell \\ \ell & \ell \end{bmatrix} = 0$$

$$\begin{bmatrix} \ell & \ell \\ \ell & \ell \end{bmatrix} = 0$$

$$\begin{bmatrix} \ell & \ell \\ \ell & \ell \end{bmatrix} = 0$$

$$\begin{bmatrix} \ell & \ell \\ \ell & \ell \end{bmatrix} = 0$$

$$\begin{bmatrix} \ell & \ell \\ \ell$$

We thus see that the up-right lattice paths perform staircase-like movements most of the time. Occasionally, however, these staircases move up or down according to the weights of the vertices (1,0;1,0) and (0,1;0,1), respectively. Subtracting the staircase movement, rescaling the vertical direction by the factor of (v-u)/u(1-t), and interpreting it as time lead to the following continuous time particle system on \mathbb{Z} .

The particles are ordered as $y_1(\tau) > y_2(\tau) > \cdots$, and at most one particle per site is allowed. The six-vertex boundary condition translates into the step initial condition $y_i(0) = -i$, $i \ge 1$. In continuous time, each particle y_ℓ tries to jump to the right by one at rate $(u - st^\ell)/(u - st^{\ell-1})$ and to the left by one at rate $t((u - st^{\ell-1})/(u - st^\ell))$. If the destination is occupied, the corresponding jump is blocked and y_ℓ does not move; see Figure 2 in Section 1. Thus, one can say that our dynamic ASEP is a generalization of the ASEP with certain particle-dependent jump rates. The connection to spin Hall–Littlewood measures might provide tools for asymptotic analysis of this model.

The dynamic version of the ASEP obtained above is somewhat similar to the one of [Bor17b, BC17] coming from vertex models at elliptic level. However, these two models are different. In particular, in our model, the dynamic dependence on the height function is via the quantities

 $h_x = \#\{\text{number of particles to the right of } x\},\$

while in [Bor17b, BC17], the dynamic parameter is $s_x = 2h_x + x$ which incorporates both the particle's number and location.

A.14. Finite vertical spin. Setting $s = t^{-1/2}$, where $I \in \mathbb{Z}_{\geq 1}$, turns the vertical representation giving rise to the vertex weights (3.2) into a spin I/2 one. This gives rise to a vertex model with at most I vertical arrows per edge allowed. Let us briefly discuss what this means for the main constructions of the present paper. For simplicity, we only consider the case I = 1 when the higher spin six-vertex model turns into the six-vertex model.



Call a signature $\lambda \in \mathsf{Sign}_N$ *strict* if $\lambda_1 > \lambda_2 > \cdots > \lambda_N$. Observe that for $s = t^{-1/2}$, the weight

$$\left[\underbrace{g - 1}_{g} \right]_{u} = \frac{(1 - t^{g-2})u}{1 - ut^{-1/2}}$$

vanishes for g=2. Thus, $G^c_{\mu/\nu}(v)$ also vanishes if ν is strict and μ is not; see Section 4.2.2. At the same time, the function $G^c_{\lambda/(0^N)}$ entering the spin Hall–Littlewood measure (6.1) is not well-defined since (0^N) is not strict. This presents an obstacle in degenerating spin Hall–Littlewood measures and processes to $s=t^{-1/2}$ in a straightforward way.

On the other hand, the vertex weights for $s=t^{-1/2}$ satisfy a Yang–Baxter equation, and bijectivization can be applied to it too. Following the lines of Section 5, one can define forward transition probabilities $\mathsf{U}^{\mathrm{fwd}}(\kappa \to \nu \mid \lambda, \mu)$, where $\kappa, \lambda \in \mathsf{Sign}_{N-1}$ and $\mu, \nu \in \mathsf{Sign}_N$ are strict. Using these probabilities, it is possible to define an analogue of the Yang–Baxter field $\lambda^{(x,y)}$, $x,y \in \mathbb{Z}_{\geqslant 0}$, with boundary conditions $\lambda^{(x,0)} = \varnothing, \lambda^{(0,y)} = (-1,-2,\ldots,-y)$. It is not clear whether this version of the Yang–Baxter field leads via Markov projections to an analogue of the DS6V model of Section 7, and we do not discuss this issue here.

Appendix B. Yang-Baxter equation

Here we write out all the explicit identities between rational functions which comprise the Yang–Baxter equation. This equation states that certain combinations of vertex weights (3.2) and (3.3) are equal to each other. Writing all possible cases out, we arrive at the following 16 identities. For better notation, in the vertex weights, we put cross vertices together with pairs of vertices and use the shorthand

$$[\cdots] := [\cdots]_{u,v}, \quad [\cdots]' := [\cdots]_{v,u} \tag{B.1}$$

for the vertex weights. Moreover, by agreement, the weights of the cross vertices are not affected by the swapping of spectral parameters and are given by (3.3) on both sides of each of the identities.

Below are all the 16 identities comprising the Yang–Baxter equation. They depend on an arbitrary nonnegative integer g subject to the agreement that once an arrow configuration on either side of a formula contains g-1 or g-2, we assume that $g\geqslant 1$ or $g\geqslant 2$, respectively. Each of the identities below is readily verified by hand:



$$\begin{bmatrix} \underbrace{ \begin{bmatrix} g - 1 \\ g - 1 \end{bmatrix} } \\ = \underbrace{ (1 - s^2 t^{g-1}) u (1 - st^{g-1} u) }_{(1 - su)(1 - sv)} \underbrace{ (1 - st^g v) (1 - s^2 t^{g-1}) u }_{u - tv} + \underbrace{ \frac{ (1 - st^g v) (1 - s^2 t^{g-1}) u }_{u - tv} u - v }_{u - tv}$$

$$= \underbrace{ \begin{bmatrix} g - 1 \\ g - 1 \\ g - 1 \end{bmatrix} }_{(1 - sv)(1 - su)} \underbrace{ \begin{bmatrix} g - 1 \\ g - 1 \\ g - 1 \end{bmatrix} }_{v - tv} \underbrace{ \begin{bmatrix} g - 1 \\ g - 1 \\ g - 1 \end{bmatrix} }_{s - tv} \underbrace{ \begin{bmatrix} g - 1 \\ g - 1 \\ g - 1 \end{bmatrix} }_{s - tv} \underbrace{ \begin{bmatrix} (YB1.2) \\ (1 - su)(1 - sv) \end{bmatrix} }_{s - tv} \underbrace{ \begin{bmatrix} (1 - st^g u) (1 - s^2 t^{g-1}) v \\ (1 - su)(1 - sv) \end{bmatrix} }_{s - tv} \underbrace{ \underbrace{ \begin{bmatrix} (1 - st^g u) (1 - s^2 t^{g-1}) v \\ (1 - sv)(1 - su) \end{bmatrix} }_{s - tv} \underbrace{ \underbrace{ \begin{bmatrix} (1 - st^g v) (1 - st^{g-1} u) t \\ (1 - sv)(1 - su) \end{bmatrix} }_{s - tv} \underbrace{ \underbrace{ \begin{bmatrix} (1 - s^2 t^{g-1}) v (1 - st^{g-1} u) t \\ (1 - sv)(1 - su) \end{bmatrix} }_{s - tv} \underbrace{ \underbrace{ \begin{bmatrix} (1 - s^2 t^{g-1}) u (1 - s^2 t^{g-2}) v \\ (1 - su)(1 - sv) \end{bmatrix} }_{s - tv} \underbrace{ \underbrace{ \begin{bmatrix} (1 - s^2 t^{g-1}) u (1 - s^2 t^{g-2}) v \\ (1 - su)(1 - sv) \end{bmatrix} }_{s - tv} \underbrace{ \underbrace{ \begin{bmatrix} (1 - t^{g+1}) (1 - st^{g+1} u) t \\ (1 - su)(1 - sv) \end{bmatrix} }_{s - tv} \underbrace{ \underbrace{ \begin{bmatrix} (1 - t^{g+1}) (1 - st^{g+1} u) t \\ (1 - su)(1 - sv) \end{bmatrix} }_{s - tv} \underbrace{ \underbrace{ \begin{bmatrix} (1 - t^{g+1}) (1 - st^{g+1} u) t \\ (1 - sv)(1 - su) \end{bmatrix} }_{s - tv} \underbrace{ \underbrace{ \begin{bmatrix} (1 - t^{g+1}) (1 - st^{g+1} u) t \\ (1 - sv)(1 - su) \end{bmatrix} }_{s - tv} \underbrace{ \underbrace{ \begin{bmatrix} (1 - t^{g+1}) (1 - st^{g+1} u) t \\ (1 - sv)(1 - sv) \end{bmatrix} }_{s - tv} \underbrace{ \underbrace{ \begin{bmatrix} (1 - t^{g+1}) (1 - st^{g+1} u) t \\ (1 - sv)(1 - sv) \end{bmatrix} }_{s - tv} \underbrace{ \underbrace{ \begin{bmatrix} (1 - t^{g+1}) (1 - st^{g+1} u) t \\ (1 - sv)(1 - sv) \end{bmatrix} }_{s - tv} \underbrace{ \underbrace{ \begin{bmatrix} (1 - t^{g+1}) (1 - st^{g+1} u) t \\ (1 - sv)(1 - sv) \end{bmatrix} }_{s - tv} \underbrace{ \underbrace{ \begin{bmatrix} (1 - t^{g+1}) (1 - st^{g+1} u) t \\ (1 - sv)(1 - sv) \end{bmatrix} }_{s - tv} \underbrace{ \underbrace{ \begin{bmatrix} (1 - t^{g+1}) (1 - st^{g+1} u) t \\ (1 - sv)(1 - sv) t \end{bmatrix} }_{s - tv} \underbrace{ \underbrace{ \begin{bmatrix} (1 - t^{g+1}) (1 - st^{g+1} u) t \\ (1 - sv)(1 - sv) t \end{bmatrix} }_{s - tv} \underbrace{ \underbrace{ \begin{bmatrix} (1 - t^{g+1}) (1 - t^{g+1} u) t \\ (1 - sv)(1 - sv) t \end{bmatrix} }_{s - tv} \underbrace{ \underbrace{ \begin{bmatrix} (1 - t^{g+1}) (1 - t^{g+1} u) t \\ (1 - sv)(1 - sv) t \end{bmatrix} }_{s - tv} \underbrace{ \underbrace{ \begin{bmatrix} (1 - t^{g+1}) (1 - t^{g+1} u) t \\ (1 - t^{g+1}) (1 - t^{g+1} u) t \end{bmatrix} }_{s - tv} \underbrace{ \underbrace{ \begin{bmatrix} (1 - t^{g+1}) (1 - t^{g+1} u) t \\ (1 - t^{g+1} u) t \end{bmatrix} }_{s - tv} \underbrace{ \underbrace{ \begin{bmatrix} (1 - t^{g+1}) (1 - t^{g+1} u) t \\ (1 - t^$$



$$= \begin{bmatrix} \frac{g}{g} & \frac{g}{g} & \frac{1}{g} \end{bmatrix}' + \begin{bmatrix} \frac{g}{g+1} & \frac{g}{g} \\ \frac{g}{g+1} & \frac{g}{g} \end{bmatrix}'; \qquad (YB2.2)$$

$$\begin{bmatrix} \frac{g}{g+1} & \frac{g}{g} & \frac{1}{g} \\ \frac{g}{g+1} & \frac{g}{g} & \frac{g}{g} \\ \frac{g}{g} & \frac{g}{g} & \frac{g}{g} & \frac{g}{g} & \frac{g}{g} \\ \frac{g}{g} & \frac{g}{g} & \frac{g}{g} & \frac{g}{g} & \frac{g}{g} \\ \frac{g}{g} & \frac{g}{g} & \frac{g}{g} & \frac{g}{g} & \frac{g}{g} \\ \frac{g}{g} & \frac{g}{g} & \frac{g}{g} & \frac{g}{g} & \frac{g}{g} \\ \frac{g}{g} & \frac{g}{g} & \frac{g}{g} & \frac{g}{g} & \frac{g}{g} \\ \frac{g}{g} & \frac{g}{g} & \frac{g}{g} & \frac{g}{g} & \frac{g}{g} \\ \frac{g}{g} & \frac{g}{g} & \frac{g}{g} & \frac{g}{g} & \frac{g}{g} \\ \frac{g}{g} & \frac{g}{g} & \frac{g}{g} & \frac{g}{g} & \frac{g}{g} \\ \frac{g}{g} & \frac{g}{g} & \frac{g}{g} & \frac{g}{g} & \frac{g}{g} \\ \frac{g}{g} & \frac{g}{g} & \frac{g}{g} & \frac{g}{g} & \frac{g}{g} & \frac{g}{g} \\ \frac{g}{g} & \frac{g}{g} & \frac{g}{g} & \frac{g}{g} & \frac{g}{g} \\ \frac{g}{g} & \frac{g}{g} & \frac{g}{g} & \frac{g}{g} & \frac{g}{g} \\ \frac{g}{g} & \frac{g}{g} & \frac{g}{g} & \frac{g}{g} & \frac{g}{g} \\ \frac{g}{g} & \frac{g}{g} & \frac{g}{g} & \frac{g}{g} & \frac{g}{g} \\ \frac{g}{g} & \frac{g}{g} & \frac{g}{g} & \frac{g}{g} & \frac{g}{g} \\ \frac{g}{g} & \frac{g}{g} & \frac{g}{g} & \frac{g}{g} & \frac{g}{g} \\ \frac{g}{g} & \frac{g}{g} & \frac{g}{g} & \frac{g}{g} & \frac{g}{g} \\ \frac{g}{g} & \frac{g}{g} & \frac{g}{g} & \frac{g}{g} & \frac{g}{g} \\ \frac{g}{g} & \frac{g}{g} & \frac{g}{g} & \frac{g}{g} & \frac{g}{g} \\ \frac{g}{g} & \frac{g}{g} & \frac{g}{g} & \frac{g}{g} & \frac{g}{g} \\ \frac{g}{g} & \frac{g}{g} & \frac{g}{g} & \frac{g}{g} & \frac{g}{g} & \frac{g}{g} \\ \frac{g}{g} & \frac{g}{g} & \frac{g}{g} & \frac{g}{g} & \frac{g}{g} & \frac{g}{g} \\ \frac{g}{g} & \frac{g}{g} \\ \frac{g}{g} & \frac$$



$$= \left[\underbrace{\frac{g}{g-1}}_{g} \underbrace{\frac{g}{g}}_{f} \right]' + \left[\underbrace{\frac{g}{g}}_{g} \underbrace{\frac{g}{g}}_{f} \right]';$$
 (YB3.2)
$$= \frac{(1-t)v}{u-tv} \underbrace{(1-st^{g}u)(v-st^{g})}_{(1-su)(1-sv)} + \frac{u-v}{u-tv} \underbrace{(1-t^{g+1})(1-s^{2}t^{g})v}_{(1-su)(1-sv)}$$

$$= \frac{(1-st^{g}v)(u-st^{g})}{(1-sv)(1-su)} \underbrace{\frac{(1-t)v}{u-tv}}_{u-tv} + \underbrace{\frac{(1-s^{2}t^{g-1})v(1-t^{g})}{(1-sv)(1-su)}}_{u-tv} \underbrace{\frac{t(u-v)}{u-tv}}_{u-tv}$$

$$= \left[\underbrace{\frac{g}{g-1}}_{g} \underbrace{\frac{g}{g-1}}_{g} \right]';$$
 (YB3.3)
$$\begin{bmatrix} \underbrace{\frac{g}{g-1}}_{g} \\ \underbrace{\frac{g}{g-1}}_{g} \end{bmatrix} + \underbrace{\underbrace{\frac{g}{g-1}}_{g} \\ \underbrace{\frac{g}{g-1}}_{g} \end{bmatrix}' \\ = \underbrace{\frac{(1-t)v}{u-tv}}_{u-tv} \underbrace{\frac{(1-s^{2}t^{g-1})u(v-st^{g-1})}{(1-su)(1-sv)}}_{u-tv} + \underbrace{\frac{u-v}{u-tv}}_{u-tv} \underbrace{\frac{(u-st^{g})(1-s^{2}t^{g-1})v}{(1-su)(1-sv)}}_{u-tv}$$

$$= \underbrace{\frac{(1-s^{2}t^{g-1})v(u-st^{g-1})}{(1-sv)(1-su)}}_{u-tv} = \underbrace{\begin{bmatrix} \frac{g}{g}+2}\\ \frac{g}{g}+1 \\ \frac{g}{g} \end{bmatrix}' ;$$
 (YB3.4)
$$\begin{bmatrix} \underbrace{\frac{g}{g}+2}\\ \frac{g}{g}+1 \\ \frac{g}{g} \end{bmatrix} = \underbrace{\frac{(1-t)^{g+1})(1-t^{g+2})}{(1-su)(1-sv)}}_{u-tv} + \underbrace{\frac{(1-t^{g+1})(u-st^{g+1})}{(1-sv)(1-su)}}_{u-tv} + \underbrace{\frac{v-v}{u-tv}}_{u-tv} + \underbrace{\frac{v$$



$$= \frac{(1 - t^{g+1})(u - st^{g+1})}{(1 - sv)(1 - su)} \frac{(1 - t)v}{u - tv} + \frac{(v - st^g)(1 - t^{g+1})}{(1 - sv)(1 - su)} \frac{t(u - v)}{u - tv}$$

$$= \left[\underbrace{\frac{g + 1}{g + 1}}_{g} \right]' + \left[\underbrace{\frac{g + 1}{g}}_{g} \right]'; \tag{YB4.3}$$

$$\begin{bmatrix} \swarrow \xrightarrow{g} \xrightarrow{g} \end{bmatrix} = \frac{(u - st^g)(v - st^g)}{(1 - su)(1 - sv)} = \begin{bmatrix} \xrightarrow{g} \xrightarrow{g} & \swarrow \\ \xrightarrow{g} & \swarrow \end{bmatrix}.$$
 (YB4.4)

Appendix C. Another form of the skew Cauchy identity

The spin Hall–Littlewood symmetric functions satisfy another form of Cauchy identities which is worth mentioning. These identities involve the functions G^c (Section 4.2.2) along with the functions G. The latter are variations of the F functions (Section 4.2.1), the only difference is that the boundary condition on the left as in Figure 8 (left) is also empty. We refer to [Bor17a, Section 3] for a detailed definition of the functions G. Let us focus on the variant of the skew Cauchy identity with single variables (analogue of Theorem 4.2).

PROPOSITION C.1. Under assumption (4.9), let λ , $\mu \in \text{Sign}_N$. We have

$$\sum_{\kappa \in \operatorname{Sign}_N} G_{\lambda/\kappa}^c(v^{-1}) G_{\mu/\kappa}(u) = \sum_{\nu \in \operatorname{Sign}_N} G_{\nu/\mu}^c(v^{-1}) G_{\nu/\lambda}(u). \tag{C.1}$$

Proof. The proof is analogous to our proof of Theorem 4.2 presented in Section 5.2. The only difference is that we consider boundary conditions as in Figure 20 instead of Figure 9. Namely, one defines the modified transition probabilities on signatures $\bar{\sf U}^{\rm fwd}_{v,u}(\kappa \to \nu \mid \lambda, \mu)$ ($\bar{\sf U}^{\rm bwd}_{v,u}(\nu \to \kappa \mid \lambda, \mu)$) obtained by dragging the cross vertex \times from $-\infty$ to $+\infty$ (from $+\infty$ to $-\infty$, respectively), proves an analogue of Proposition 5.6, and obtains a bijective proof of (C.1). \square

Proposition C.1 is new. Its s = 0 degeneration was mentioned in [BM18, Sections 3.1 and 3.7]. The significance of this variation of the skew Cauchy identity is in the fact that it does not have any prefactors, which is neat from the combinatorial point of view. Another property which is better visible in this variation is a symmetry between λ and μ .

PROPOSITION C.2. Let $\bar{\mathsf{U}}^{\mathrm{fwd}}_{v,u}(\kappa \to \nu \mid \lambda, \mu)$ and $\bar{\mathsf{U}}^{\mathrm{bwd}}_{v,u}(\nu \to \kappa \mid \lambda, \mu)$ be transition probabilities defined in the proof of Proposition C.1. We have

$$\bar{\mathsf{U}}^{\mathrm{fwd}}_{\boldsymbol{\nu},\boldsymbol{u}}(\kappa \to \boldsymbol{\nu} \mid \boldsymbol{\lambda}, \boldsymbol{\mu}) = \bar{\mathsf{U}}^{\mathrm{fwd}}_{\boldsymbol{u}^{-1},\boldsymbol{\nu}^{-1}}(\kappa \to \boldsymbol{\nu} \mid \boldsymbol{\mu}, \boldsymbol{\lambda}),$$



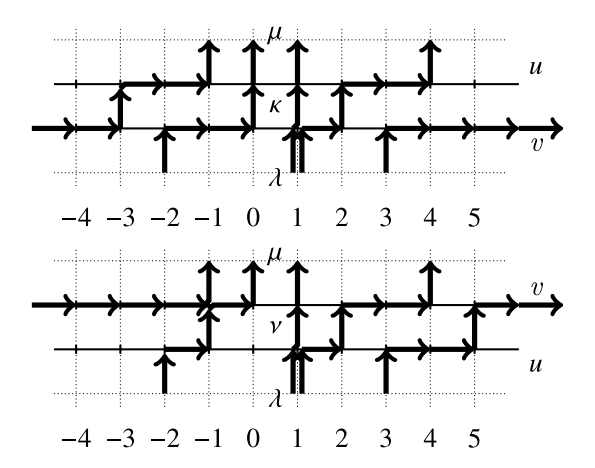


Figure 20. Illustration of the sums on both sides of identity (C.1).

$$\bar{\mathsf{U}}^{\mathrm{bwd}}_{\boldsymbol{v},\boldsymbol{u}}(\boldsymbol{v} \to \boldsymbol{\kappa} \mid \boldsymbol{\lambda}, \boldsymbol{\mu}) = \bar{\mathsf{U}}^{\mathrm{bwd}}_{\boldsymbol{u}^{-1},\boldsymbol{v}^{-1}}(\boldsymbol{v} \to \boldsymbol{\kappa} \mid \boldsymbol{\mu}, \boldsymbol{\lambda}).$$

Proof. The proof readily follows from Proposition 3.4.

Note also that in the Hall–Littlewood case (s = 0), Proposition C.2 becomes fully symmetric:

$$\bar{\mathsf{U}}^{\mathrm{fwd}}_{v,u}(\kappa \to \nu \mid \lambda, \mu) = \bar{\mathsf{U}}^{\mathrm{fwd}}_{v,u}(\kappa \to \nu \mid \mu, \lambda),$$
$$\bar{\mathsf{U}}^{\mathrm{bwd}}_{v,u}(\nu \to \kappa \mid \lambda, \mu) = \bar{\mathsf{U}}^{\mathrm{bwd}}_{v,u}(\nu \to \kappa \mid \mu, \lambda).$$

Indeed, this is because the local transition probabilities (Figures 4 and 5) are invariant under the swap $(u, v) \rightarrow (v^{-1}, u^{-1})$ if s = 0.

Appendix D. Inhomogeneous modifications

Most constructions and results of the present paper can be generalized to allow the spectral parameter u and the spin parameter s in the higher spin weights (3.2) vary along columns. Versions of the spin Hall-Littlewood functions F and G^c with this type of inhomogeneity, as well as Cauchy summation identities for these functions, are discussed in detail in [BP18a]. Such Cauchy identities were employed in that work to compute observables of the inhomogeneous stochastic higher spin six-vertex model which are amenable to asymptotic analysis (performed in, for example, [BP18b]).

Let us briefly discuss the modifications needed to introduce inhomogeneity parameters into our constructions. These parameters form two families, $\{\xi_i\}_{i\in\mathbb{Z}}$



and $\{s_i\}_{i\in\mathbb{Z}}$. The vertex weights (3.2) in the column number i now depend on the parameters $\xi_i u$ (replacing u) and s_i . These parameters ξ_i , s_i do not enter the cross vertex weights (3.3) involved in the Yang–Baxter equation. However, they do enter the local transition probabilities P^{fwd} , P^{bwd} : in the tables in Figures 4 and 5, one should replace the parameters u, v, s with $\xi_i u$, $\xi_i v$, s_i , respectively, where $i \in \mathbb{Z}$ is the location through which the cross vertex is dragged.

Next, the definitions of the functions F and G^c should be modified as in [BP18a] by first replacing $(u,s) \to (\xi_m u,s_m)$ in (4.2) and $(u^{-1},s) \to (\xi_m^{-1}u^{-1},s_m)$ in (4.5) and then defining the multivariable functions as in Section 4.2.3. Note that in Cauchy identities (for example, in (4.12)) the parameters in the functions F and G^c should be $u_i \xi_m$ and $v_j^{-1} \xi_m^{-1}$, respectively. Remarkably, the double product $\prod \prod ((v_j - u_i)/(v_j - tu_i))$ entering (4.12) remains the same in the inhomogeneous setting.

Having inhomogeneous versions of the spin Hall–Littlewood functions F and G^c , one can define the corresponding measures and processes as in Section 6.1. The local transition probabilities assembled into $U^{\text{fwd}}_{v,u}$ and $U^{\text{bwd}}_{v,u}$ thus give rise to an inhomogeneous version of the Yang–Baxter field depending on t, the parameters $\{u_i\}$, $\{v_j\}$ as in Figure 12, and two series of inhomogeneous parameters $\{\xi_m\}$ and $\{s_m\}$. The latter parameters may be thought of as belonging to the third dimension in Figure 12, the one where the signatures $\lambda^{(x,y)}$ live.

The DS6V model arising in Section 7 as a Markov projection of the Yang–Baxter field onto the column number zero does not feel the inhomogeneous parameters $\{\xi_m\}$ and $\{s_m\}$ for $m \ge 1$. This follows by the very construction of the Yang–Baxter field using the probabilities $U_{v,u}^{\text{fwd}}$. In other words, we have the following.

COROLLARY D.1. The distribution of the number of zero parts $\lambda^{[0]}$ under the inhomogeneous version of the spin Hall–Littlewood measure described above does not depend on the inhomogeneity parameters ξ_m , s_m for $m \ge 1$. A similar statement holds for spin Hall–Littlewood processes.

On the other hand, the parameters $\{u_i\}$, $\{v_j\}$ entering the Yang–Baxter field carry over to the DS6V model. The height function in this inhomogeneous DS6V model is identified with $\lambda^{[0]}$ under a spin Hall–Littlewood measure, in which the inhomogeneous parameters u_i , v_j serve as variables in the functions F and G^c ; see Corollary 7.4. The presence of the inhomogeneous parameters $\{u_i\}$ and $\{v_j\}$ carries over to most of the degenerations of the DS6V model considered in Appendix A. An exception is the ASEP type limit of Appendix A.13 since this limit is performed along the diagonal of the quadrant.



Acknowledgements

We appreciate helpful discussions with Alexei Borodin, Ivan Corwin, Grigori Olshanski, and Nicolai Reshetikhin. The work was started when the authors attended the 2017 IAS PCMI Summer Session on Random Matrices, and we are grateful to the organizers for their hospitality and support. L.P. is partially supported by the NSF grant DMS-1664617.

Conflict of Interest: None

References

- [Agg17] A. Aggarwal, 'Dynamical stochastic higher spin vertex models', *Selecta Math.* **24**(3) (2018), 2659–2735.
- [ABB18] A. Aggarwal, A. Borodin and A. Bufetov, 'Stochasticization of solutions to the Yang-Baxter equation', Ann. Henri Poincaré 20(8) (2019), 2495–2554.
- [BDJ99] J. Baik, P. Deift and K. Johansson, 'On the distribution of the length of the longest increasing subsequence of random permutations', J. Amer. Math. Soc. 12(4) (1999), 1119–1178.
- [Bar01] Y. Baryshnikov, 'GUEs and queues', Probab. Theory Related Fields 119 (2001), 256–274.
- [Bax07] R. Baxter, Exactly Solved Models in Statistical Mechanics (Courier Dover Publications, Mineola, NY, 2007).
- [BBB+14] D. Betea, C. Boutillier, J. Bouttier, G. Chapuy, S. Corteel and M. Vuletić, 'Perfect sampling algorithm for Schur processes', *Markov Process. Related Fields* 24(3) (2017), 381–418.
 - [BW16] D. Betea and M. Wheeler, 'Refined Cauchy and Littlewood identities, plane partitions and symmetry classes of alternating sign matrices', J. Combin. Theory Ser A 137 (2016), 126–165.
- [BWZJ15] D. Betea, M. Wheeler and P. Zinn-Justin, 'Refined Cauchy/Littlewood identities and six-vertex model partition functions: II. Proofs and new conjectures', J. Algebraic Combin. 42(2) (2015), 555–603.
 - [Bor11] A. Borodin, 'Schur dynamics of the Schur processes', *Adv. Math.* **228**(4) (2011), 2268–2291.
 - [Bor16] A. Borodin, 'Stochastic higher spin six vertex model and Macdonald measures', J. Math. Phys. 59(2) (2018), 023301.
 - [Bor17a] A. Borodin, 'On a family of symmetric rational functions', *Adv. Math.* **306** (2017), 973–1018.
 - [Bor17b] A. Borodin, 'Symmetric elliptic functions, IRF models, and dynamic exclusion processes', Preprint, 2017, arXiv:1701.05239 [math-ph].
- [BBW18] A. Borodin, A. Bufetov and M. Wheeler, 'Between the stochastic six vertex model and Hall–Littlewood processes', *Duke Math. J.* **167**(13) (2018), 2457–2529.
 - [BC14] A. Borodin and I. Corwin, 'Macdonald processes', Probab. Theory Related Fields 158 (2014), 225–400.
 - [BC15] A. Borodin and I. Corwin, 'Discrete time *q*-TASEPs', *Int. Math. Res. Not. IMRN* **2015**(2) (2015), 499–537.



- [BC17] A. Borodin and I. Corwin, 'Dynamic ASEP, duality and continuous q^{-1} -Hermite polynomials', Preprint, 2017, arXiv:1705.01980 [math.PR].
- [BCFV15] A. Borodin, I. Corwin, P. Ferrari and B. Veto, 'Height fluctuations for the stationary KPZ equation', Math. Phys. Anal. Geom. 18(1) (2015), 1–95.
- [BCG16] A. Borodin, I. Corwin and V. Gorin, 'Stochastic six-vertex model', *Duke J. Math.* 165(3) (2016), 563–624.
- [BCGS16] A. Borodin, I. Corwin, V. Gorin and S. Shakirov, 'Observables of Macdonald processes', Trans. Amer. Math. Soc. 368(3) (2016), 1517–1558.
- [BCPS15a] A. Borodin, I. Corwin, L. Petrov and T. Sasamoto, 'Spectral theory for interacting particle systems solvable by coordinate Bethe ansatz', *Commun. Math. Phys.* 339(3) (2015), 1167–1245.
- [BCPS15b] A. Borodin, I. Corwin, L. Petrov and T. Sasamoto, 'Spectral theory for the q-Boson particle system', *Compos. Math.* 151(1) (2015), 1–67.
 - [BF08] A. Borodin and P. Ferrari, 'Large time asymptotics of growth models on space-like paths I: PushASEP', Electron. J. Probab. 13 (2008), 1380–1418.
 - [BF14] A. Borodin and P. Ferrari, 'Anisotropic growth of random surfaces in 2+1 dimensions', *Commun. Math. Phys.* **325** (2014), 603–684.
 - [BG15] A. Borodin and V. Gorin, 'General β-Jacobi corners process and the Gaussian free field', *Comm. Pure Appl. Math.* **68**(10) (2015), 1774–1844.
 - [BP14] A. Borodin and L. Petrov, 'Integrable probability: From representation theory to Macdonald processes', *Probab. Surv.* 11 (2014), 1–58.
 - [BP16] A. Borodin and L. Petrov, 'Nearest neighbor Markov dynamics on Macdonald processes', Adv. Math. 300 (2016), 71–155.
 - [BP18a] A. Borodin and L. Petrov, 'Higher spin six vertex model and symmetric rational functions', *Selecta Math.* **24**(2) (2018), 751–874.
 - [BP18b] A. Borodin and L. Petrov, 'Inhomogeneous exponential jump model', *Probab. Theory Related Fields* **172** (2018), 323–385.
 - [BM18] A. Bufetov and K. Matveev, 'Hall–Littlewood RSK field', Selecta Math. 24(5) (2018), 4839–4884.
 - [BP15] A. Bufetov and L. Petrov, 'Law of large numbers for infinite random matrices over a finite field', *Selecta Math.* **21**(4) (2015), 1271–1338.
 - [Cor12] I. Corwin, 'The Kardar–Parisi–Zhang equation and universality class', Random Matrices Theory Appl. 1(1) (2012), 1130001.
 - [Cor16] I. Corwin, 'Kardar-Parisi-Zhang universality', Notices Amer. Math. Soc. 63(3) (2016), 230–239.
- [COSZ14] I. Corwin, N. O'Connell, T. Seppäläinen and N. Zygouras, 'Tropical combinatorics and Whittaker functions', Duke J. Math. 163(3) (2014), 513–563.
 - [CP15] I. Corwin and L. Petrov, 'The *q*-PushASEP: a new integrable model for traffic in 1 + 1 dimension', *J. Stat. Phys.* **160**(4) (2015), 1005–1026.
 - [CP16] I. Corwin and L. Petrov, 'Stochastic higher spin vertex models on the line', Comm. Math. Phys. 343(2) (2016), 651–700.
 - [DF90] P. Diaconis and J. A. Fill, 'Strong stationary times via a new form of duality', Ann. Probab. 18 (1990), 1483–1522.
 - [Dim16] E. Dimitrov, 'KPZ and Airy limits of Hall-Littlewood random plane partitions', Ann. Inst. Henri Poincaré Probab. Stat. 54(2) (2018), 640–693.
- [DLSS91] B. Derrida, J. Lebowitz, E. Speer and H. Spohn, 'Dynamics of an anchored Toom interface', J. Phys. A 24(20) (1991), 4805–4834.
 - [Fer08] P. Ferrari, 'The universal Airy₁ and Airy₂ processes in the totally asymmetric simple



- exclusion process', in *Integrable Systems and Random Matrices: In Honor of Percy Deift*, (eds. J. Baik, T. Kriecherbauer, L.-C. Li, K. T.-R. McLaughlin and C. Tomei) Contemporary Mathematics (American Mathematical Society, Providence, RI, 2008), 321–332.
- [Fom86] S. Fomin, 'Generalized Robinson-Schnested-Knuth correspondence', Zap. Nauchn. Sem. (LOMI) 155 (1986), 156–175 (in Russian).
- [Fom95] S. Fomin, 'Schensted algorithms for dual graded graphs', J. Algebraic Combin. 4(1) (1995), 5–45.
- [GM14] G. Gimmett and I. Manolescu, 'Bond percolation on isoradial graphs: criticality and universality', *Probab. Theory Related Fields* **159**(1–2) (2014), 273–327.
- [GS92] L.-H. Gwa and H. Spohn, 'Six-vertex model, roughened surfaces, and an asymmetric spin Hamiltonian', *Phys. Rev. Lett.* **68**(6) (1992), 725–728.
- [HHT15] T. Halpin-Healy and K. Takeuchi, 'A KPZ cocktail-shaken, not stirred ...', J. Stat. Phys. 160(4) (2015), 794–814.
 - [Joh00] K. Johansson, 'Shape fluctuations and random matrices', Comm. Math. Phys. 209(2) (2000), 437–476.
 - [Kir01] A. N. Kirillov, 'Introduction to tropical combinatorics', in *Physics and Combinatorics*, Proceedings of the Nagoya 2000 International Workshop (Singapore) (eds. A. N. Kirillov and N. Liskova) (World Scientific, Singapore, 2001), 82–150.
 - [KR87] A. N. Kirillov and N. Reshetikhin, 'Exact solution of the integrable XXZ Heisenberg model with arbitrary spin. I. The ground state and the excitation spectrum', J. Phys. A 20(6) (1987), 1565–1585.
- [KBI93] V. Korepin, N. Bogoliubov and A. Izergin, Quantum Inverse Scattering Method and Correlation Functions, (Cambridge University Press, Cambridge, 1993).
- [KR83] P. Kulish and N. Reshetikhin, 'Quantum linear problem for the Sine–Gordon equation and higher representations', New York J. Math. Sci. 23 (1983), 2435–2441.
- [KRS81] P. Kulish, N. Reshetikhin and E. Sklyanin, 'Yang–Baxter equation and representation theory: I', Lett. Math. Phys. 5 (1981), 393–403.
- [Lie67] E. H. Lieb, 'Residual entropy of square ice', Phys. Rev. 162(1) (1967), 162–172.
- [MGP68] C. MacDonald, J. Gibbs and A. Pipkin, 'Kinetics of biopolymerization on nucleic acid templates', *Biopolymers* **6**(1) (1968), 1–25.
- [Mac95] I. G. Macdonald, Symmetric Functions and Hall Polynomials, 2nd edn, (Oxford University Press, Oxford, UK, 1995).
- [Man14] V. Mangazeev, 'On the Yang-Baxter equation for the six-vertex model', Nuclear Phys. B 882 (2014), 70–96.
- [MP17] K. Matveev and L. Petrov, 'q-randomized Robinson-Schensted-Knuth correspondences and random polymers', Ann. Inst. Henri Poincare D 4(1) (2017), 1–123.
- [NY04] M. Noumi and Y. Yamada, 'Tropical Robinson-Schensted-Knuth correspondence and birational Weyl group actions', in *Representation Theory of Algebraic Groups* and Quantum Groups, Adv. Stud. Pure Math., 40 (Math. Soc. Japan, Tokyo, 2004), 371–442.
- [O'C03a] N. O'Connell, 'A path-transformation for random walks and the Robinson–Schensted correspondence', *Trans. Amer. Math. Soc.* **355**(9) (2003), 3669–3697.
- [O'C03b] N. O'Connell, 'Conditioned random walks and the RSK correspondence', J. Phys. A 36(12) (2003), 3049–3066.
- [O'C12] N. O'Connell, 'Directed polymers and the quantum Toda lattice', *Ann. Probab.* **40**(2) (2012), 437–458.



- [OP13] N. O'Connell and Y. Pei, 'A q-weighted version of the Robinson–Schensted algorithm', Electron. J. Probab. 18(95) (2013), 1–25.
- [OSZ14] N. O'Connell, T. Seppäläinen and N. Zygouras, 'Geometric RSK correspondence, Whittaker functions and symmetrized random polymers', *Invent. Math.* 197 (2014), 361–416.
- [OY02] N. O'Connell and M. Yor, 'A representation for non-colliding random walks', *Electron. Commun. Probab.* **7** (2002), 1–12.
- [Oko01] A. Okounkov, 'Infinite wedge and random partitions', *Selecta Math.* **7**(1) (2001), 57–81.
- [OR03] A. Okounkov and N. Reshetikhin, 'Correlation function of Schur process with application to local geometry of a random 3-dimensional Young diagram', J. Amer. Math. Soc. 16(3) (2003), 581–603.
- [Pau35] L. Pauling, 'The structure and entropy of ice and of other crystals with some randomness of atomic arrangement', J. Amer. Chem. Soc. 57(12) (1935), 2680–2684.
- [Pei13] Y. Pei, 'A symmetry property for q-weighted Robinson–Schensted algorithms and other branching insertion algorithms', *J. Algebraic Combin.* **40** (2013), 743–770.
- [Pei16] Y. Pei, 'A *q*-Robinson–Schensted–Knuth Algorithm and a *q*-polymer', Preprint, 2016, arXiv:1610.03692 [math.CO].
- [Pet20] L. Petrov, 'PushTASEP in inhomogeneous space', In preparation, 2020.
- [Pov13] A. Povolotsky, 'On integrability of zero-range chipping models with factorized steady state', J. Phys. A 46 465205 (2013).
- [PS02] M. Prähofer and H. Spohn, 'Scale invariance of the PNG droplet and the Airy process', J. Stat. Phys. 108 (2002), 1071–1106.
- [Sep12] T. Seppäläinen, 'Scaling for a one-dimensional directed polymer with boundary conditions', Ann. Probab. 40(1) (2012), 19–73.
- [Spi70] F. Spitzer, 'Interaction of Markov processes', Adv. Math. 5(2) (1970), 246–290.
- [Spo15] A. Sportiello, Personal communication, 2015.
- [Tsi06] N. Tsilevich, 'Quantum inverse scattering method for the q-boson model and symmetric functions', *Funct. Anal. Appl.* **40**(3) (2006), 207–217.
- [VK86] A. Vershik and S. Kerov, 'The characters of the infinite symmetric group and probability properties of the Robinson–Shensted–Knuth algorithm', SIAM J. Algebra Discrete Math. 7(1) (1986), 116–124.
- [WW09] J. Warren and P. Windridge, 'Some examples of dynamics for Gelfand–Tsetlin patterns', *Electron. J. Probab.* **14** (2009), 1745–1769.
- [Wey97] H. Weyl, The Classical Groups. Their Invariants and Representations, (Princeton University Press, Princeton, NJ, 1997).
- [WZJ16] M. Wheeler and P. Zinn-Justin, 'Refined Cauchy/Littlewood identities and six-vertex model partition functions: III. Deformed bosons', Adv. Math. 299 (2016), 543–600.
- [Yan67] C. N. Yang, 'Some exact results for the many-body problem in one dimension with repulsive delta-function interaction', *Phys. Rev. Lett.* 19(23) (1967), 1312.